A microbe-derived treatment to help inhibit White-nose Syndrome in hibernating North American bats

By

Mayara Mejri

A Thesis Submitted to

Saint Mary's University, Halifax, Nova Scotia

in Partial Fulfillment of the Requirements for

the Degree of Bachelor of Science with Honours in Biology

April, 2023, Halifax, Nova Scotia

Approved: Dr. Clarissa Sit

Supervisor

Approved: Dr. David Chiasson

Examiner

Date: Submitted: April 26, 2023

A microbe-derived treatment to help inhibit White-nose Syndrome in hibernating North American bats

By Mayara Mejri

ABSTRACT

Pseudogymnoascus destructans (*P. destructans*) is known to be the causative agent of White-Nose Syndrome in hibernating North American bats. To date, this disease has caused large-scale mortality in bat populations present in 25 US states and 5 Canadian provinces. White Nose Syndrome is associated with a decrease in fat reserves and a substantial loss in water and electrolytes. This disturbance in normal metabolism leads to frequent arousal periods during hibernation. While fighting against the disease, exhaustion of compensatory mechanisms leads to mortality.

Probiotics and microbe-derived treatments are the likely solution for managing White Nose Syndrome since introducing foreign antifungals can affect an already sensitive cave environment. This study examines the inhibitory effect of one *Penicillium spp.* isolate on *P. destructans*. Sanger sequencing and NCBI BLAST confirmed the identity of the *Penicillium spp.* The isolate was identified to be *Penicillium herquei*. Using pairwise testing plates, the fungus has been shown to inhibit the growth of *P. destructans* over the course of two weeks. The growth curve of the isolate was tracked by measuring the dry mass and the absorbance of different liquid cultures over 10 days. The inhibition could either be due to resource or interference competition. The cell-free liquid culture was added to fresh media to make up plates that were subsequently inoculated with *P. destructans*. These plates had no to little growth which showed that the presence of the *P. herquei* is not crucial to the inhibition and that there is no resource competition between the two fungi. This indicates that the isolate probably secretes an inhibitory compound. Plates inoculated with the isolate were extracted with solvents of different polarities and then analyzed using a quadrupole time-of-flight mass spectrometer to determine the mass-to-charge ratio and the retention time of the inhibitory compound.

April 26, 2023

ACKNOWLEDGMENTS

I would like to thank my supervisor, Dr. Clarissa Sit, for her constant support and guidance. I was honoured to have the opportunity to be part of the bat research group and work in both microbiology and organic chemistry. This project was a huge learning process for me, and I could not have done it without your encouragement, feedback and support. Thank you!

I would also like to thank my thesis reader, Dr. David Chiasson, who was also my mentor for more than a year and a half. I started in Dr. Chiasson's lab with no prior research experience. I owe everything I know about microbiology and genetics to you, and I am forever grateful for recruiting me as a brand-new first-year student. Thank you for your guidance throughout my university life and for providing valuable feedback throughout my thesis research.

Also, a special thanks to both the Biology and Chemistry department, for all the work opportunities that helped me develop important skill sets that were valuable for my research. Thank you to Mary Jane MacNeil and to the department chairs Dr. Jason Masuda and Dr. David Dansereau for all the technical help and support throughout this year.

A big thank you to all the Biology and Chemistry Department Technicians, especially Patricia Granados and Carmen Cranley for training me on the different equipment, Dr. Najwan Albarghouthi and Dr. Bitu Hurisso . Thank you Patricia for your support and guidance while I was trying to figure out how the QTOF worked and thank you for answering all my questions and for allowing me to reflect on each part of my research. Bitu and Najwan, thank you for your constant support. It's been a pleasure working with both of you.

Thank you to my Honours classmates and to the professors, Dr Anne Dalziel and Dr. Ellie Goud for all your support and all your feedback.

I would like to thank the former and current Sit Research Group members: Lauren Grant, Janine Mombourquette, Julie Dayrit, Cassie Burns, Olivia Roland, Tanisha Ballard, Nicola Augustin, Prashansa Kooshna but especially Logan Cox for training me and being an amazing and supportive lab mate and Jennifer Kolwich (who I never met in person!). Thank you, Jenn, for all your work. Your research and thesis were guidelines for me, and I was so honoured to talk to you and brainstorm ideas for the project with you!

Finally, I would like to thank my parents, my brother, my best friends, my Mima and the rest of my family in Canada. Thank you for all your support when everything seemed dark and blurry. We made it!

Table of Content

Table of Figures and Table

1. Introduction

1.1 Chiropterans: Important anatomy and physiology

Chiropterans or bats are one of the most diverse mammalian groups after rodents. The order Chiroptera includes 18 families and more than 1116 bat species to date (Heard et al., 2007). It is also one of the most largely spread-out groups that inhabit tropical areas as well as oceanic islands and some of the colder regions in both hemispheres (Heard et al., 2007). Members of the Chiropterans family undergo hibernation. It is a response to seasonal periods that have high energy demand and low energy availability. During hibernation, bats experience a variety of physiological, behavioural, and morphological changes. A regular hibernation season contains different periods of torpor (Carey et al., 2003). For brown bats (*Eptesicus fuscus*), torpor lasts approximately 3.3 days (Halsall et al., 2012). Bats are homeotherms which means that they can control their metabolic rate and body temperature (Zagmajster et al., 2019). During this torpor period, basal metabolic rate is decreased by about 2 – 4% (Carey et el., 2003). However, necessary physiological functions continue at a lower rate whereas some functions are suspended till the end of the torpor. During this hibernation period, the heart rate is decreased from its normal value of 200-300 beats/min to 3-5 beats/min. Respiration rate also decreases from 100-200 breaths/min to 4-6 breaths/min (Carey et al., 2003). Hibernating bats do not need food ingestion during the torpor periods. Instead, they rely on their fat reserves. In fact, the process of lipid hydrolysis from the white adipose tissue results in fatty acids and glycerol. These products constitute the primary fuel source for bats during torpor (Carey et al., 2003). Torpor can also affect other physiological processes and biological systems including the immune system (Fritze et al., 2019). In fact, the immune response is a very costly process because it includes an increase in metabolic rate.

Consequently, the immune system is generally downregulated during these periods of torpor in bats (Fritze et al., 2019).

The wing structure is a very important anatomical and morphological structure in bats. The wing tissue is composed of two epithelial tissues with a bundle of blood and lymphatic vessels, nerves, and connective tissues in between (Cryan et al., 2010). Wings play a critical role in maintaining water balance within bats. During hibernation, the exposed wing membranes, and the bat's large lungs both contribute to evaporative water loss. This loss accounts for 99% of total water loss in hibernating bats (Cryan et al., 2010).

The body temperature of bats during hibernation can range between 1 to 15^{o} C (Cryan et al., 2010). To conserve energy, bats also choose to cluster around humid areas of the cave to conserve energy and decrease evaporative water loss. In addition to that, the bat's anatomy and morphology make them predisposed to evaporative water loss during hibernation (Cryan et al., 2010). All these reasons combined make hibernating bats a vulnerable target for various infections.

1.2 *Pseudogymnoascus destructans* and White-nose Syndrome

White-nose syndrome was first documented in North America in 2006 at Howe's Cave, New York City (Frick et al., 2016). In the late winter of 2007, the Department of Environmental Conservation discovered hundreds of dead bats on the floors of various caves. Bats were also seen flying out of the caves in the middle of the winter and into the snowy landscapes (Frick et al., 2016). White-nose syndrome results in white fuzzy hyphae and conidia on the muzzle and the wing membranes of bats (Gargas et al., 2009). By 2014, White-nose Syndrome was found in 25 US states and five Canadian provinces. A confirmed case of White-nose syndrome is determined after histopathological examination (Frick et a., 2016). This disease has affected 47 different bat species

in North America (Frank et al., 2016) and 5.7 to 6.7 million North American bats (Moore et al., 2013).

Pseudogymnoascus destructans is the causative agent of White-nose syndrome. In April 2009, the white-nose syndrome fungus was isolated from four different bat species: Little Brown, Northern Long-eared, Big Brown and Tricolored bats (Gargas et al., 2009). The initial species identification was done by sequencing small subunit (SSU) and internal transcribed spacer (ITS) RNA sequences. The results placed the causative fungus within the genus *Geomyces* (Gargas et al., 2009). However, the fungus was later reclassified to be *P. destructans* due to its different morphology from *Geomyces* and based on other sequencing and phylogenetic evidence (Blehert et al., 2009; Minnis and Linder, 2013). For a while, *P. destructans* was not confirmed to be the causative agent of White-nose Syndrome. In fact, *P. destructans* is not native to North America and is present in Europe. However, large-scale mortality has never been recorded in European bats (Johnson et al., 2014). *P. destructans* was finally found to be the cause of White-nose Syndrome in 2011-2012 by inoculating Little Brown Bats (*Myotis lucifugus*) with *P. destructans* (Reeder et al., 2012). This inoculation induced White-nose Syndrome and the fungus could be isolated from infected bats which are the necessary criteria for a primary pathogen (Reeder et al., 2012). *P. destructans* is part of the Ascomycota phylum (Vanderwolf et al., 2016). It is a saprophytic fungus that requires a host to survive. It persists on the walls and in the soil of caves which could explain the continuous infection (Farina and Lankton, 2018).

White-nose Syndrome symptoms are associated with a decrease in fat reserves and a cascade of physiological responses that lead to mortality in bat populations (Verant et al., 2014). Early stages of the disease include the colonization of the wing membrane by the fungus causing apparent lesions on the epidermis. Infected bats undergo a significant increase in energy

consumption, along with respiratory acidosis and hyperkalemia (Verant et al., 2014). Respiratory acidosis results from the accumulation of high CO_2 levels in the blood. This accumulation can be due to the bats trying to further decrease their metabolic rates (Verant et al., 2014). Hyperkalemia is defined by high potassium levels in the blood. It was first though that the increase in electrolyte concentration in the blood (Potassium, Sodium and Chloride) was due to renal failure. However, histological examination found that there was no kidney damage (Warnecke et al., 2013). Hyperkalemia can be explained by ions from the cell leaking through the damaged tissues (Verant et al., 2014). In later stages of the infection, CO_2 levels elevate beyond a tolerable threshold and hyperventilation is stimulated which causes arousal periods. The removal of excess CO_2 from the blood is energetically costly which contributes to the faster depletion of fat reserves (Verant et al., 2014). Increased hyperventilation and an increased body temperature during the arousal periods contribute to a greater evaporative water loss and electrolyte loss through the ulcerations causing dehydration and more frequent arousals (Verant et al., 2014; Warnecke et al., 2013). The worsening of the infection leads to other physiological disturbances such as hypoglycemia and hypocapnia (Verant et al., 2014). Mortality is the result of the exhaustion of all physiological compensatory mechanisms such as cellular buffering and metabolic regulation (Verant et al., 2014).

1.3 White-nose Syndrome and the emergence of infectious disease in Wildlife hypotheses

The mass death that the bat population across North American underwent raises a very critical question about the origin of the New York outbreak in 2006. There are two major hypotheses that could explain the emergence of infectious disease in wildlife: the endemic pathogen hypothesis and the novel or invasive pathogen hypothesis (Warnecke et al., 2012). The

endemic pathogen hypothesis states that the pathogen has been present in wildlife before, but it recently increased its pathogenicity due to environmental changes or human intervention (Rachowicz et al., 2005). On the other hand, the novel pathogen hypothesis suggests that the pathogen or the newly evolved virulent variant, has spread out to a new geographic area where the hosts are more naïve and susceptible to being infected (Rachowicz et al., 2005). The endemic pathogen hypothesis was rejected when phylogenetic analysis failed to find a closely related species that *Pseudogymnoascus* could have evolved from in North America (Minnis and Linder). Phylogenetic evidence showed that *Pseudogymnoascus* evolved independently from closely related genera like *Geomyces* (Minnis and Linder, 2013). Accumulated research suggests that *Pseudogymnoascus destructans* is an exotic species that was introduced to North America (Minnis and Linder, 2013). In fact, *P. destructans* is widespread in different regions in Europe without an associated mass mortality (Puechmaille et al., 2011). In addition, two different mating types were found in Europe (Palmer et al., 2014). Consequently, it is possible that European bats have evolved to cohabitate with the fungus by incorporating the fungus into their skin's flora (Wibbelt at al., 2010). To confirm that the difference in the degree of pathogenicity between European and North American bats is not the cause of the different mortality rates across continents, North American bats were inoculated with the European isolate of *P. destructans*. North American bats displayed the same symptoms associated with White-nose Syndrome (Warnecke et al., 2012). Thus, White-nose Syndrome associated *P. destructans* probably originated from Eastern Europe and was transferred to North America (Drees et al., 2017; Leopardi et al., 2015). It is important to note that *P. destructans* can also be found in China and Mongolia with no associated mass mortality (Hoyt et al., 2020). Further phylogenetic analysis and molecular dating have shown that the *P.*

destructans strains in North America and Europe have diverged from their ancestors and the Asian isolates about 3400 years ago (Drees et al., 2017).

1.4 Resistance to White-nose Syndrome

The differences between how European and North American bats react to *P. destructans* pose multiple questions about the resistance of bats to White-nose Syndrome. Research on Little Brown Bats (*Myotis lucifugus*) revealed that infected bats undergo an inflammatory response stimulated by the fungus (Moore et al., 2013). It was shown that anti- *P. destructans* antibodies play no role in immunity against White-nose Syndrome since studies on European bats demonstrated a low anti- *P. destructans* antibody level (Lilley et al., 2017). However, it was found that the infection triggers a local inflammatory response at the infection site (Lilley et al., 2017). Transcriptomic studies revealed that the infection induced the expression of an inflammatory cytokine compound that is associated with the immune response. Examination of gene expression of cytokines showed that the inflammatory cytokine is expressed in lymphatic nodes of infected bats as opposed to uninfected bats (Lilley et al., 2017). However, it is very difficult to fight the fungus with just these immune system mechanisms. Consequently, *Pseudogymnoascus destructans* proliferates and invades more of the cutaneous tissues in bats (Field et al., 2015). In this case, the classic host-immunity systems might not be efficient in fighting against White-nose Syndrome in North American bats. Therefore, microbe-derived treatment might be a better solution against White-nose Syndrome.

1.5 Immunobiome and microbe-derived treatments

Treatment with Probiotics may be an efficient solution for managing disease in wildlife. Unlike manufactured fungicides and chemicals, probiotics have the advantage of being able to potentially co-evolve with the pathogen, reducing the disease from within the natural microbiota of the host (Hoyt et al., 2015). The term immunobiome is defined as the interactions between the immune system of a host and the organisms that can live on or in that host (Horrocks et al., 2011). Immunobiome also includes the possibility of co-evolution between the host and associated microbes, to enhance the host's current immune responses. The ability of the microbes to shape the host's immune defenses is referred to as immubiotic pressure (Horrocks et al., 2011). In the wild, hosts interact with a variety of microbes that can be benign (commensals), beneficial, or harmful (pathogens) and provide the host with diverse immunobiotic pressures (Horrocks et al., 2011).

Microbial protection against pathogens is a result of metabolic secretions of compounds that can either weaken the defense mechanisms of the pathogen, slow its growth, or inhibit it completely. Microbes could also be strong competitors for nutrients, which leaves the pathogen with not enough resources to survive (Cheng et al., 2017; Cornelison et al., 2014a; Cornelison et al., 2014b; Hoyt et al., 2015; Micalizzi et al., 2017). For this reason, microbe-derived treatments may be a therapeutic solution for infectious diseases like White-nose Syndrome.

The first treatment using antifungal volatile compounds against *Pseudogymnoascus destructans* was found in 2013 and was produced by soil bacteria (Cornelison et al., 2014a). This technique was based on isolated volatile compounds from *Pseudomonas* and *Bacillus* spp., and it demonstrated broad antifungal activity (Fernando et al., 2004). Six volatile organic compounds were screened including decanal, 2-ethyl-1-hexanol, nonanal, benzothiazole, benzaldehyde, and

N, N-dimethyloctylamine. These compounds reduced conidia growth and mycelial extension (Cornelison et al., 2014a). However, there are ecological issues that can affect both the host and the ecosystem if volatile compounds are introduced to an already fragile ecosystem (Kolwich, 2019).

Efforts were undertaken to isolate microbes from the ecosystem itself, either from the soil or from the microbiota of the bats (Kolwich, 2019). *Trichoderma polysporum* was isolated from a hibernaculum infected with White-nose Syndrome (Zhang at al., 2015). A study conducted by Zhang *et al.* (2015) was the first to isolate a microbe from the soil of the cave and grow it in a laboratory environment. This isolate was able to produce secondary metabolites to inhibit the growth of *P. destructans*, but the compounds were not identified (Zhang at al., 2015).

In 2015, Hoyt *et al.* tried to isolate bacteria from the skin of different bat species in Eastern North America. The research identified another species of *Pseudomonas* that inhibits the growth of *P. destructans*. This group of bacteria can produce mycolysing enzymes that act on mycelia and conidia and inhibit the growth of *P. destructans* (Hoyt et al., 2015).

Further research tested the effectiveness of one isolate *Pseudomonas fluorescens* (designated Pf1 strain) on infected captivate bats (Cheng et al., 2017). Uninfected bats were also exposed to the strain and no harm was observed (Cheng et al., 2017). Five characteristics (called metrics) were measured to identify the severity of the disease. These include the surface area of the wing covered by *P. destructans* and number of tissue lesions. The bats were divided into different groups based on various treatments which included simultaneous application of Pf1 and *P. destructans*, pre-expose to Pf1, *P. destructans* control and Pf1 control. Results showed that the severity of the disease is highly reduced when the bats were inoculated with Pf1and *P. destructans* simultaneously. Bats in the Pf1 pre-exposure and the *P. destructans* control treatments suffered

severe metrics (Cheng et al., 2017). Consequently, at the presence of *P. destructans*, *Pseudomonas fluorescens* reduced the mortality rate of bats infected with White-nose Syndrome. The effect of the isolate on *P. destructans* relies heavily on the treatment mechanism. Simultaneous disease exposure and Pf1 treatment prevented the colonization of the pathogen (Cheng et al., 2017).

In conclusion, microbe-derived treatment has the potential to be effective in fighting infectious-based disease like White-nose Syndrome. Other treatments like relying on the immune system's antibodies and Volatile Organic Compounds may not be very effective (Cornelison et al., 2014a). Consequently, it is very important to explore the immunobiome concept and the microorganisms living with the host in the same ecosystem. This technique is beneficial because it reduces disturbance of the host and its environment, and it helps create a more diversified microbiota (Kolwich, 2019).

1.6 Objectives

The objective of this study is to find a microbe-derived treatment from a cave isolate to help inhibit the growth of *P. destructans*, the cause of White-nose Syndrome in North American bats. This study focuses on three main questions: 1) What is S5 (the isolate)?, 2) What is the inhibitory effect of S5 on *P.* destructans? And 3) How does S5 inhibit the growth of *P.* destructans? The isolate (S5) in an unknown fungus belonging to *Penicillium spp.* that was isolated from a soil sample in Gatineau, Quebec by Dr. Myron Smith's lab at Carleton University (Micalizzi et al., 2017). Through DNA extraction, PCR and sequencing this paper aims to identify to which species S5 belongs to. This research also aims to characterize the growth of S5 by creating a growth and calibration curve. To answer the second question, the inhibition will be visualized through pairwise testing plates where each pure strain (S5 and *P. destructans*) will be put on each side of the well and grown together. For the third question, this study aims to address two main scenarios. The first

scenario is that inhibition is due to resource competition, meaning that S5 is a better competitive resulting in exhausting all the available resources and thus inhibiting the growth of *P. destructans*. The second scenario is that the inhibition is due to interference competition where S5 secretes secondary metabolites to inhibit the growth of *P. destructans*. If this is the case, the paper aims to identify some of the compound's properties using quadrupole time-of-flight (QTOF) Mass Spectrometry (including retention time and mass-to-charge ratio). The complete workflow is included below (Figure 1).

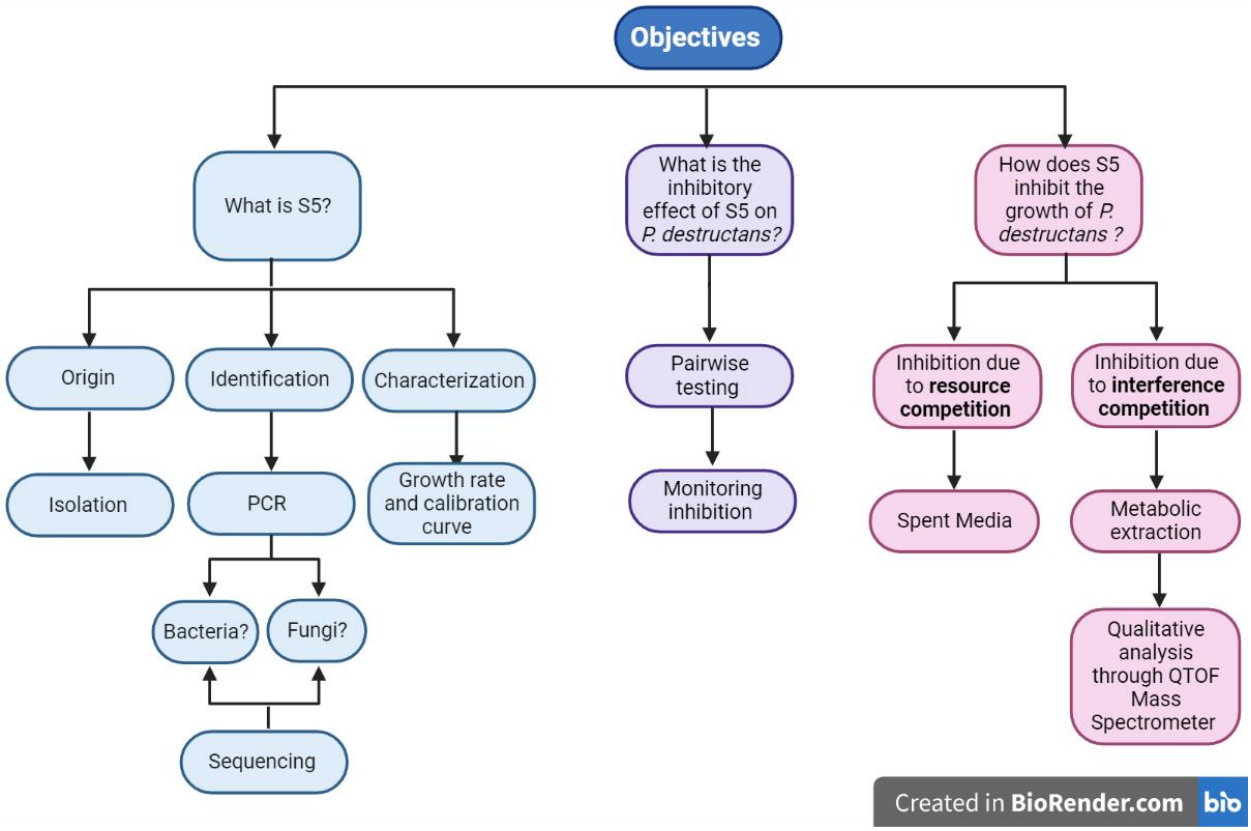

Figure 1: Work Flowchart including the objectives and various experiments performed under every objective. This project is trying to answer three main questions: 1) What is S5, 2) What is the inhibitory effect of S5 on *P. destructans* and 3) How does S5 inhibit the growth of *P. destructans*.

2. Methods and Materials

The experimental work was performed in a Containment Level 2 Laboratory according to the Canadian Biosafety Standards and Guidelines. Lab work containing living organisms was predominantly executed in an ESCO Class II, Type A2 biological safety cabinet (BSC). All waste was disposed of in a sealed biohazard container for subsequent sterile cycling and disposal. The standard operating procedures for autoclaving, the use of the biological safety cabinet, decontamination and waste disposal are outlined in the Saint Mary's University Biosafety Manual. Media and non-sterile items (glass media bottles, glassware, micropipettes, etc.) as well as any item that was introduced into the BS cabinet environment, were sterilized using a Gentinge SL5000 autoclave. The autoclave cycle was a 30-minute liquid cycle, with a minimum temperature of 121°C and a pressure of 15 psi. Before putting the items in the BSC, all items were surface sterilized with a solution of 70% v/v ethanol.

2.1 Fungi Acquisition

The S5 fungus was originally extracted from soil, specifically from a rock outcropping in Gatineau, Quebec. The unknown S5 microbe was isolated by Dr. Myron Smith's Lab at Carleton University (Ottawa, Ontario) (Micalizzi et al., 2017). *P. destructans* (strain US-15) was originally obtained from Agriculture and Agrifood Culture Collection, Ottawa, Ontario. S5 and *P. destructans* were cultured and sent to us from the Smith research group on BD Difco^{TM} Potato Dextrose Agar plates. The preliminary work on the different isolates obtained from the Smith group was done by Jennifer Kolwich as part of her Honours Thesis in Chemistry (Kolwich, 2019). The cultures of *P. destructans* were primarily cultivated in a Danby Refrigerator (Model: DCR059WE; 48L capacity) attached to an Inkbird Thermostat Controller (Model: ITC-308). The refrigerator was kept at 14.0±1.0 °C. S5 cultures were grown in the lab cupboard at room

temperature (22-25 °C). The first S5 cultures were inoculated from a 50% glycerol stock stored at a Z-SCI Twincore ultra-low temperature freezer kept at -80 °C.

2.2 Media Used

Yeast Malt Broth and Yeast Malt Agar were used to cultivate S5 and *P. destructans* throughout this project. The Yeast Malt Broth (YMB) was composed of 5.0g peptone, 3.0g yeast extract, 3.0g malt extract and 10.0g dextrose dissolved in 1000mL of deionized water (dH_2O) (pH: 6.2 ±0.2) All reagents were obtained from VWR International (Radnor, Pennsylvania, USA). The Yeast Malt Agar (YMA) contained the same components as YMB with an addition of 20g EMD Millipore Agar Powder per litre (pH: 6.2 ±0.2).

2.3 Identification of S5: DNA extraction, PCR and DNA sequencing

The DNA extraction protocol used in this thesis was a modified version of the Promega procedure (Promega, 2021) and the protocol outlined by Micalizzi et al. (2017). S5 was streaked on a YMA plate and grown at room temperature (22 °C). After 4 days of growth, one colony was selected and placed inside a small microcentrifuge tube (0.2 mL) using a micropipette. 25 µL of 70% ethanol and approximately 25 µL of 0.5 mm Glass beads from BioSpec (or the tip of a micro spatula) were added into the microcentrifuge. The mixture was then vortexed using a Fisher STD Vortex mixer 120 V (Speed: 9) for 1 to 3 minutes. The 16S region was amplified using the IDT 16S rRNA Forward primer (5’ - AGA GTT TGA TCC TGG CTC AG – 3’) and the IDT 16S rRNA Reverse primer (5’ - ACG GCT ACC TTG TTA CGA CTT – 3’). The Internal Transcribed Spacer (ITS) region characteristic of filamentous fungi was amplified using IDT ITS1 (5’ - TCC GTA GGT GAA CCT GCG G – 3’), IDT ITS2 (5’ - GCT GCG TTC TTC ATC GAT GC – 3’), IDT ITS3 (5’ - GCA TCG ATG AAG AAC GCA GC – 3’) and IDT ITS4 (5’ - TCC TCC GCT TAT

TGSA TAT GC – 3') (Figure 2). The primers were diluted to 20 µM from a 100 µM stock solution. Standard PCR reactions were 50 µL and contained 19 µL Nuclease-free Water, 25 µL Promega GoTaq® Green Master Mix (which has Taq DNA polymerase, dNTPs, $MgCl_2$ and reaction buffers), 2 µL forward primer, 2 µL reverse primer and 2 µL DNA template (from the colony extraction) (Promega, 2021). The negative controls included all components without the DNA template. The positive controls included the DNA template from the S5 colony and the ITS1 and ITS4 primers (Figure 2). Products were amplified using the BIO-RAD C1000 Touch™ Thermocycler with a 5 minutes denaturation at 94 °C followed by: 25 cycles each with denaturation for 30 s at 94 °C, annealing for 30 s at 56 °C and extension for 30 s at 72 °C. The product was preserved at 12 °C (Micalizzi et al., 2017). For the 16S primers the annealing temperature was increased to 60 °C to improve primer specificity (Micalizzi et al., 2017). The bands were visualized on a 1.5% Ethidium Bromide agarose gel made with 0.5x TBE and 5-6 µL ethidium bromide. The BIO-RAD Gel Doc™ XRT Imaging System was used to visualize the bands. When there was no smearing of the bands, the PCR products were sent to Genome Quebec (Montreal, QC) for Sanger sequencing (using an Applied Biosystems 3730xl DNA Analyzer) (https://cesgq.com/en-services#en-sequencing).

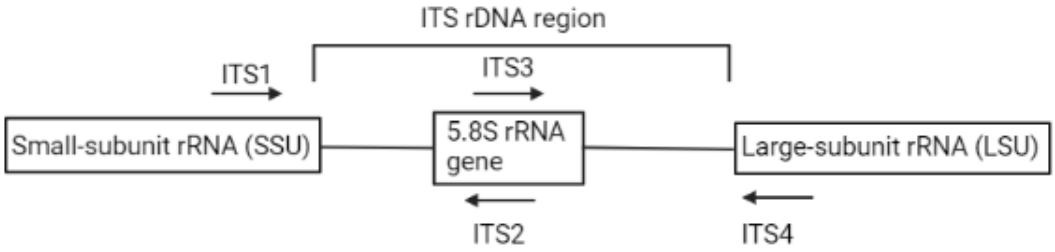

Figure 2: The ITS region of filamentous fungi, including the ITS1, ITS2, ITS3 and ITS4 primers in their approximate positions (Porras-Alfaro et al., 2014).

2.4 Quantification of *P. destructans*: Dry mass vs Absorbance

The quantification method used was originally outlined in Jennifer Kolwich's Master's Thesis (Kolwich, 2021). Three liquid stocks were made by mixing 5 mL of a seven-day culture with 45 mL of YMB. The stocks were grown for seven more days. A 35mL dilution series was prepared containing 0, 5, 10, 20, 40, 60, 80, and 100% stocks of fresh YMB. To measure the absorbance of the culture at 630 nm, a BIOCHROM NovaSpec Plus Visible Spectrophotometer and a quartz cuvette (10 mm path length) were used and compared to fresh YMB as a blank. Each sample was measured ten times. To record the dry mass associated with each dilution, a sample of 10 mL was collected on a pre-dried (in a desiccator), pre-weighed filter paper (Whatman No1) by vacuum filtration. The mycelia and the filter paper were rinsed with deionized water and placed to dry in a desiccator for 24 h). The filter paper was subsequently weighed. The mean absorbance data was plotted against the dry mass for each sample.

2.5 Quantification of S5: Dry mass vs Absorbance

Forty 15 mL disposable, sterile tubes were inoculated with 100 µL of an S5 culture in 10 mL of fresh YMB. Measurements were taken each day for a total of 10 days. Each absorbance sample and three dry mass samples were measured. To measure the absorbance, the 10 mL culture was poured into a tissue grinder (homogenizer) (Granade et al., 1985) and ground for 1 to 2 minutes. The absorbance at 630 nm was then measured in a quartz cuvette (10 mm pathlength) using a BIOCHROM NovaSpec Plus Visible Spectrophotometer. Each sample was quantified 10 times to account for the deviation. S5 fungal mass was calculated by weighing the 15 mL tube before the YMB and culture was added and after the YMB was discarded using a micropipette while the fungal mass was at the bottom. As for *P. destructans* the absorbance data was plotted against dry mass.

2.6 Pairwise testing of S5 and *P. destructans*

A 12-well plate was made using 2-4 mL of fresh YMA in each well. The wells were inoculated with 20 µL of a *P. destructans* culture on one side and 20 µL of a S5 culture on the other (outlined in figure 3, third row). The plates were incubated in the refrigerator at 14 °C for 14 days. For subsequent analysis and colony comparison, 50 µL of pure *P. destructans* and pure S5 strains were inoculated in separate 12-well plates (outlined in figure 3, first and second row) and incubated at 14 °C for 14 days. The number of plates used depended on the experiment. 24-well plates were also used to serve the same purpose.

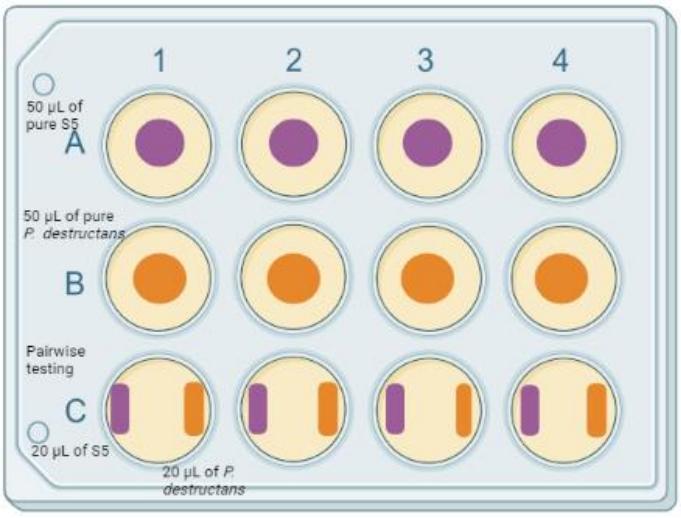

Figure 3: Layout of the 12-well plates. The pure strains and the pairwise tests were made in separate 12-well plates but were outline in this figure in the same plate.

2.7 Spent Media testing of S5

This assay was made to assess whether the inhibition was cause by interference competition where a microbe (S5) secretes inhibitory metabolites that affect *P. destructans* or by resource competition where the microbe (S5) deprives *P. destructans* from shared resources. 300 µL of S5 was grown in 300 mL of YMB for three weeks at room temperature (varying between 22 and 25 °C) (Method outlined in figure 4). After, the media was filtered through a 0.22 µm nylon filter top into a presterilized bottle. The cell-free extract (or the spent media) was preserved in the fridge at 5 °C. 10% and 20% (v/v) spent media YMA was created by mixing 10 mL and 20 mL of spent media with 90% and 80% (v/v) YMA consecutively. This media was used to pour 12-well plates.

10% and 20% spent media YMB media was also made using the same principle. The 12-well plates were inoculated with 50 µL *P. destructans*. The 100 mL of the liquid media were inoculated with 100 µL of *P. destructans*. Both plates and liquid media were incubated at 14 °C for three weeks.

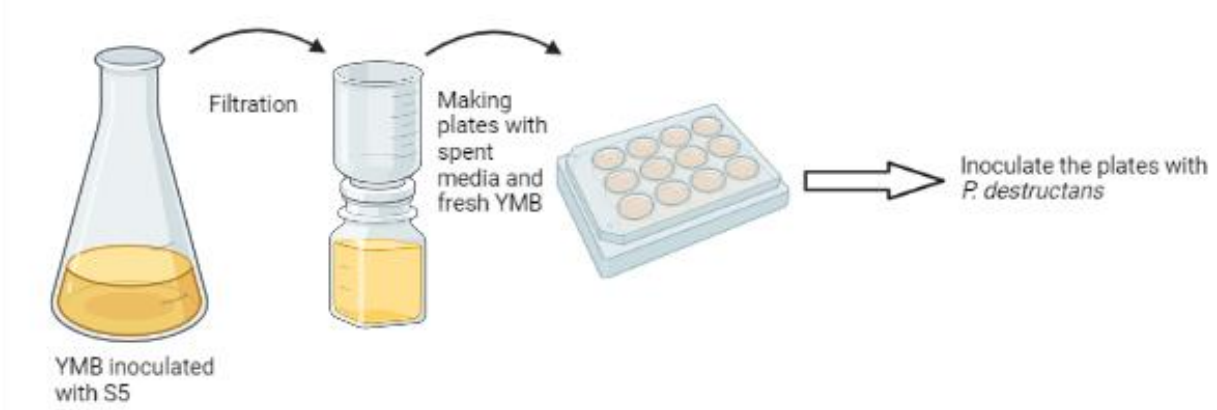

Figure 4: Flow chart for the spent media testing experiment. This experiment was used to test if S5 inhibited *P. destructans* through resource competition. The experiment involved using S5 cell-free extract (spent media) to make agar-baased media that was subsequently inoculated with *P. destructans*.

2.8 Metabolic extraction from agar plates

The pairwise test plates described in section 2.6 along with the pure *P. destructans* and S5 12-well plates were extracted using a 2:1:1 ratio of methanol, ethyl acetate and chloroform mixture (Method outlined in figure 5). The discs of the 12-well plates were 2 cm in diameter and contained 2-4 mL of YMA along with either *P. destructans*, S5, or both S5 and *P. destructans* and were removed from the plate and submerged with the 2:1:1 mixture for two hours in an Erlenmeyer sealed with tin foil. This mixture was chosen for a maximal compound extraction. Based on the "like likes like" principle, compounds can be extracted using the solvent that most is similar to them. Methanol is a polar protic solvent while chloroform is non-polar and ethyl acetate is polar aprotic. The most obvious difference between polar protic and polar aprotic solvents is the ability

to form hydrogen bonds (Huffman et al., 2012). After two hours, the mixture was filtered through a filter paper (Whatman No 1) by vacuum filtration. The soaking and filtration procedure was performed two more times. The resultant mixture was poured into a pre-weighed round bottom flask. The solvents were evaporated off by rotary evaporation using the appropriate pressure for each solvent. The extracted solids were weighed and redissolved in methanol at a concentration of 25mg/mL. The extracts were passed through a 0.22 µm filter and stored in a scintillation vial in the freezer. Blank agar plates were also extracted using the same outlined protocol. This extract was treated as the control (or the background signals) in subsequent analysis.

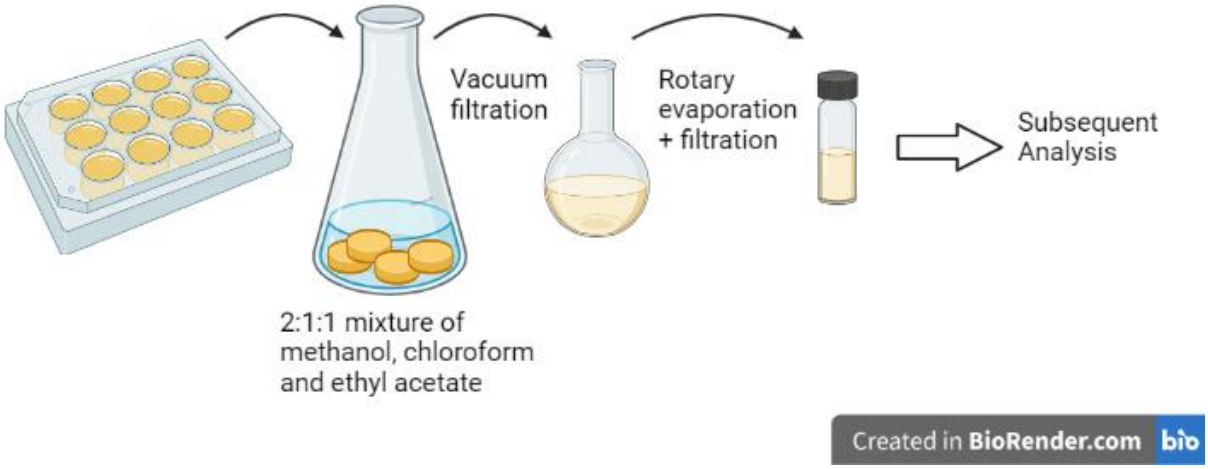

Figure 5: Flow chart for the metabolic extraction experiment from a S5 12-well plate. The plates were extracted using solvents with different polarities. The metabolic extract was used to make agar-based media and for subsequent qualitative analysis.

2.9 Metabolic extract testing

Similar to the spent media testing, twelve well plates were made from YMA adding with 10% (v/v) S5 extract, S5 and *P. destructans* extract or 20% (v/v) of the S5 and *P. destructans* extract. The plates were incubated at 14 °C for three weeks.

2.10 Thin Film Layer Testing

The metabolic extract protocol outlined in section 2.8 was redone using S5 12-well plates extracted with either Acetonitrile (ACN) or Chloroform ($CHCl_3$). The metabolic extract was redissolved in its original solvent (either ACN or $CHCl_3$) to a final concentration of 25 mg/mL. 100 µL of each extract was placed on each agar well (from a 12-well plate). After all the solvent had evaporated from the 12-well plate, making a thin film, 10 µL of *P. destructans* was inoculated. The plates were incubated for two weeks at 14 °C. Using the same thin film principle, 100 µL pure ACN and $CHCl_3$ was pipetted into each agar well of a 12-well plate (used as a control). After the solvent had evaporated, 10 µL of *P. destructans* was inoculated on top of the thin film. The plates were also incubated at 14 °C for two weeks. These plates served as positive controls.

2.11 Extract Analysis

A mass spectrometer is an instrument that measures the mass-to-charge ratio of ions (Ferrer and Thurman, 2003). It ionizes the sample and separates the ion using either an electric or a magnetic field. A quadrupole mass spectrometer is a type of mass spectrometer that utilises a quadrupole filter system to separate ions based on their mass-to-charge ratio (Ferrer and Thurman, 2003). An alternating electric potential passes through four rods arranged in a square configuration. Ions that pass through the electric field are filtered based on their mass-to-charge ratio. Only ions with a mass-to-charge ratio that fits within the pre-set range (parameter) can pass through the quadrupole and reach the detector. A time-of-flight (TOF) mass spectrometer is a type of mass spectrometer that measures the time taken by the ion to travel a certain distance (Ferrer and Thurman, 2003). The sample is ionized and then the ions are accelerated to a higher velocity using an electric field. The ions are allowed to travel through a drift region and are detected at the end. The time it takes for the ion to reach the detector is measured and used to calculate the mass-to-

charge ratio of the ions. A quadrupole time-of-flight mass spectrometer (QTOF MS) is a hybrid instrument that combines the capabilities of a quadrupole mass spectrometer and a time-of-flight mass spectrometer (Ferrer and Thurman, 2003) (Figure 6). It first filters ions of a pre-set mass-to-charge ratio range using a quadrupole mass filter, and then measures the different times the ions take to travel a certain distance using a time-of-flight detector (Ferrer and Thurman, 2003).

High Resolution mass spectrometry (HRMS) was used to determine the different masses of the compounds present in the metabolic extracts (section 2.8 and the ones used in section 2.10) and the spent media samples (section 2.7) following the protocol outlined in Jennifer Kolwich's Master's in Applied Science thesis (Kolwich, 2021). The fungal extracts were dissolved in HPLC (High-performance Liquid Chromatography) grade methanol (Fisher Scientific International, Hampton, New Hampshire, United States) for the analysis with a concentration of 1mg/mL. Spent Media samples were diluted in HPLC grade water (250 µL of spent media in 750 µL of water). Blank agar plates were used as controls to account for the background noise due to the media. Extracts were analysed using an Agilent 1260 Infinity II HPLC equipped with an Agilent 6530 quadrupole time-of-flight (QTOF) mass spectrometer. Extracts were pipetted into 1.8 mL LC vials. 1.5 µL of each sample was injected through a Poroshell 120EC C18 (3 x 150mm, 2.7 um) column at 30^{o}C. The solvents used for the analysis were labeled A through D. All the solvents used were HPLC grade. Solvent A consisted of water with 0.1% formic acid. Solvent B was 95% acetonitrile in water with 0.1% formic acid. A and B constituted the gradient mobile phase system. Solvents C and D were water and acetonitrile respectively and were used for the cleaning protocol. The sample was eluted through the column at a flow rate of 0.5mL/min following a linear increase from 20% to 35% of solvent B over 5 minutes, an increase from 35% to 75% of solvent B over 20 minutes and an increase from 75% to 100% of solvent B over 2 minutes. Afterwards, solvent B

was administered at 100% for another 10 minutes. The QTOF parameters were set to positive electrospray ionisation (+ESI) mode, Gas Temp: 350 °C, Drying Gas: 12 L/min, Nebuliser 60 psi, VCap: 3000V. The Mass spectrometer parameter were set to 100-1700 m/z (Low mass range), Collision energy: 42 V, Fragmentor: 175 V, Skimmer: 65 V and Oct 1 RF Vpp: 750 V. The data collected was a Total Ion Chromatogram (TIC).

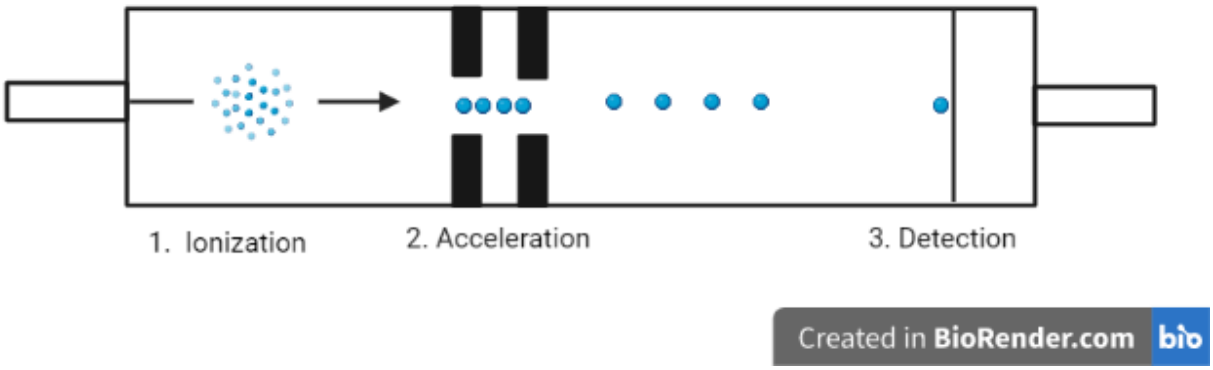

Figure 6: A simplified diagram of a Quadrupole time-of-flight (QTOF) Mass Spectrometery (Cho et al., 2015). It was used to analyse different S5 metabolic extracts.

3. Results

3.1 PCR, DNA sequencing, and Database interrogation using Basic Local Alignment Search Tool (BLAST®)

Regions of the Internal Transcribed Spacer (ITS) region and 16S ribosomal rRNA (16S) were amplified to allow for species identification of S5. The first PCR run shown in figure 7 (lanes 1-4) was dedicated to the amplification of the 16S region, characteristic of bacteria. Lanes 1 and 3 acted as a negative control to verify that the primers and the PCR mixes are not contaminated. Lanes 2 and 4 contained the DNA extracted from an S5 colony and amplified through the 16S forward and reverse primers. No DNA band was observed in lanes 2 and 4 which suggested that

the 16S region was not present in S5. The second set of PCR samples was amplified using the Internal Transcribed Spacer (ITS) region. The bands in lanes 5 and 7 were at about 500 – 600 bp in length (Figure 7). This observation suggested that the ITS region was present in S5. However, the DNA bands from the ITS1/ITS4 primers were smeared implying that the thermocycler run was not optimal. Figure 8 shows the same PCR set with an optimized thermocycler procedure. The bands were clearer, and the product was between 500 and 600 bps in length. These samples were deemed suitable for Sanger Sequencing. To further identify S5, more PCR amplifications were run. In figure 9, lanes 4 and 7 were the DNA samples amplified with ITS1/ITS2. The bands seemed to fall within the range of 200 to 300 bps in length. Lanes 5 and 8 were the DNA samples amplified with the ITS3/ITS4 primer set. The bands were between 300-400 bps in length. Figure 10 was an optimized version of the samples in figure 9. Lanes 2 through 4 showed the same results obtained in figure 9 (lanes 3,4 and 5). However, the bands were clearer, and the samples were fit to be sent for Sanger Sequencing.

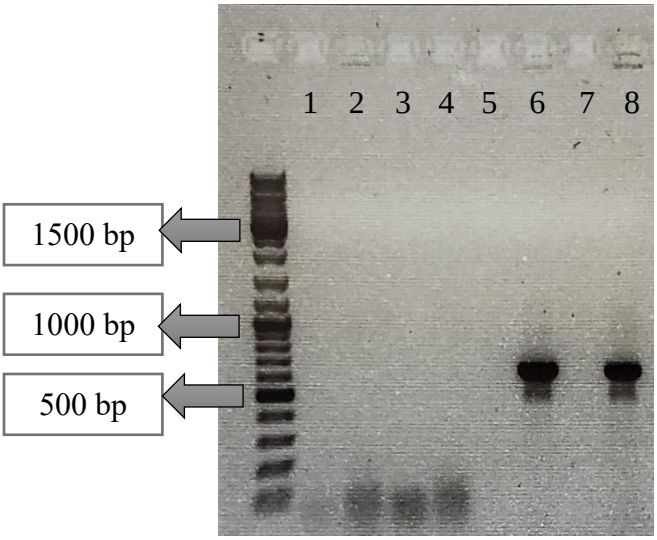

Figure 7: Product of PCR of S5 DNA amplified with ITS1/ITS4 and 16S primers viewed on a 1.5% agarose gel with a 1kb DNA ladder. Lanes 1 and 3 contain negative controls for the 16S forward and reverse primers; lanes 2 and 4 contain 16S forward and reverse primers + DNA; lanes 5 and 7 contain negative controls for the ITS1/ITS4 primers; lanes 6 and 8 contain ITS1/ITS4 primers + DNA.

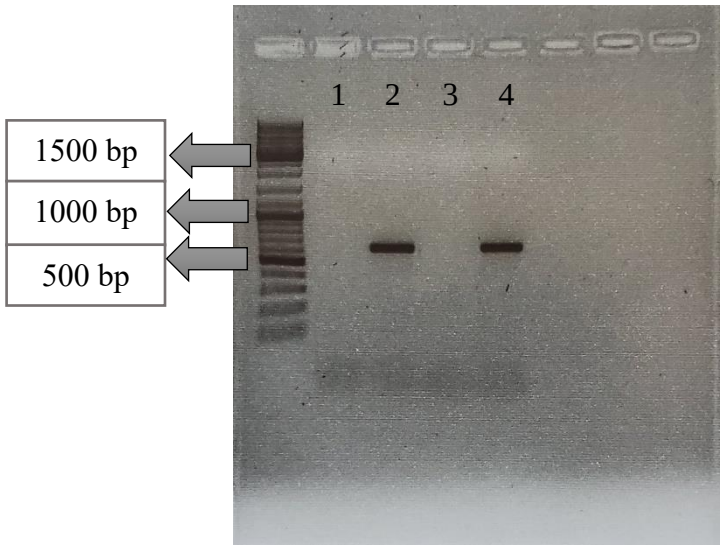

Figure 8: Product of PCR of S5 DNA amplified with ITS1/ITS4 with an optimized procedure viewed on a 1.5% agarose gel with a 1kb DNA ladder. Lanes 1 and 3 are the negative controls for the 1 the ITS1/ITS4 primers; lanes 2 and 4 contain the ITS1/ITS4 primers + DNA.

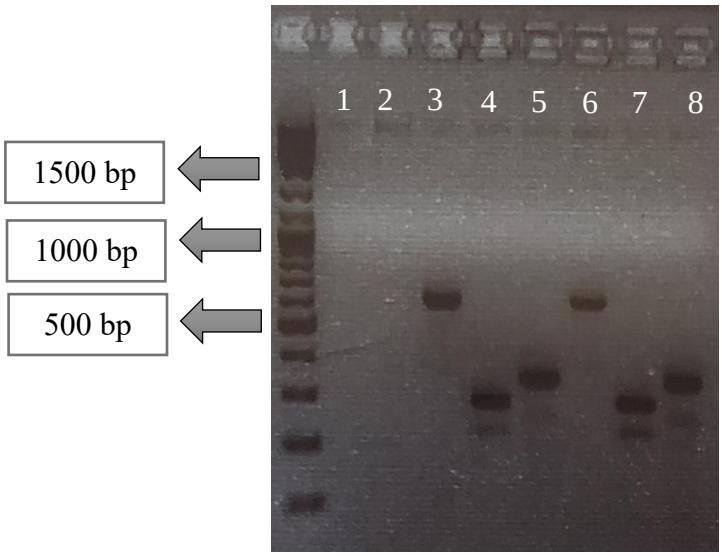

Figure 9: Product of PCR of S5 DNA amplified with ITS region primers viewed on a 1.5% agarose gel with a 1kb DNA ladder. Lane 1 contains the negative control for the ITS1/ITS2 primers; lane 2 contains the negative control for the ITS3/ITS4 primers; lanes 3 and 6 contain ITS1/ITS4 primers + DNA; lanes 4 and 7 contain ITS1/ITS2 primers + DNA; lanes 5 and 8 contain ITS3/ITS4 primers + DNA.

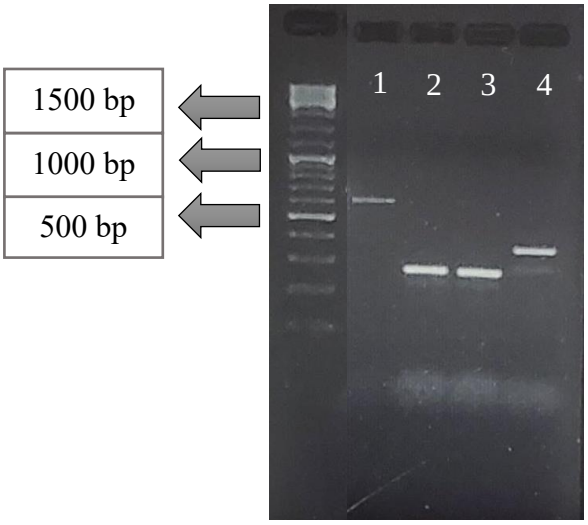

Figure 10: Product of PCR of S5 DNA amplified with ITS region with an optimized procedure viewed on a 1.5% agarose gel with a 1kb DNA ladder. Lane 1 contains a positive control with ITS1/ITS4 + DNA; lanes 2 and 3 contain ITS1/ITS2 primers + DNA; lane 4 contains ITS3/ITS4 primers + DNA.

The chromatograms obtained from Genome Quebec outlined the length and sequence of the PCR samples (Table 1). Figures 5 to 8 showed the first 19 to 20 hits of the samples sequenced using ITS1, ITS2, ITS3 and ITS4 as sequencing primers. For the samples sequenced through ITS1, the very first hit was 100% *Penicillium herquei* while the rest was ranging between 98.57% and 99.42% *Penicillium herquei* (Figure 11). The sample sequenced with ITS2 showed a match of a 100% *Penicillium herquei* (Figure 12). The samples sequenced with ITS3, showed a match of 98.57% to *Penicillium herquei* while the rest ranged between 97.91% to 97.45% (Figure 13). Finally, the samples sequenced with ITS4 showed a match of 100% to *Penicillium herquei* (Figure 14).

Table 1: The primers used for the Sanger Sequencing of S5 samples sequenced using different primers , the length and the sequence of the fragments. Results were obtained through the Genome Quebec portal (Nanuq)

Primer	Length	Sequence of the S5 sample
ITS1	552	tgcggaggatcattactgagtgagggccctctgggtNN Ncctcccacccgtgtttattgtaccttgttgcttcggcaggcccgcctcacggccgccgg ggggcttctcgcccccgggcccgcgcctgccggagacacctttgaacgctgtctgaagtt tgcagtctgagcgattagctaaattagttaaaactttcaacaacggatctcttggttccg gcatcgatgaagaacgcagcgaaatgcgataattaatgtgaattgcagaattcagtgaat catcgagtctttgaacgcacattgcgccccctggtattccgggggggcatgcctgtccgag cgtcattgctgccctcaagcccggcttgtgtgttgggcctcgtcccccttccgggggacg ggcccgaaaggcagcggcggcaccgtgtccggtcctcgagcgtatggggctttgtcaccc gctctgtaggcccggccggcgccttagccgacgacacaacttttttttcaggttgacctc ggatcaggtagggatacccgctgaacttaagcatatcNNNNNNNNNgagga
ITS2	187	tNNNNNNNtcgctcagactgcaaacttcagaca gcgttcaaaggtgtctccggcaggcgcgggcccgggggcgagaagccc cccggcggccgt gaggcgggcctgccgaagcaacaaggtacaataaacacgggtgggaggtt ggacccagagggccctcactcagtaatgatccttccgcaggttcacctacgga
ITS3	268	tcNNtNaNNNcgagtctttgaacNNNattgcgcccccctg gtattccgggggggcatgcctgtccgagcgtcattgctgccctcaagcccggcttgtgtgt tgggcctcgtcccccttccgggggacgggcccgaaaggcagcggcggcaccgtgtccggt cctcgagcgtatggggctttgtcacccgctctgtaggcccggccggcgccttagccgacg acacaacttttttttcaggttgacctcggatcaggtagggatacccgctgaacttaagca tatcaataagcggagg
ITS4	545	acctgaaaaaagttgtgtcgtcggctaaggcgccgg ccgggcctacagagcgggtgacaaagccccatacgctcgaggaccggacacggtgccgcc gctgcctttcgggcccgtcccccggaaggggggacgaggcccaacacacaagccgggcttg agggcagcaatgacgctcggacaggcatgcccccccggaataccaggggggcgcaatgtgcg ttcaaagactcgatgattcactgaattctgcaattcacattaattatcgcatttcgctgc gttcttcatcgatgccggaaccaagagatccgttgttgaaagttttaactaatttagcta atcgctcagactgcaaacttcagacagcgttcaaaggtgtctccggcaggcgcgggcccg ggggcgagaagccccccggcggccgtgaggcgggcctgccgaagcaacaaggtacaataa acacgggtgggaggttggacccagagggccctcactcagtaatgatccttccgcaggttc acctacggaaaccttgttacgacttttacttcctctaNNNgaccaag

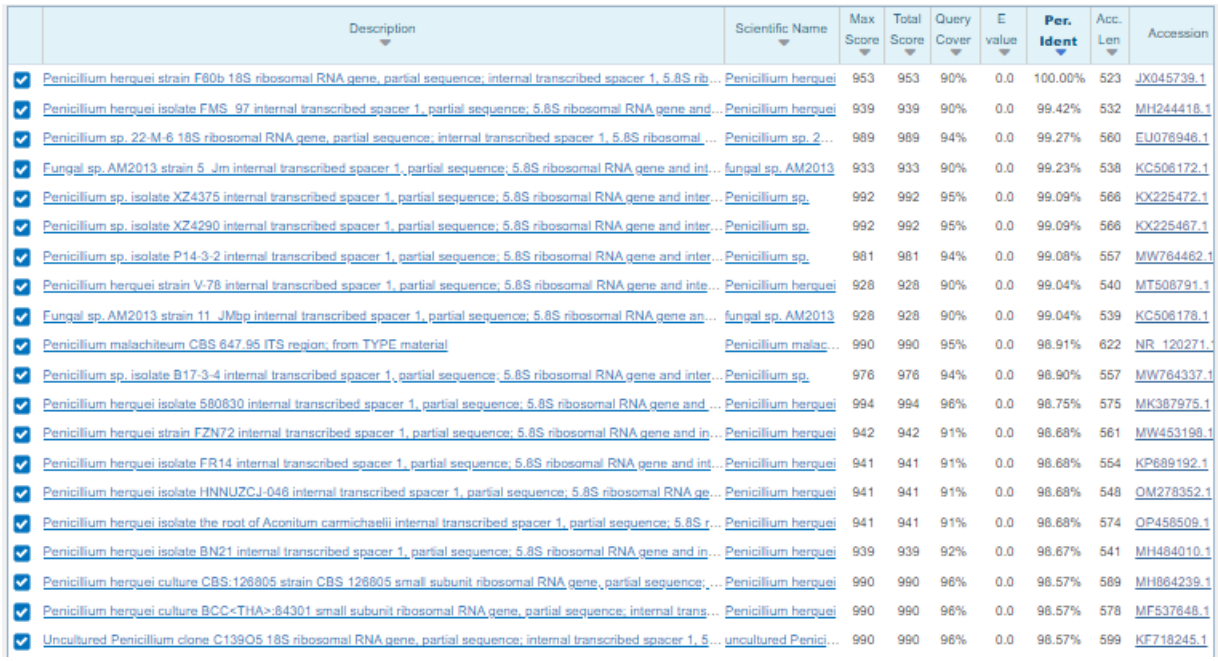

Description	Scientific Name	Max Score	Total Score	Query Cover	E value	Per. Ident	Acc. Len	Accession
Penicillium herquei strain F60b 18S ribosomal RNA gene, partial sequence; internal transcribed spacer 1, 5.8S rib...	Penicillium herquei	953	953	90%	0.0	100.00%	523	JX045739.1
Penicillium herquei isolate FMS_97 internal transcribed spacer 1, partial sequence; 5.8S ribosomal RNA gene and...	Penicillium herquei	939	939	90%	0.0	99.42%	532	MH244418.1
Penicillium sp. 22-M-6 18S ribosomal RNA gene, partial sequence; internal transcribed spacer 1, 5.8S ribosomal ...	Penicillium sp. 2...	989	989	94%	0.0	99.27%	560	EU078946.1
Fungal sp. AM2013 strain 5_Jm internal transcribed spacer 1, partial sequence; 5.8S ribosomal RNA gene and int...	fungal sp. AM2013	933	933	90%	0.0	99.23%	538	KC506172.1
Penicillium sp. isolate XZ4375 internal transcribed spacer 1, partial sequence; 5.8S ribosomal RNA gene and inter...	Penicillium sp.	992	992	95%	0.0	99.09%	566	KX225472.1
Penicillium sp. isolate XZ4290 internal transcribed spacer 1, partial sequence; 5.8S ribosomal RNA gene and inter...	Penicillium sp.	992	992	95%	0.0	99.09%	566	KX225467.1
Penicillium sp. isolate P14-3-2 internal transcribed spacer 1, partial sequence; 5.8S ribosomal RNA gene and inter...	Penicillium sp.	981	981	94%	0.0	99.08%	557	MW764462.1
Penicillium herquei strain V-78 internal transcribed spacer 1, partial sequence; 5.8S ribosomal RNA gene and inte...	Penicillium herquei	928	928	90%	0.0	99.04%	540	MT508791.1
Fungal sp. AM2013 strain 11_JMbp internal transcribed spacer 1, partial sequence; 5.8S ribosomal RNA gene an...	fungal sp. AM2013	928	928	90%	0.0	99.04%	539	KC506178.1
Penicillium malachiteum CBS 647.95 ITS region; from TYPE material	Penicillium malac...	990	990	95%	0.0	98.91%	622	NR_120271.1
Penicillium sp. isolate B17-3-4 internal transcribed spacer 1, partial sequence; 5.8S ribosomal RNA gene and inter...	Penicillium sp.	976	976	94%	0.0	98.90%	557	MW764337.1
Penicillium herquei isolate 580630 internal transcribed spacer 1, partial sequence; 5.8S ribosomal RNA gene and ...	Penicillium herquei	994	994	96%	0.0	98.75%	575	MK387975.1
Penicillium herquei strain FZN72 internal transcribed spacer 1, partial sequence; 5.8S ribosomal RNA gene and in...	Penicillium herquei	942	942	91%	0.0	98.68%	561	MW453198.1
Penicillium herquei isolate FR14 internal transcribed spacer 1, partial sequence; 5.8S ribosomal RNA gene and int...	Penicillium herquei	941	941	91%	0.0	98.68%	554	KP689192.1
Penicillium herquei isolate HNNUZCJ-046 internal transcribed spacer 1, partial sequence; 5.8S ribosomal RNA ge...	Penicillium herquei	941	941	91%	0.0	98.68%	548	OM278352.1
Penicillium herquei isolate the root of Aconitum carmichaelii internal transcribed spacer 1, partial sequence; 5.8S r...	Penicillium herquei	941	941	91%	0.0	98.68%	574	OP458509.1
Penicillium herquei isolate BN21 internal transcribed spacer 1, partial sequence; 5.8S ribosomal RNA gene and in...	Penicillium herquei	939	939	92%	0.0	98.67%	541	MH484010.1
Penicillium herquei culture CBS:126805 strain CBS 126805 small subunit ribosomal RNA gene, partial sequence;...	Penicillium herquei	990	990	96%	0.0	98.57%	589	MH864239.1
Penicillium herquei culture BCC<THA>:84301 small subunit ribosomal RNA gene, partial sequence; internal trans...	Penicillium herquei	990	990	96%	0.0	98.57%	578	MF537648.1
Uncultured Penicillium clone C139O5 18S ribosomal RNA gene, partial sequence; internal transcribed spacer 1, 5...	uncultured Penici...	990	990	96%	0.0	98.57%	599	KF718245.1

Figure 11: The results of a BLAST® (Basic Local Alignment Search Tool) search of the segment from S5 amplified by the ITS1 primer. The sequence was outlined in Table 1 and was obtained after Sanger Sequencing from Genome Quebec.

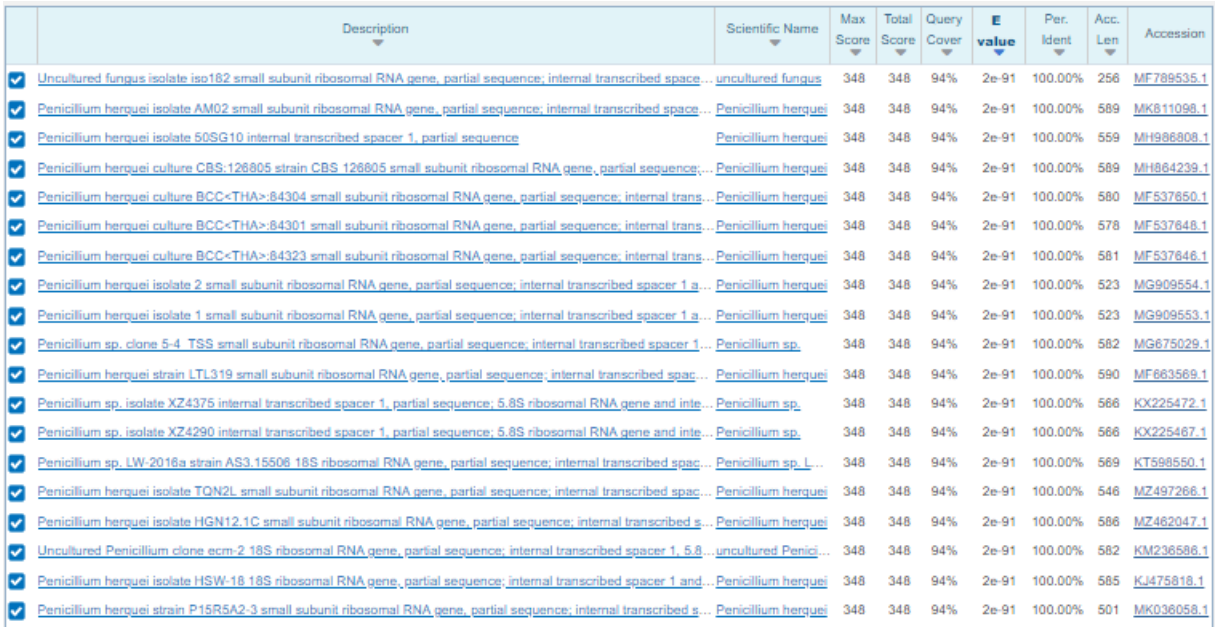

Description	Scientific Name	Max Score	Total Score	Query Cover	E value	Per. Ident	Acc. Len	Accession
Uncultured fungus isolate iso162 small subunit ribosomal RNA gene, partial sequence; internal transcribed space...	uncultured fungus	348	348	94%	2e-91	100.00%	256	MF789535.1
Penicillium herquei isolate AM02 small subunit ribosomal RNA gene, partial sequence; internal transcribed space...	Penicillium herquei	348	348	94%	2e-91	100.00%	589	MK811098.1
Penicillium herquei isolate 50SG10 internal transcribed spacer 1, partial sequence	Penicillium herquei	348	348	94%	2e-91	100.00%	559	MH986808.1
Penicillium herquei culture CBS:126805 strain CBS 126805 small subunit ribosomal RNA gene, partial sequence;...	Penicillium herquei	348	348	94%	2e-91	100.00%	589	MH864239.1
Penicillium herquei culture BCC<THA>:84304 small subunit ribosomal RNA gene, partial sequence; internal trans...	Penicillium herquei	348	348	94%	2e-91	100.00%	580	MF537650.1
Penicillium herquei culture BCC<THA>:84301 small subunit ribosomal RNA gene, partial sequence; internal trans...	Penicillium herquei	348	348	94%	2e-91	100.00%	578	MF537648.1
Penicillium herquei culture BCC<THA>:84323 small subunit ribosomal RNA gene, partial sequence; internal trans...	Penicillium herquei	348	348	94%	2e-91	100.00%	581	MF537646.1
Penicillium herquei isolate 2 small subunit ribosomal RNA gene, partial sequence; internal transcribed spacer 1 a...	Penicillium herquei	348	348	94%	2e-91	100.00%	523	MG909554.1
Penicillium herquei isolate 1 small subunit ribosomal RNA gene, partial sequence; internal transcribed spacer 1 a...	Penicillium herquei	348	348	94%	2e-91	100.00%	523	MG909553.1
Penicillium sp. clone 5-4_TSS small subunit ribosomal RNA gene, partial sequence; internal transcribed spacer 1...	Penicillium sp.	348	348	94%	2e-91	100.00%	582	MG675029.1
Penicillium herquei strain LTL319 small subunit ribosomal RNA gene, partial sequence; internal transcribed spac...	Penicillium herquei	348	348	94%	2e-91	100.00%	590	MF663569.1
Penicillium sp. isolate XZ4375 internal transcribed spacer 1, partial sequence; 5.8S ribosomal RNA gene and inte...	Penicillium sp.	348	348	94%	2e-91	100.00%	566	KX225472.1
Penicillium sp. isolate XZ4290 internal transcribed spacer 1, partial sequence; 5.8S ribosomal RNA gene and inte...	Penicillium sp.	348	348	94%	2e-91	100.00%	566	KX225467.1
Penicillium sp. LW-2016a strain AS3.15506 18S ribosomal RNA gene, partial sequence; internal transcribed spac...	Penicillium sp. L...	348	348	94%	2e-91	100.00%	569	KT598550.1
Penicillium herquei isolate TQN2L small subunit ribosomal RNA gene, partial sequence; internal transcribed spac...	Penicillium herquei	348	348	94%	2e-91	100.00%	546	MZ497266.1
Penicillium herquei isolate HGN12.1C small subunit ribosomal RNA gene, partial sequence; internal transcribed s...	Penicillium herquei	348	348	94%	2e-91	100.00%	586	MZ462047.1
Uncultured Penicillium clone ecm-2 18S ribosomal RNA gene, partial sequence; internal transcribed spacer 1, 5.8...	uncultured Penici...	348	348	94%	2e-91	100.00%	582	KM236586.1
Penicillium herquei isolate HSW-18 18S ribosomal RNA gene, partial sequence; internal transcribed spacer 1 and...	Penicillium herquei	348	348	94%	2e-91	100.00%	585	KJ475818.1
Penicillium herquei strain P15R5A2-3 small subunit ribosomal RNA gene, partial sequence; internal transcribed s...	Penicillium herquei	348	348	94%	2e-91	100.00%	501	MK036058.1

Figure 12: The results of a BLAST® (Basic Local Alignment Search Tool) search of the segment from S5 amplified by the ITS2 primer. The sequence was outlined in Table 1 and was obtained after Sanger Sequencing from Genome Quebec.

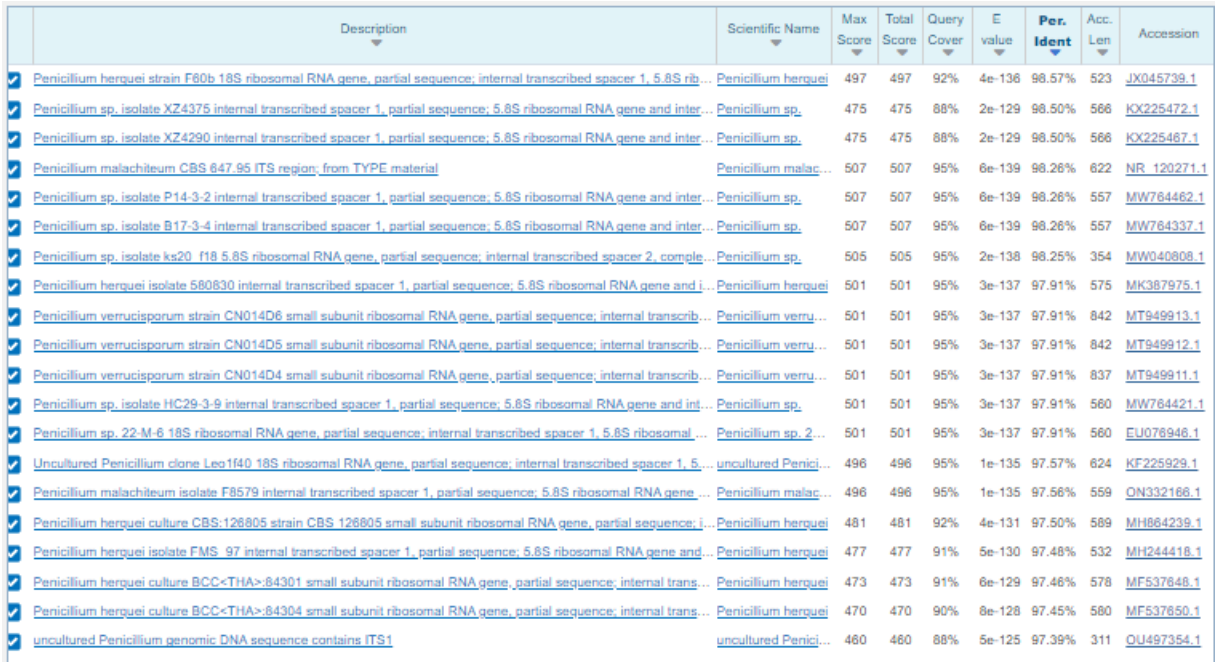

Description	Scientific Name	Max Score	Total Score	Query Cover	E value	Per. Ident	Acc. Len	Accession
Penicillium herquei strain F60b 18S ribosomal RNA gene, partial sequence; internal transcribed spacer 1, 5.8S rib...	Penicillium herquei	497	497	92%	4e-136	98.57%	523	JX045739.1
Penicillium sp. isolate XZ4375 internal transcribed spacer 1, partial sequence; 5.8S ribosomal RNA gene and inter...	Penicillium sp.	475	475	88%	2e-129	98.50%	566	KX225472.1
Penicillium sp. isolate XZ4290 internal transcribed spacer 1, partial sequence; 5.8S ribosomal RNA gene and inter...	Penicillium sp.	475	475	88%	2e-129	98.50%	566	KX225467.1
Penicillium malachiteum CBS 647.95 ITS region; from TYPE material	Penicillium malac...	507	507	95%	6e-139	98.26%	622	NR_120271.1
Penicillium sp. isolate P14-3-2 internal transcribed spacer 1, partial sequence; 5.8S ribosomal RNA gene and inter...	Penicillium sp.	507	507	95%	6e-139	98.26%	557	MW764462.1
Penicillium sp. isolate B17-3-4 internal transcribed spacer 1, partial sequence; 5.8S ribosomal RNA gene and inter...	Penicillium sp.	507	507	95%	6e-139	98.26%	557	MW764337.1
Penicillium sp. isolate ks20_f18 5.8S ribosomal RNA gene, partial sequence; internal transcribed spacer 2, comple...	Penicillium sp.	505	505	95%	2e-138	98.25%	354	MW040808.1
Penicillium herquei isolate 580830 internal transcribed spacer 1, partial sequence; 5.8S ribosomal RNA gene and i...	Penicillium herquei	501	501	95%	3e-137	97.91%	575	MK387975.1
Penicillium verrucisporum strain CN014D6 small subunit ribosomal RNA gene, partial sequence; internal transcrib...	Penicillium verru...	501	501	95%	3e-137	97.91%	842	MT949913.1
Penicillium verrucisporum strain CN014D5 small subunit ribosomal RNA gene, partial sequence; internal transcrib...	Penicillium verru...	501	501	95%	3e-137	97.91%	842	MT949912.1
Penicillium verrucisporum strain CN014D4 small subunit ribosomal RNA gene, partial sequence; internal transcrib...	Penicillium verru...	501	501	95%	3e-137	97.91%	837	MT949911.1
Penicillium sp. isolate HC29-3-9 internal transcribed spacer 1, partial sequence; 5.8S ribosomal RNA gene and int...	Penicillium sp.	501	501	95%	3e-137	97.91%	560	MW764421.1
Penicillium sp. 22-M-6 18S ribosomal RNA gene, partial sequence; internal transcribed spacer 1, 5.8S ribosomal ...	Penicillium sp. 2...	501	501	95%	3e-137	97.91%	560	EU076946.1
Uncultured Penicillium clone Leo1f40 18S ribosomal RNA gene, partial sequence; internal transcribed spacer 1, 5....	uncultured Penici...	496	496	95%	1e-135	97.57%	624	KF225929.1
Penicillium malachiteum isolate F8579 internal transcribed spacer 1, partial sequence; 5.8S ribosomal RNA gene ...	Penicillium malac...	496	496	95%	1e-135	97.56%	559	ON332166.1
Penicillium herquei culture CBS:126805 strain CBS 126805 small subunit ribosomal RNA gene, partial sequence; i...	Penicillium herquei	481	481	92%	4e-131	97.50%	589	MH864239.1
Penicillium herquei isolate FMS_97 internal transcribed spacer 1, partial sequence; 5.8S ribosomal RNA gene and...	Penicillium herquei	477	477	91%	5e-130	97.48%	532	MH244418.1
Penicillium herquei culture BCC<THA>:84301 small subunit ribosomal RNA gene, partial sequence; internal trans...	Penicillium herquei	473	473	91%	6e-129	97.46%	578	MF537648.1
Penicillium herquei culture BCC<THA>:84304 small subunit ribosomal RNA gene, partial sequence; internal trans...	Penicillium herquei	470	470	90%	8e-128	97.45%	580	MF537650.1
uncultured Penicillium genomic DNA sequence contains ITS1	uncultured Penici...	460	460	88%	5e-125	97.39%	311	OU497354.1

Figure 13: The results of a BLAST® (Basic Local Alignment Search Tool) search of the segment from S5 amplified by the ITS3 primer. The sequence was outlined in Table 1 and was obtained after Sanger Sequencing from Genome Quebec.

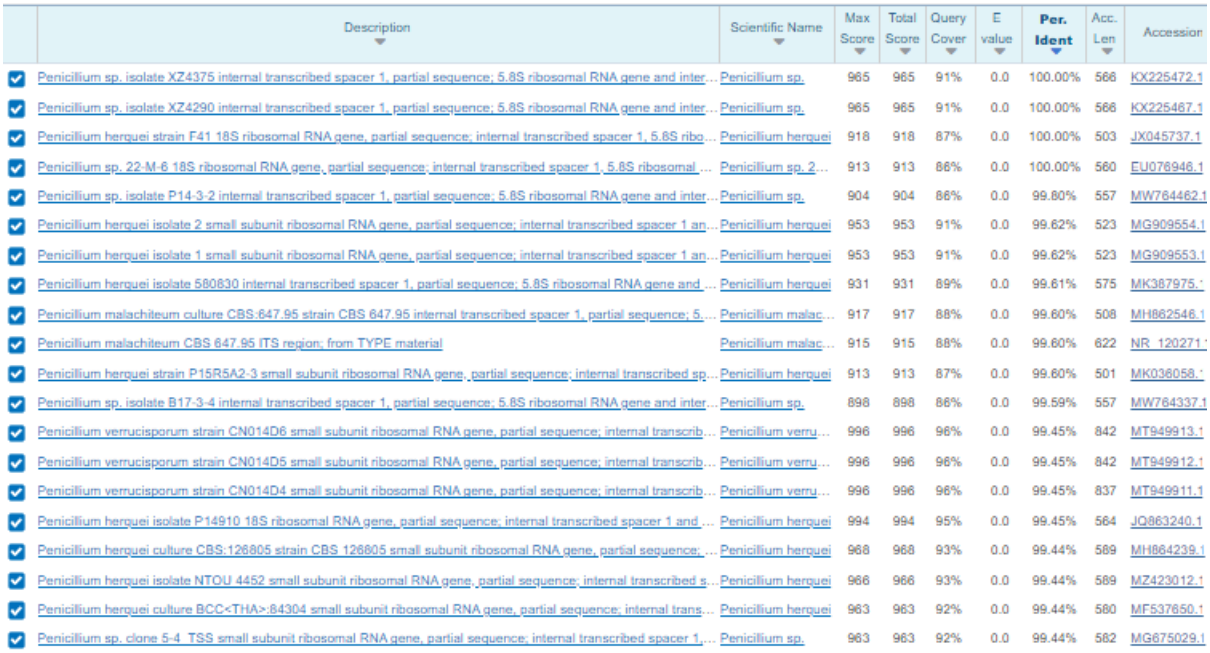

Description	Scientific Name	Max Score	Total Score	Query Cover	E value	Per. Ident	Acc. Len	Accession
Penicillium sp. isolate XZ4375 internal transcribed spacer 1, partial sequence; 5.8S ribosomal RNA gene and inter...	Penicillium sp.	965	965	91%	0.0	100.00%	566	KX225472.1
Penicillium sp. isolate XZ4290 internal transcribed spacer 1, partial sequence; 5.8S ribosomal RNA gene and inter...	Penicillium sp.	965	965	91%	0.0	100.00%	566	KX225467.1
Penicillium herquei strain F41 18S ribosomal RNA gene, partial sequence; internal transcribed spacer 1, 5.8S ribo...	Penicillium herquei	918	918	87%	0.0	100.00%	503	JX045737.1
Penicillium sp. 22-M-6 18S ribosomal RNA gene, partial sequence; internal transcribed spacer 1, 5.8S ribosomal ...	Penicillium sp. 2...	913	913	86%	0.0	100.00%	560	EU076946.1
Penicillium sp. isolate P14-3-2 internal transcribed spacer 1, partial sequence; 5.8S ribosomal RNA gene and inter...	Penicillium sp.	904	904	86%	0.0	99.80%	557	MW764462.1
Penicillium herquei isolate 2 small subunit ribosomal RNA gene, partial sequence; internal transcribed spacer 1 an...	Penicillium herquei	953	953	91%	0.0	99.62%	523	MG909554.1
Penicillium herquei isolate 1 small subunit ribosomal RNA gene, partial sequence; internal transcribed spacer 1 an...	Penicillium herquei	953	953	91%	0.0	99.62%	523	MG909553.1
Penicillium herquei isolate 580830 internal transcribed spacer 1, partial sequence; 5.8S ribosomal RNA gene and ...	Penicillium herquei	931	931	89%	0.0	99.61%	575	MK387975.1
Penicillium malachiteum culture CBS:647.95 strain CBS 647.95 internal transcribed spacer 1, partial sequence; 5....	Penicillium malac...	917	917	88%	0.0	99.60%	508	MH862546.1
Penicillium malachiteum CBS 647.95 ITS region; from TYPE material	Penicillium malac...	915	915	88%	0.0	99.60%	622	NR_120271.1
Penicillium herquei strain P15R5A2-3 small subunit ribosomal RNA gene, partial sequence; internal transcribed sp...	Penicillium herquei	913	913	87%	0.0	99.60%	501	MK036058.1
Penicillium sp. isolate B17-3-4 internal transcribed spacer 1, partial sequence; 5.8S ribosomal RNA gene and inter...	Penicillium sp.	898	898	86%	0.0	99.59%	557	MW764337.1
Penicillium verrucisporum strain CN014D6 small subunit ribosomal RNA gene, partial sequence; internal transcrib...	Penicillium verru...	996	996	96%	0.0	99.45%	842	MT949913.1
Penicillium verrucisporum strain CN014D5 small subunit ribosomal RNA gene, partial sequence; internal transcrib...	Penicillium verru...	996	996	96%	0.0	99.45%	842	MT949912.1
Penicillium verrucisporum strain CN014D4 small subunit ribosomal RNA gene, partial sequence; internal transcrib...	Penicillium verru...	996	996	96%	0.0	99.45%	837	MT949911.1
Penicillium herquei isolate P14910 18S ribosomal RNA gene, partial sequence; internal transcribed spacer 1 and ...	Penicillium herquei	994	994	95%	0.0	99.45%	564	JQ863240.1
Penicillium herquei culture CBS:126805 strain CBS 126805 small subunit ribosomal RNA gene, partial sequence; ...	Penicillium herquei	968	968	93%	0.0	99.44%	589	MH864239.1
Penicillium herquei isolate NTOU 4452 small subunit ribosomal RNA gene, partial sequence; internal transcribed s...	Penicillium herquei	966	966	93%	0.0	99.44%	589	MZ423012.1
Penicillium herquei culture BCC<THA>:84304 small subunit ribosomal RNA gene, partial sequence; internal trans...	Penicillium herquei	963	963	92%	0.0	99.44%	580	MF537650.1
Penicillium sp. clone 5-4_TSS small subunit ribosomal RNA gene, partial sequence; internal transcribed spacer 1,...	Penicillium sp.	963	963	92%	0.0	99.44%	582	MG675029.1

Figure 14: The results of a BLAST® (Basic Local Alignment Search Tool) search of the segment from S5 amplified by the ITS4 primer. The sequence was outlined in Table 1 and was obtained after Sanger Sequencing from Genome Quebec.

3.2 Quantification of S5: growth rate and calibration curve

Absorbance and dry mass measurements were recorded for 10 liquid cultures during 10 consecutive days. The goal of this experiment was to create a growth curve and a calibration curve to monitor the growth phases of S5. Figure 15 shows the growth curve of S5 measured over the span of 10 days. This graph enabled the tracking of the growth behaviour of S5. Between day 0 and 1, the growth was at it's minimal. In day 1 to day 4, the growth rate accelerated slightly. This acceleration w as represented by a slightly steeper curve. Between days 4 and 6, the growth rate was at its maximal, which was represents with a steeper curve. Starting from day 6 to day 7, the growth rate decelerated. Finally, between days 8 and 9, the growth rate plateaued. Figure 16 represents the calibration curve obtained by measuring the absorbance and the dry mass of S5 liquid cultures. The graph represents a positive linear correlation between the absorbance and the dry mass.

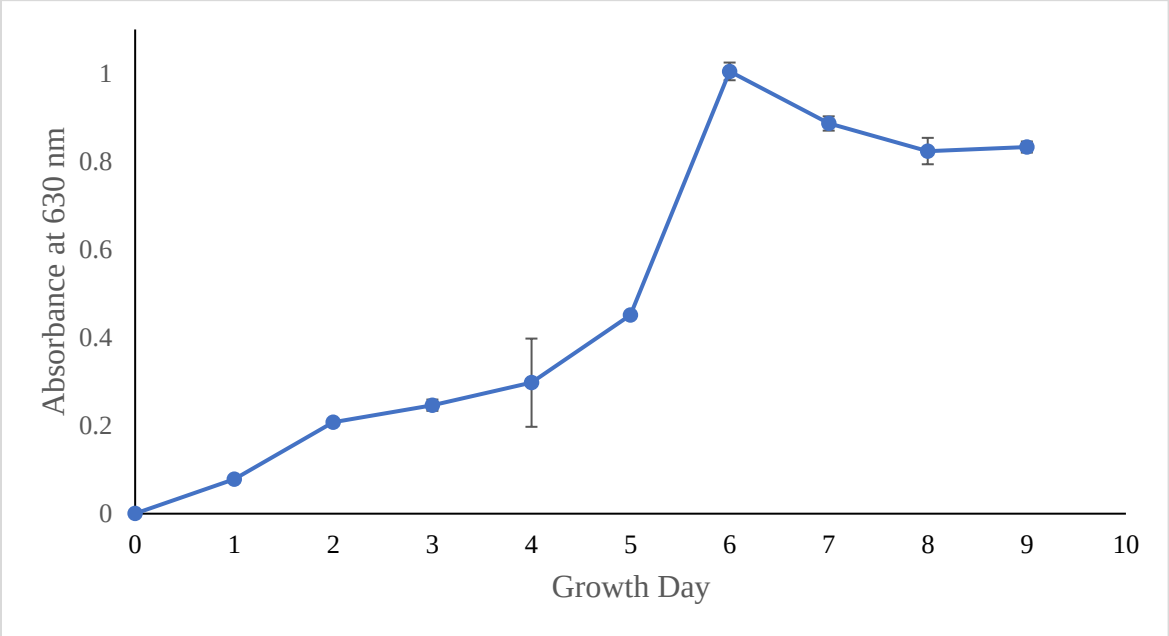

Figure 15: Growth curve to determine the log phase time span for S5. The absorbance was measured at 630 nm from liquid cultures during 10 consecutive days. The measurements were done in triplicates and the cultures were grown in tubes in YMB media. The error bars represent the standard deviation and dots represent mean absorbances (taken from triplicates for each day). The log phase for S5 was between days 4 and 6.

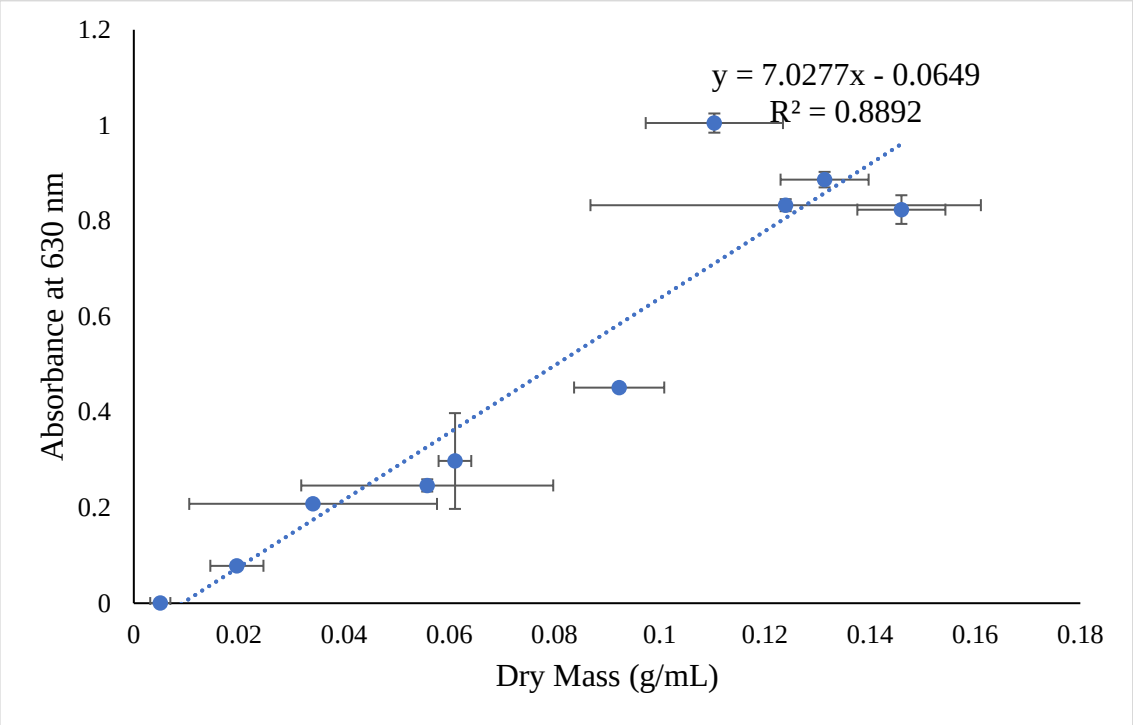

Figure 16: Calibration curve of S5 fungal mass versus absorbance at 630 nm. The dry mass was measured in triplicates. The trend was linear with an equation of y = 7.0277x – 0.0649 and R^2 = 0.8892. The error bars represent the standard deviation and dots represent the mean values.

3.3 Pairwise testing of S5 and *P. destructans*

Pairwise testing enabled the visualization of the inhibition of *P. destructans* by S5. Figure 17 showed the regular growth pattern of S5. It grew as a beige lawn on agar plates. Figure 18 shows the different growth patterns of *P. destructans*. It had different growth patterns depending on the environmental and weather changes (humidity for example). A pairwise test plate is set up by placing two pure cultures on each side of an agar well. The plates were grown for two weeks. Figure 19 is an example of a pairwise testing plate. S5, on the right side, did not grow as much as it did in figure 17. However, there was no *P. destructans* growth on the plate which indicated inhibition.

Figure 17: Growth pattern of S5 on solid Yeast Malt Agar (YMA) media made in 12-well plates that were 4mL deep and 2cm in diameter. 100 µL of S5 was inoculated from a 4-day liquid culture.

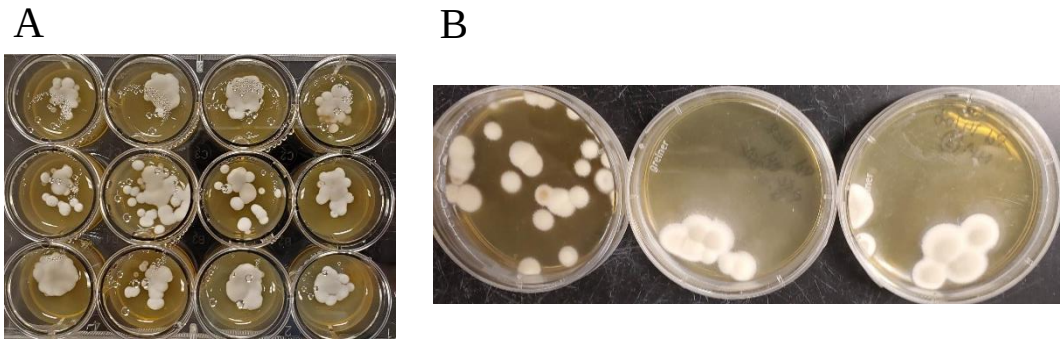

Figure 18: Growth pattern of P. destructans on solid Yeast Malt Agar (YMA) media made in either 12-well plates (A) or 60 mm x 15 mm Petri Dishes (B). The inoculations were made in different days. 100 µL of *P. destructans* was inoculated from a 7-day liquid culture for both the 12-well plates and the Petri Dishes.

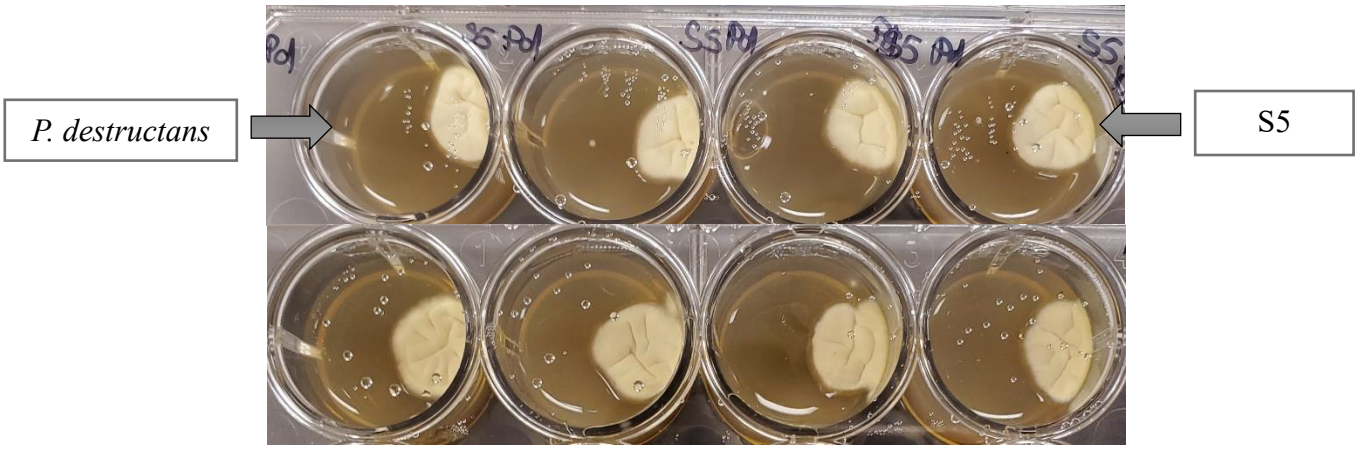

Figure 19: Test for pairwise inhibition between S5 (inoculated on the right side of the plate) and P. destructans (inoculated on the left side of the plate). Both pure cultures were inoculated on each side of a well in a 12-well plate. The media used was Yeast Malt Agar (YMA) media.

3.4 Spent Media testing

Spent Media testing was a way to address the hypothesis that S5 and *P. destructans* were in resource competition meaning that the inhibition occurs because S5 is a better competitor. Varying volumes (either 10 or 20% v/v) of an S5 cell-free extract was used to make Yeast Malt Broth (Figure 20) and Yeast Malt Agar plates (Figure 21). Subsequently, *P. destructans* was grown in the different media. Yeast Malt Broth in Figure 20 A was the only one not containing *P. destructans* growth. Figures 20 B and 21 (A and B) contained minimal to moderate *P. destructans* growth compared to the positive controls of *P. destructans* grown on regular agar-based and liquid media. This test showed that the presence of S5 is not necessary for the inhibition of *P. destructans* (Figure 20A).

A 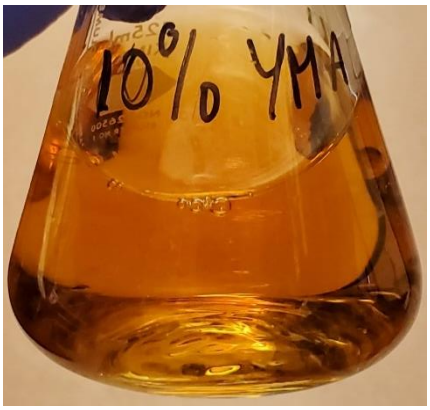  B

Figure 20: Fresh Yeast Malt Broth (YMB) supplemented with 10% v/v S5 cell-free extract (or spent media, A) or 20% v/v S5 cell-free extract (B) and inoculated with 100 µL of P. destructans.

A 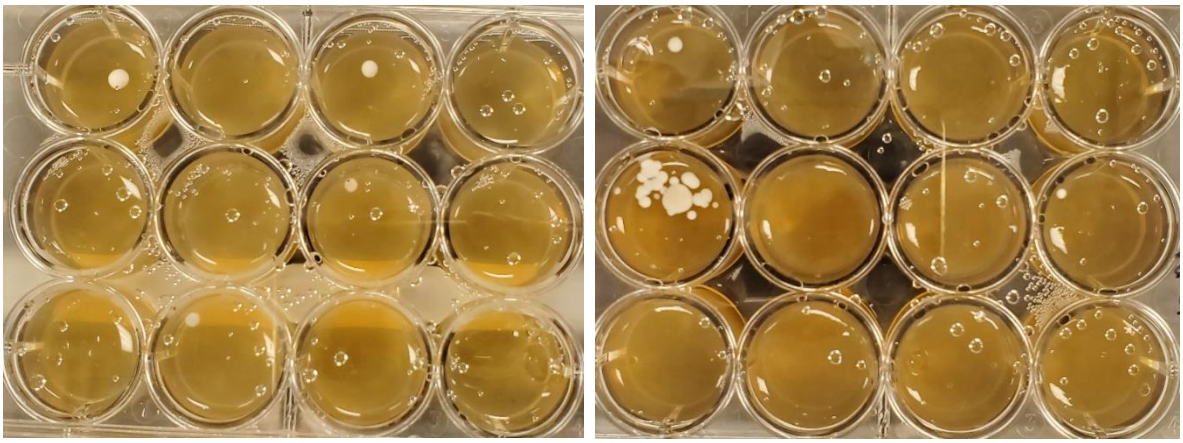 B

Figure 21: Fresh Yeast Malt Agar (YMA) supplemented with 10% v/v S5 cell-free extract (A) or 20% v/v S5 cell-free extract (B) and inoculated with 20 µL of P. destructans.

3.5 Metabolic extraction testing

Metabolic extraction testing was a way to address the hypothesis that S5 might have been secreting a secondary metabolite to inhibit the growth of *P. destructans*. Metabolic extracts from S5 12-well plates and S5 and *P. destructans* 12-well plates were extracted with a 2:1:1 ratio of methanol, chloroform and ethyl acetate. The extracts were used to make agar-based media which was inoculated with *P. destructans*. Figures 22 and 23 show the different metabolic extracts used in different ratios. *P. destructans* did not grow on any of the plates, suggesting that S5 did not have to be present for the inhibition to occur. S5 might be secreting a secondary metabolite that is contributing to the inhibition.

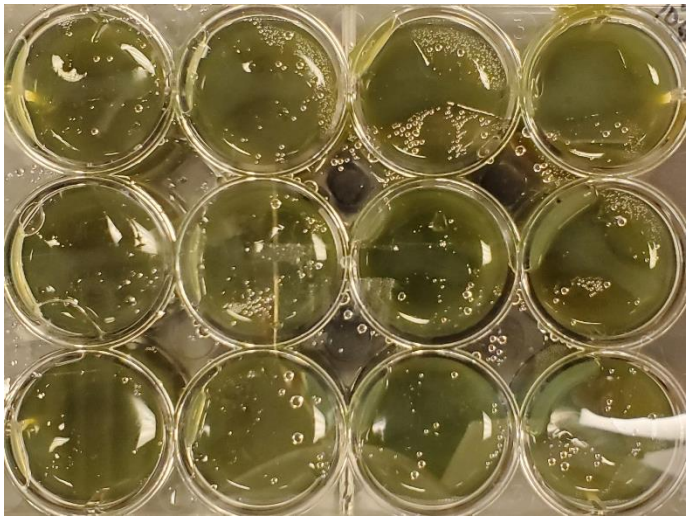

Figure 22: Fresh Yeast Malt Agar (YMA) supplemented with 10% v/v S5 metabolic extract (using 2:1:1 ratio of methanol, chloroform, and ethyl acetate) and inoculated with 20 µL of *P. destructans*. No growth was present on the plate.

A

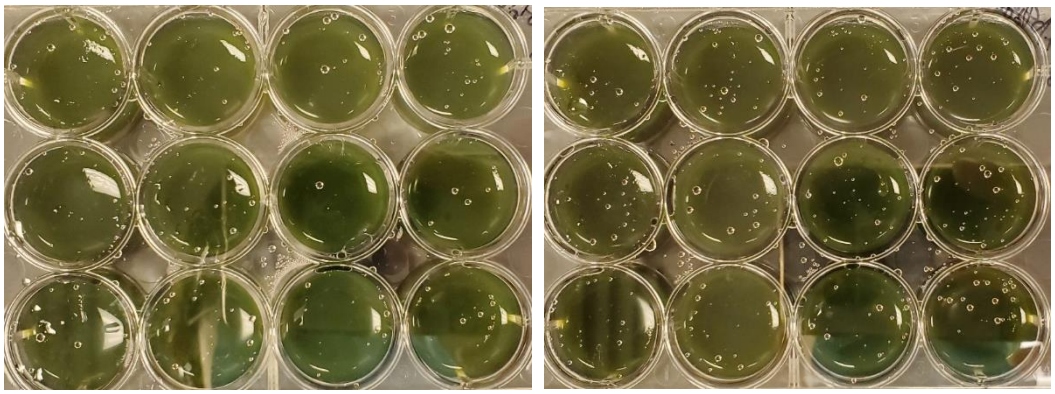

B

Figure 23: Fresh Yeast Malt Agar (YMA) supplemented with 10% v/v (A) and 20% v/v (B) S5 and P. destructans metabolic extract using 2:1:1 ratio of methanol, chloroform, and ethyl acetate, inoculated with 20 µL of *P. destructans*. No growth was present on the plates.

3.6 Thin film testing

Figure 24 shows a thin film test of an S5 extract with chloroform. *P. destructans* did grow on the chloroform thin film indicating (Figure 24 A) that chloroform had no inhibition effect. However, *P. destructans* did not grow when S5 extract from chloroform was applied (Figure 24 B). Figure 25 showed the same pattern. When the acetonitrile thin film was applied on agar, *P.*

destructans grew. When the S5 metabolic extract using acetonitrile was applied, there was no *p. destructans* growth.

A 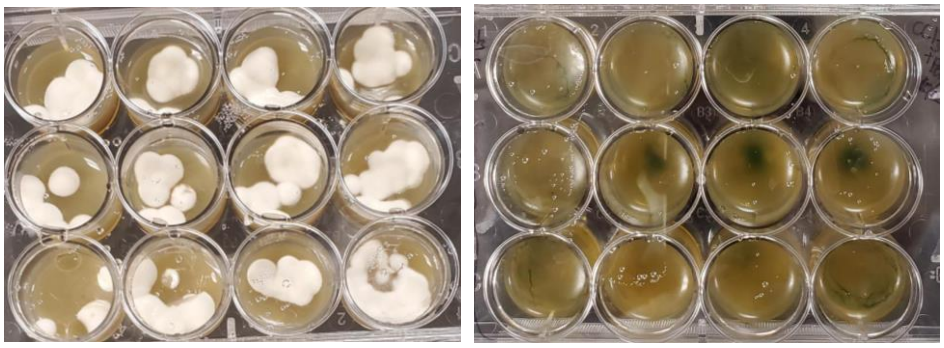 B

Figure 24: Two 12-well plates made of Yeast Malt Agar (YMA) media and inoculated with 10 µL of P. destructans. Plate A) P. destructans grown on YMA with an evaporated thin film of 100 µL of pure chloroform ($CHCl_3$) acting as a control. Plate B) P. destructans grown on evaporated thin film created using 100 µL S5 plates extracted with chloroform ($CHCl_3$)

A 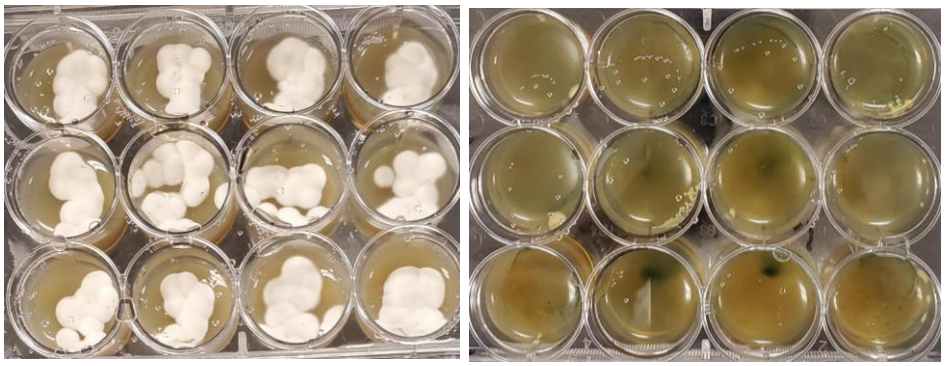 B

Figure 25: Two 12-well plates made of Yeast Malt Agar (YMA) media and inoculated with 10 µL of P. destructans. Plate A) P. destructans grown on YMA with an evaporated thin film of 100 µL of pure acetonitrile (ACN) acting as a control. Plate B) P. destructans grown on evaporated thin film created using 100 µL S5 plates extracted with acetonitrile (ACN)

3.7 Qualitative analysis of the S5 metabolic extracts

Figure 26 shows the chromatograms of the cell-free extracts (or spent media samples) from S5 alone, S5 and *P. destructans* co-cultures, and *P. destructans* alone. No peak patterns were observed during this experiment. All chromatograms didn't have any peaks in common but had several peaks dispersed throughout the chromatogram. In figures 27 and 28, the background chromatograms were subtracted to display the chromatogram without the background signals.

Figure 27 showed the different chromatograms for the different samples. In the first Total Ion Chromatogram (TIC) for the acetonitrile extract, the highest peak had an average retention time of 12.516 minutes (Figure 27). The peak started at 12.388 min and ended at 12.766 min (Sample Chromatograms, Appendix 1). This peak also corresponded to a base peak of 327.0865 m/z (Figure 28) which was 100% abundant (Sample Spectra, Appendix 1). The second TIC is an analysis of the chloroform extract (Figure 27). In this TIC, the highest peak had an average retention time of 12.570 minutes (Figure 27). The peak started at 12.408 min and ended at 12.969 min (Sample Chromatograms, Appendix 2). In the sample spectra outlined in figure 28, the most abundant base peak (Sample Spectra, Appendix 2) was 327.0867 m/z (Figure 28). Another region on interest had an average retention time of 13.151 min (Figure 27). The peak started at 13.063 min and ended at 13.282 min (Sample Chromatograms, Appendix 2). Based on the spectrum in figure 28, the most abundant base peak (100%) has a mass-to-charge ratio of 327.0865 m/z (Sample Spectra, Appendix 2; Figure 28). The third TIC corresponded to the *P. destructans* sample. One peak of interest was the one with an average retention time of 12.353min, which started at 12.219 min and ended at 12.407 min (Sample Chromatograms, Appendix 3). In this area the most abundant base peak was 420.2445 m/z (Sample Spectra, Appendix 3; Figure 28). The fourth TIC in figure 27 analyzed the S5 + *P. destructans* extract. One peak of interest had an average retention time of 12.677 min (Figure 27). The peak started at 12.532 min and ended at 12.825 min (Sample Chromatograms, Appendix 4). Based on the spectrum in figure 28, the most abundant base peak (100%) has a mass-to-charge ratio of 327.0872 m/z (Sample Spectra, Appendix 4; Figure 28). The fifth and last TIC was of the S5 sample. One peak of interest had an average retention time of 12.638 min (Figure 27). The peak started at 12.511 min and ended at 12.799 min (Sample

Chromatograms, Appendix 5). Based on the spectrum in figure 28, the most abundant base peak (90.16%) has a mass-to-charge ratio of 327.0863 m/z (Sample Spectra, Appendix 5; Figure 28).

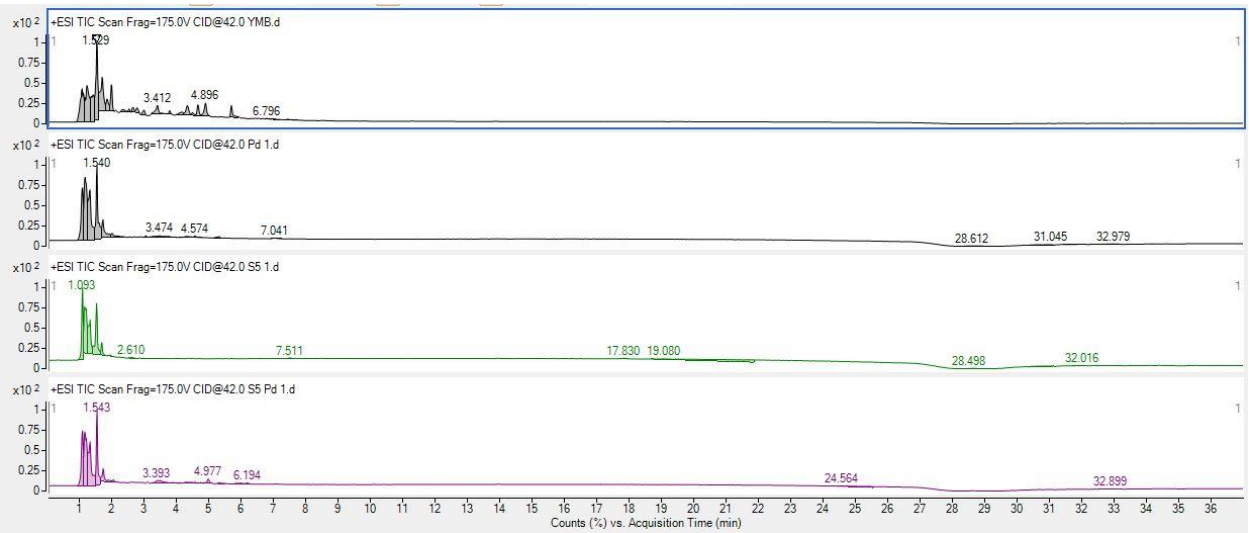

Figure 26: Integrated Total Ion Chromatogram (TIC) measured on a Quadrupole Time-of-flight (QTOF) Mass Spectrometer of different spent media samples: fresh Yeast Malt Broth (YMB) (first black TIC) and 250 µL cell-free extracts or spent media samples from *P. destructans* (second black TIC), S5 (third, green TIC) and the *P. destructans* + S5 diluted with HPLC grade water to a total volume of 1 mL. Each peak was a representation of a compound. The average retention times were indicated on top of each peak. The chromatogram shows the acquisition time (minutes) versus the intensity or the abundance of the peaks.

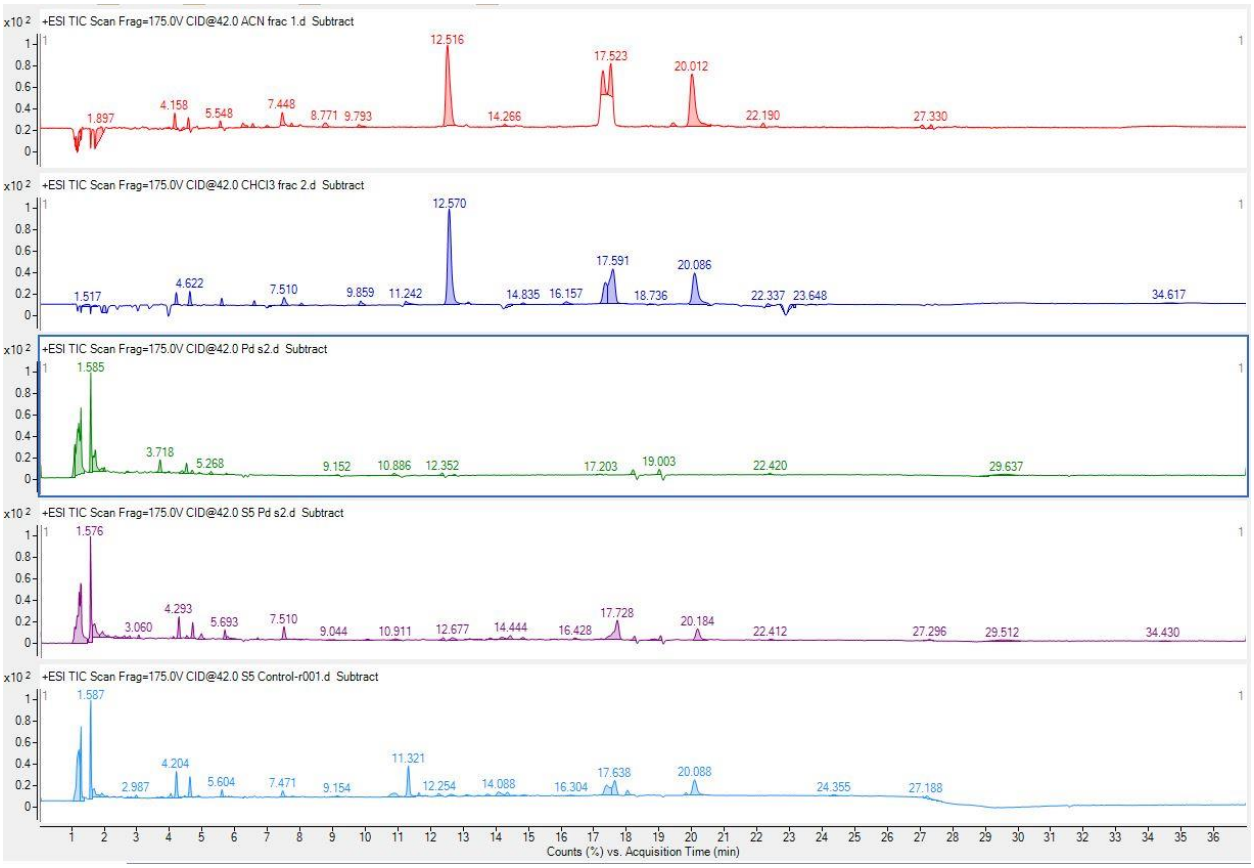

Figure 27: Total Ion Chromatogram (TIC) of different metabolic extracts measured on a Quadrupole Time-of-flight (QTOF) Mass Spectrometer and showing the percent count versus the acquisition time in minutes. First (red) TIC: sample of S5 12-well plates extracted with acetonitrile. The used blank was empty agar wells also extracted with acetonitrile. Second (dark blue) TIC: sample of S5 12-well plates extracted with chloroform. The used blank was empty agar wells also extracted with chloroform. For TICs 3, 4, and 5: S5 12-well plates, *P. destructans* plates and pairwise testing plates of S5 and *P. destructans* were extracted with a 2:1:1 ration of methanol, chloroform, and ethyl acetate. The used blank was empty agar plates extracted using the same method. All the extracts were diluted to 1mg/mL using HPLC grade methanol. Third (green) TIC: *P. destructans* extract. Fourth (purple) TIC: S5 and *P. destructans* extract. Fifth (light blue) TIC: S5 extract. Peaks represented the different compounds. Average retention times were indicated on top of each peak.

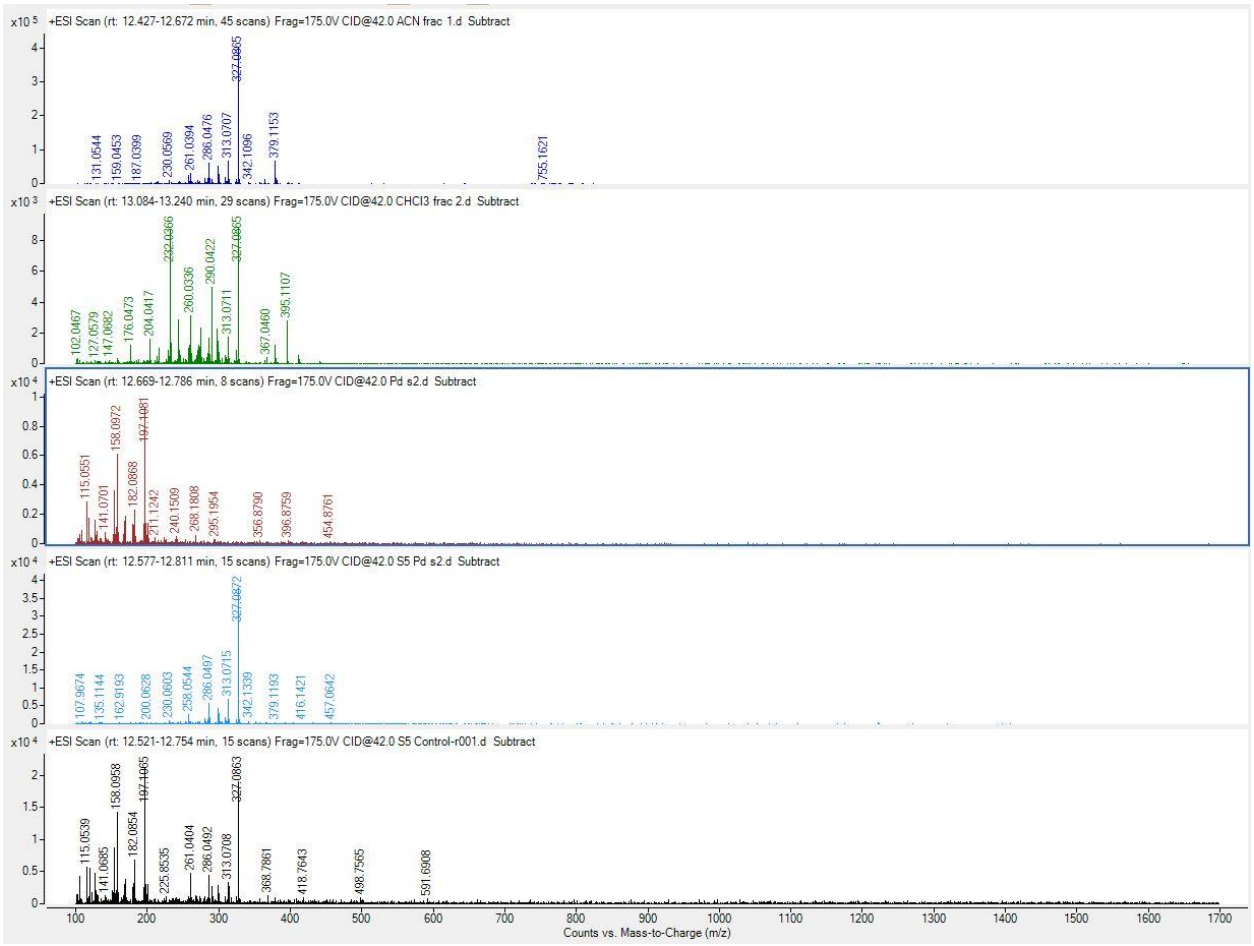

Figure 28: Spectra of different metabolic extracts representing the count versus the mass to charge ratio (m/z). First (dark blue) spectrum: sample of S5 12-well plates extracted with acetonitrile. The used blank was empty agar wells also extracted with acetonitrile. Second (green) spectrum: sample of S5 12-well plates extracted with chloroform. The used blank was empty agar wells also extracted with chloroform. For spectra 3, 4, and 5: S5 12-well plates, *P. destructans* plates and pairwise testing plates of S5 and *P. destructans* were extracted with a 2:1:1 ration of methanol, chloroform, and ethyl acetate. The used blank was empty agar plates extracted using the same method. All the extracts were diluted to 1mg/mL using HPLC grade methanol. Third (brown) spectra: *P. destructans* extract. Fourth (light blue) spectra: S5 and *P. destructans* extract. Fifth (black) spectra: S5 extract. Peaks represented the different compounds. The mass-to-charge ratios were indicated on top of each peak.

4. Discussion

White-nose syndrome is an emerging disease that has affected many bat populations in Eastern USA and Canada (Frank et al., 2016) and is still spreading across the continent (Micalizzi et al., 2017; Warnecke et al., 2012). To fight against this infectious disease, probiotic and microbe-derived treatments might be an efficient solution since they provide a new source of naturally derived compounds (Kolwich, 2019). This thesis aims to find a microbe-derived inhibitory compound from a soil sample isolate extracted from a cave in Gatineau, Quebec. The main results were the following. The isolate was first named S5 and was after identified, using PCR and sequencing, to be *Penicillium herquei* (*P. herquei*). The growth curve and calibration curve of *P. herquei* were also determined by measuring the pellet mass and the absorbance of liquid cultures. Using pairwise testing, it was determined that *P. herquei* inhibits the growth of *P. destructans*. Spent media testing was not conclusive in determining whether the inhibition was due to resource competition or interference competition. However, metabolic extract testing showed that the presence of *P. herquei* was not necessary for the inhibition to occur. Further qualitative analysis of the metabolic extract was done to determine the molecular weight, retention time and mass-to-charge ratio of the inhibitory compound. A certain peak was seen consistently across multiple chromatograms of different S5 metabolic extracts.

4.1 What is S5?

4.1.1 Isolate (S5) Identification: *P. herquei*:

Micalizzi et al. (2017) have isolated a library containing multiple microbes from different cave sites across Canada. S5 was one of the isolates that were sent to our research group from Dr. Myron Smith's lab at Carleton University. The filamentous fungi (including S5) and yeast were

amplified using the Internal Transcribed Spacer region (Micalizzi et al., 2017). The paper also amplified the *beta-tubulin* gene which is a region characteristic of *Penicillium spp.* S5 was determined to be part of the *Penicillium spp.* (Micalizzi et al., 2017). Using DNA extraction, PCR amplification and sequencing, S5 was identified to be *Penicillium herquei*. The NCBI nucleotide BLAST results showed that the first targets, using ITS 1, ITS2 and ITS4 were *P. herquei* (Figures 11, 12 and 14). However, the BLAST results for the segment sequenced with ITS3 had a lower percent identity match (Figure 13). The ITS 3 region might be a conserved region across multiple *Penicillium spp.* which would explain the lower percent identity match. *P. herquei* is part of the subgenus *Aspergilloides*. Specifically, it belongs to the section *Sclerotiora*, which contains about 17 *Penicillium spp.* (Wang et al., 2017). *P. herquei* is the only taxa in *Sclerotiora* that contains conidiophores with two branches (or biverticillate conidiophores). It usually grows on different media at 25 ^{o}C and it has been isolated from different substrates including soil, plant material (like rotten fruits), and insects (Wang et al., 2017). The colony characteristics mentioned in the literature confirm the characteristics observed on the solid media in our lab (Enomoto et al., 1995; Visagie et al., 2013; Wang et al., 2017). On Malt Agar media, *P. herquei* covers 10 to 25 mm after incubation at 25 ^{o}C (Figure 17). The colony is velvety, and the reverse side has a yellow to cream colour between day 4 and day 6 (Figure 17). These observations were consistent throughout the different literature papers (Enomoto et al., 1995; Visagie et al., 2013; Wang et al., 2017). Visagie et al., (2013) also showed that *P. herquei* grew moderately at 30 ^{o}C but did not grow at all at a temperature of 37 ^{o}C which matches and justifies our 25 ^{o}C growth temperature.

4.1.2 Quantification of S5: growth and calibration curve:

This experiment enables the quantification of *P. herquei* growth by measuring the fungal dry mass and the absorbance of liquid cultures over 10 days. The quantification keeps the number

of cells in a liquid culture consistent across all experiments and enables the liquid cultures to be used when the cell growth is at its maximum. Cell growth is defined as a balanced increase in cell content over time (Deacon, 2006). Cell content includes proteins, biomass, cell number, dry weight, nucleic acid content, etc. (Deacon, 2006). The propagation of filamentous fungi occurs in five phases. The lag phase is characterized by little to no growth. The exponential or logarithmic growth phase is when the growth rate is at its maximum which can be visualized by the steep slope on the growth curve. During this phase, cells duplicate rapidly. The growth continues until the available resources can no longer support the growth or when a harmful by-product starts to accumulate. The deceleration phase is when the growth rate slows down (Deacon, 2006). The stationary phase is when growth is offset by cell death which causes the curve to plateau (Kolwich, 2021). The last phase is autolysis or cell death (Deacon, 2006). Ensuring that all liquid cultures are in the exponential phase increases the number of cells in the liquid culture, optimizing the subsequent experiments. Based on Figure 15, the exponential phase of *P. herquei* in YMA liquid cultures is between days 4 and 6.

The calibration curve is made by plotting the measurement of absorbance at 630 nm against the dry mass of the filamentous fungi. The relationship between absorbance and dry mass is linear. The dry mass of a liquid culture increases proportionally as its absorbance increases (Langvad, 1999). It enables the determination of the dry mass based on the absorbance of a certain liquid culture using the linear slope equation. This ensures consistency across experiments. The measurements of the dry mass in liquid cultures were not very successful which was represented by the high standard error bars in Figure 16. To measure the absorbance, the liquid culture had to be homogenized using a tissue grinder (Granade et al., 1985). The measurement of the dry mass was problematic. First, the dry mass was measured on filter paper, dried in a desiccator for 24

hours then weighed on an analytical balance based on the procedure made by Jennifer Kolwich and originally adapted from Langvad's (1999) protocol. The dry mass values were not consistent due to the residual water trapped in the filter paper, as well as static electricity buildup on the filter paper and the balance. While weighing the filter paper, static electricity causes the numbers on the balance to fluctuate almost constantly. The experiment was rerun using a modified protocol (outlined in Methods and Materials, section 2.5). The results were then plotted in the graph. The standard error bars were significantly high for the dry mass variable (Figure 16). This indicates that the values between the triplicates were significantly different. The difference can be explained by a balance error, the presence of leftover YMB or differences in growth in each tube that could influence the measurement. Langvad (1999) proposed a more efficient method to calculate the calibration curve of filamentous fungi that could be considered for future attempts to quantify S5 growth. The paper suggests using a 96-well microtiter plate and a microplate reader to measure the absorbance. The dry weight was measured using glass fibre filters which absorb a minimal amount of water. The glass filters were then oven-dried overnight at 105 ^{o}C (Langvad, 1999). An oven would dry out the water left in the glass filter which contributes to an accurate reading of the dry mass.

4.2 What is the inhibitory effect of *P. herquei* (S5) on *P. destructans*?

Pairwise testing enables the visualization of the inhibition. After growing *P. destructans* for 7 days and *P. herquei* for 4 to 6 days each pure strain was inoculated on each side of the agar and incubated. The two inoculates did not come in contact with each other and were 15 mm apart. Figure 19 represents a pairwise test in a 12-well plate. In the plate, no *P. destructans* growth was observed and *P. herquei* growth was decreased. The absence of *P. destructans* suggests that *P. herquei* acted as an inhibitor for the growth of *P. destructans*. The mode of inhibition between *P.*

destructans and *P. herquei* is the focus of the next section. The decrease in the *P. herquei* colony might be due to the decreased number of available resources on the agar well. The two fungi were being grown on the same plate and both grew on the same media and needed the same compounds for survival (including dextrose and peptone) (Alexopoulos et al., 1996). At the start, *P. destructans* was using the resource to establish a colony, and so did *P. herquei*. However, the inhibition hindered *P. destructans* from growing and resulted in *P. herquei* decreasing its growth (colony size) due to the available resources (Pirt, 1967).

It is important to mention that the inhibition was only observed when *P. herquei* and *P. destructans* were inoculated at the same time. If *P. destructans* was given time to establish its colonies *P. herquei* could not kill the already present *P. destructans* colonies.

4.3 How does *P. herquei* inhibit the growth of *P. destructans*?

The main result is that *P. herquei* inhibits the growth of *P. destructans*. The next two sections discuss the inhibition modes based on the observed results.

4.3.1 Inhibition due to resource competition:

Resource competition happens when there is a simultaneous demand for the same resources by two different populations. The resources might not be sufficient to meet the demands of both populations (Dighton et al., 1992). Exploitation competition happens when one individual depletes all available resources and leaves the second individual with little to no survival sources. In this case, a population or an individual is a better competitor (Dighton et al., 1992). To assess the inhibition mechanism, a cell-free extract of *P. herquei* was used to make both fresh liquid and agar-based media that were subsequently inoculated with *P. destructans*. Figure 20 A shows the absence of *P. destructans* in the liquid media, while figures 20 B and 21 (A and B) show minimal

growth of *P. destructans* compared to the *P. destructans* controls grown in regular liquid and agar-based media. These results suggest that the presence of *P. herquei* is not necessary for the inhibition to occur. Subsequently, the inhibition is not a result of resource competition between the two fungi. Since there was little *P. destructans* growth, and to dive in more on the mode of inhibition, metabolic extract testing was done to address the interference competition hypothesis.

4.3.2 Inhibition due to interference competition

Interference competition happens when one individual influences the access to resources of the other individual through behavioural (like territoriality for animals) or chemical interactions. Interference competition is also known as antagonism (Dighton et al., 1992). *Penicillium* is one of the most common fungi species in the world. This genus is primarily known for secreting different metabolites that are used in various disciplines like food spoilage, biotechnology, plant pathology, and medicine (specifically antimicrobials) (El Hajj Assaf et al., 2020). *Penicillium* is known to secrete different compounds with a wide range of biological activity. The most iconic example is the antibiotic penicillin (El Hajj Assaf et al., 2020). Natural products are usually produced as secondary metabolites through enzymatic pathways (El Hajj Assaf et al., 2020; Luo et al., 2015).

Plates made with extracts from *P. herquei* have inhibited the growth of *P. destructans*. This result suggests that the presence of *P. herquei* is not crucial to the inhibition, which implies that *P. herquei* is secreting an inhibitory compound that affects the growth of *P. destructans*. The qualitative analysis of all the different extracts was done using a QTOF Mass Spectrometer. The *P. herquei* plates were extracted with Acetonitrile (ACN) and chloroform ($CHCl_3$) separately. The two solvents have different polarities. Figures 22 and 23 show that both metabolic extracts inhibited the growth of *P. destructans*. This suggests that the inhibitory compound is present in both the ACN and the $CHCl_3$ extracts. Both the ACN and the $CHCl_3$ extract chromatograms had

one peak in common at approximately 12.5 min retention time (Figure 27). The metabolic extracts of *P. herquei* made using the 2:1:1 ratio mixture (Methods and materials, section 2.8) also had the same peak with approximately the same retention time but with a lower intensity. One specific base peak was consistent along all the spectra of the previously mentioned samples (Figure 28). The peak has a mass-to-charge ratio of a 327.09 m/z which could be informative on the molecular weight of the most stable compound within this sample. Consequently, the inhibitory compound might have an average retention time of approximately 12.5 and a base peak of 327.08 mass-to-charge ratio.

Reviewing the literature, *P. herquei* produces a variety of secondary metabolites that have a wide range of biological activities. About 40 years ago, herquline A was extracted from a strain of *P. herquei*. It was later shown that herquline A prevents platelet aggregation and has multiple antibiotic properties like inhibiting the replication of the influenza virus (Enomoto et al., 1995; Zhu et al., 2019). *P. herquei* also produces herquline B (Omura et al., 1979) and its diastereomer herquline C which seems to have the same biological activities as herquline A (Enomoto et al., 1995). It was shown that *P. herquei* produces two epimer pairs of acetaminophen derivatives called Penicilquei (A, B, C and D) (Wu et al., 2020; Zhou et al., 2019). Peniciliqueis showed broad-spectrum antifungal activity against fungi like *Colletotrichum capsica* and *Bipolaris oryzae* (Zhou et al., 2019). Stationary *P. herquei* liquid cultures seemed to produce coloured compounds that turned the media dark red. These compounds were identified to be norherqueinone and herqueinone. The compounds have antimicrobial activity (Narasimhachari and Vining, 1963). As mentioned, *P. herquei* produces a wide range of antifungal and antimicrobial compounds. However, based on the mass spectrometer data in the papers, none of these compounds have a matching mass-to-charge ratio to the one found in this paper. The closest mass-to-charge ratio was

328.1165 m/z which corresponds to (-) and (+) Scleroamide (Yu et al., 2022) suggesting that our compound of interest might be Scleroamide, a compound that has a molecular formula of $C_{18}H_{18}NO_5$. Further analysis must be done to determine the identity of the inhibitory compound. Since this compound is a secondary metabolite, it would exist in low quantities compared to the primary metabolites (Luo et al., 2015). This would explain why the spent media assay was not very successful: the compound was being produced at low levels. Its concentration decreased even more after mixing the *P. herquei* cell-free extract with fresh YMB media. However, when the 25 mg/mL metabolic extracts were mixed with fresh media, *P. destructans* was inhibited.

5. Conclusion

White-nose Syndrome is an emerging disease in Eastern USA and Canada. It has killed millions of bats from various species and is still dispersing. *P. destructans* is the causative agent of White-nose Syndrome. Chemically synthesized antimicrobials might influence the cave ecosystem. For that reason, microbe-derived treatments can be the next key solution for infections like White-nose Syndrome. The goal of this research project is to find a microbe-derived treatment from a soil sample isolate extracted from a cave in Gatineau, Quebec. The isolate was named S5 but then identified to be *Penicillium herquei*. Using pairwise testing plates, it was shown that *P. herquei* inhibits the growth of *P. destructans*. Two mechanisms of inhibition were considered: inhibition due to resource competition or interference competition. Using cell-free extracts (spent media) from *P. herquei*, it was demonstrated that the presence of *P. herquei* is not important for the inhibition to occur. This result was supported using *P. herquei* metabolic extract testing. Agar-based media was able to inhibit the growth of *P. destructans* suggesting that the physical presence of *P. herquei* does not contribute to the inhibition. This implies that *P. herquei* secretes a secondary inhibitory metabolite to inhibit *P. destructans* growth. All the metabolic extracts were analyzed

using a Quadrupole time-of-flight Mass Spectrometer. All the chromatograms have a peak in common with a retention time of 12.5 minutes. All the spectra had a common base peak with a mass-to-charge ratio m/z of 327.08. The exact molecular formula and configuration of the secondary metabolite were not determined during this research. However, based on the literature review, one candidate might be Scleroamide, a compound usually secreted by *P. herquei* that has a mass-to-charge ratio of 328.1165 and a molecular formula of $C_{18}H_{18}NO_5$.

6. Future Work

Future work involves using one dimension of a 2-Dimensional High Performance Liquid Chromatography with photodiode array detection to separate the peak of interest seen on the chromatogram of the Acetonitrile or the Chloroform metabolic extract. Having a separated sample opens the way to using other techniques to identify the compound like IR (Infrared) spectroscopy and NMR (Nuclear Magnetic Resonance) analysis. After identifying the inhibitory compound, it would be necessary to study the minimal and maximal concentrations required for the inhibition.

7. References

Alexopoulos, C. J., Mims, C. W., & Blackwell, M. (1996). Introductory mycology. *Introductory Mycology., Ed.4*. https://www.cabdirect.org/cabdirect/abstract/19971700582

Blehert, D. S., Hicks, A. C., Behr, M., Meteyer, C. U., Berlowski-Zier, B. M., Buckles, E. L., Coleman, J. T. H., Darling, S. R., Gargas, A., Niver, R., Okoniewski, J. C., Rudd, R. J., & Stone, W. B. (2009). Bat White-Nose Syndrome: An Emerging Fungal Pathogen? *Science*, *323*(5911), 227–227. https://doi.org/10.1126/science.1163874

Carey, H. V., Andrews, M. T., & Martin, S. L. (2003). Mammalian hibernation: cellular and molecular responses to depressed metabolism and low temperature. *Physiological reviews*. https://doi.org/10.1152/physrev.00008.2003

Cheng, T. L., Mayberry, H., McGuire, L. P., Hoyt, J. R., Langwig, K. E., Nguyen, H., Parise, K. L., Foster, J. T., Willis, C. K. R., Kilpatrick, A. M., & Frick, W. F. (2017). Efficacy of a probiotic bacterium to treat bats affected by the disease white-nose syndrome. *Journal of Applied Ecology*, *54*(3), 701–708. https://doi.org/10.1111/1365-2664.12757

Cho, Y.-T., Su, H., Wu, W.-J., Wu, D.-C., Hou, M.-F., Kuo, C.-H., & Shiea, J. (2015). Chapter Six—Biomarker Characterization by MALDI–TOF/MS. In G. S. Makowski (Ed.), *Advances in Clinical Chemistry* (Vol. 69, pp. 209–254). Elsevier. https://doi.org/10.1016/bs.acc.2015.01.001

Cornelison, C. T., Gabriel, K. T., Barlament, C., & Crow, S. A. (2014). Inhibition of *Pseudogymnoascus destructans* Growth from Conidia and Mycelial Extension by Bacterially Produced Volatile Organic Compounds. *Mycopathologia*, *177*(1), 1–10. https://doi.org/10.1007/s11046-013-9716-2

Cornelison, C. T., Keel, M. K., Gabriel, K. T., Barlament, C. K., Tucker, T. A., Pierce, G. E., & Crow, S. A. (2014). A preliminary report on the contact-independent antagonism of *Pseudogymnoascus destructans* by *Rhodococcus rhodochrousstrain* DAP96253. *BMC Microbiology*, *14*(1), 246. https://doi.org/10.1186/s12866-014-0246-y

Cryan, P. M., Meteyer, C. U., Boyles, J. G., & Blehert, D. S. (2010). Wing pathology of white-nose syndrome in bats suggests life-threatening disruption of physiology. *BMC Biology*, *8*(1), 135. https://doi.org/10.1186/1741-7007-8-135

Deacon, J. W. (2006). *Fungal Biology*. 80 – 90. John Wiley & Sons.

Dighton, J., White, J., & Oudemans, P. (1992). The Fungal Community: Its Organization and Role in the Ecosystem Chapter 7 Community Assembly of Phyllosphere Endophytes: A Closer Look at Fungal Life Cycle Dynamics, Competition, and Phytochemistry in the Shaping of the Fungal Community, *Second Edition*, 95. CRC Press.

Drees, K. P., Lorch, J. M., Puechmaille, S. J., Parise, K. L., Wibbelt, G., Hoyt, J. R., Sun, K., Jargalsaikhan, A., Dalannast, M., Palmer, J. M., Lindner, D. L., Marm Kilpatrick, A., Pearson, T., Keim, P. S., Blehert, D. S., & Foster, J. T. (2017). Phylogenetics of a Fungal Invasion: Origins and Widespread Dispersal of White-Nose Syndrome. *MBio*, *8*(6), e01941-17. https://doi.org/10.1128/mBio.01941-17

El Hajj Assaf, C., Zetina-Serrano, C., Tahtah, N., Khoury, A. E., Atoui, A., Oswald, I. P., Puel, O., & Lorber, S. (2020). Regulation of Secondary Metabolism in the Penicillium Genus. *International Journal of Molecular Sciences*, *21*(24), Article 24. https://doi.org/10.3390/ijms21249462

Enomoto, Y., Shiomi, K., Hayashi, M., Masuma, R., Kawakubo, T., Tomosawa, K., Iwai, Y., & Omura, S. (1996a). Herquline B, a New Platelet Aggregation Inhibitor Produced by *Penicillium herquei* Fg-372. *The Journal of Antibiotics*, *49*(1), 50–53. https://doi.org/10.7164/antibiotics.49.50

Enomoto, Y., Shiomi, K., Hayashi, M., Masuma, R., Kawakubo, T., Tomosawa, K., Iwai, Y., & Omura, S. (1996b). Herquline B, a New Platelet Aggregation Inhibitor Produced by Penicillium herquei Fg-372. *The Journal of Antibiotics*, *49*(1), 50–53. https://doi.org/10.7164/antibiotics.49.50

Farina, L. L., & Lankton, J. S. (n.d.). *Chapter 25—Chiroptera | Elsevier Enhanced Reader*. https://doi.org/10.1016/B978-0-12-805306-5.00025-0

Fernando, W. G. D., Ramarathnam, R., Krishnamoorthy, A. S., & Savchuk, S. C. (2005). Identification and use of potential bacterial organic antifungal volatiles in biocontrol. *Soil Biology and Biochemistry*, *37*(5), 955–964. https://doi.org/10.1016/j.soilbio.2004.10.021

Ferrer, I., & Thurman, E. M. (2003). Liquid chromatography/time-of-flight/mass spectrometry (LC/TOF/MS) for the analysis of emerging contaminants. *TrAC Trends in Analytical Chemistry*, *22*(10), 750–756. https://doi.org/10.1016/S0165-9936(03)01013-6

Field, K. A., Johnson, J. S., Lilley, T. M., Reeder, S. M., Rogers, E. J., Behr, M. J., & Reeder, D. M. (2015). The White-Nose Syndrome Transcriptome: Activation of Anti-fungal Host Responses in Wing Tissue of Hibernating Little Brown Myotis. *PLOS Pathogens*, *11*(10), e1005168. https://doi.org/10.1371/journal.ppat.1005168

Frank, C. L., Ingala, M. R., Ravenelle, R. E., Dougherty-Howard, K., Wicks, S. O., Herzog, C., & Rudd, R. J. (2016). The Effects of Cutaneous Fatty Acids on the Growth of

Pseudogymnoascus destructans, the Etiological Agent of White-Nose Syndrome (WNS). *PLOS ONE*, *11*(4), e0153535. https://doi.org/10.1371/journal.pone.0153535

Frick, W. F., Puechmaille, S. J., & Willis, C. K. R. (2016). White-Nose Syndrome in Bats. In C. C. Voigt & T. Kingston (Eds.), *Bats in the Anthropocene: Conservation of Bats in a Changing World* (pp. 245–262). Springer International Publishing. https://doi.org/10.1007/978-3-319-25220-9_9

Fritze, M., Costantini, D., Fickel, J., Wehner, D., Czirják, G. Á., & Voigt, C. C. (2019). Immune response of hibernating European bats to a fungal challenge. *Biology Open*, bio.046078. https://doi.org/10.1242/bio.046078

Gargas, A., Trest, M. T., Christensen, M., Volk, T. J., & Blehert, D. S. (2009). *Geomyces destructans* sp. Nov. Associated with bat white-nose syndrome. *Mycotaxon*, *108*(1), 147–154. https://doi.org/10.5248/108.147

GoTaq, A. (2021). *3. General Considerations*. Promega Corporation. ww.promega.com

Granade, T. C., Hehmann, M. F., & Artis, W. M. (1985). Monitoring of filamentous fungal growth by in situ microspectrophotometry, fragmented mycelium absorbance density, and 14C incorporation: Alternatives to mycelial dry weight. *Applied and Environmental Microbiology*, *49*(1), 101–108. https://doi.org/10.1128/aem.49.1.101-108.1985

Halsall, A. L., Boyles, J. G., & Whitaker, J. O. (2012). Body temperature patterns of big brown bats during winter in a building hibernaculum. *Journal of Mammalogy*, *93*(2), 497–503. https://doi.org/10.1644/11-MAMM-A-262.1

Horrocks, N. P. C., Matson, K. D., & Tieleman, B. I. (2011). Pathogen Pressure Puts Immune Defense into Perspective. *Integrative and Comparative Biology*, *51*(4), 563–576. https://doi.org/10.1093/icb/icr011

Hoyt, J. R., Cheng, T. L., Langwig, K. E., Hee, M. M., Frick, W. F., & Kilpatrick, A. M. (2015). Bacteria Isolated from Bats Inhibit the Growth of Pseudogymnoascus destructans, the Causative Agent of White-Nose Syndrome. *PLOS ONE*, *10*(4), e0121329. https://doi.org/10.1371/journal.pone.0121329

Hoyt, J. R., Langwig, K. E., Sun, K., Parise, K. L., Li, A., Wang, Y., Huang, X., Worledge, L., Miller, H., White, J. P., Kaarakka, H. M., Redell, J. A., Görföl, T., Boldogh, S. A., Fukui, D., Sakuyama, M., Yachimori, S., Sato, A., Dalannast, M., Jargalsaikhan, A., Batbayar, N., Yovel, Y., Amichai, E., Natradze, I., Frick, W. F., Foster, J. T., Feng, J., Kilpatrick, A. M. (2020). Environmental reservoir dynamics predict global infection patterns and population impacts for the fungal disease white-nose syndrome. *Proceedings of the National Academy of Sciences*, *117*(13), 7255–7262. https://doi.org/10.1073/pnas.1914794117

Huffman, B. A., Poltash, M. L., & Hughey, C. A. (2012). Effect of Polar Protic and Polar Aprotic Solvents on Negative-Ion Electrospray Ionization and Chromatographic Separation of Small Acidic Molecules. *Analytical Chemistry*, *84*(22), 9942–9950. https://doi.org/10.1021/ac302397b

Johnson, J. S., Reeder, D. M., McMichael, J. W., Meierhofer, M. B., Stern, D. W. F., Lumadue, S. S., Sigler, L. E., Winters, H. D., Vodzak, M. E., Kurta, A., Kath, J. A., & Field, K. A. (2014). Host, Pathogen, and Environmental Characteristics Predict White-Nose Syndrome Mortality

in Captive Little Brown Myotis (Myotis lucifugus). *PLoS ONE*, *9*(11), e112502. https://doi.org/10.1371/journal.pone.0112502

Kolwich, J. L. (2019). Discovery of anti-fungal compounds from the immunobiome of North American bat species threatened by fungal infection with Pseudogymnoascus destructans. http://library2.smu.ca/xmlui/handle/01/28589

Kolwich, J. L. (2021). An in-depth investigation on the inhibitory activity of a native cave fungus against Pseudogymnoascus destructans.

Langvad, F. (1999). A rapid and efficient method for growth measurement of filamentous fungi. *Journal of Microbiological Methods*, *37*(1), 97–100. https://doi.org/10.1016/S0167-7012(99)00053-6

Leopardi, S., Blake, D., & Puechmaille, S. J. (2015). White-Nose Syndrome fungus introduced from Europe to North America. *Current Biology*, *25*(6), R217–R219. https://doi.org/10.1016/j.cub.2015.01.047

Lilley, T. M., Prokkola, J. M., Johnson, J. S., Rogers, E. J., Gronsky, S., Kurta, A., Reeder, D. M., & Field, K. A. (2017). Immune responses in hibernating little brown myotis (*Myotis lucifugus*) with white-nose syndrome. *Proceedings of the Royal Society B: Biological Sciences*, *284*(1848), 20162232. https://doi.org/10.1098/rspb.2016.2232

Luo, Y., Li, B.-Z., Liu, D., Zhang, L., Chen, Y., Jia, B., Zeng, B.-X., Zhao, H., & Yuan, Y.-J. (2015). Engineered biosynthesis of natural products in heterologous hosts. *Chemical Society Reviews*, *44*(15), 5265–5290. https://doi.org/10.1039/C5CS00025D

Meteyer, C. U., Barber, D., & Mandl, J. N. (2012). Pathology in euthermic bats with white nose syndrome suggests a natural manifestation of immune reconstitution inflammatory syndrome. *Virulence*, *3*(7), 583–588. https://doi.org/10.4161/viru.22330

Micalizzi, E. W., Mack, J. N., White, G. P., Avis, T. J., & Smith, M. L. (2017). Microbial inhibitors of the fungus *Pseudogymnoascus destructans*, the causal agent of white-nose syndrome in bats. *PLOS ONE*, *12*(6), e0179770. https://doi.org/10.1371/journal.pone.0179770

Minnis, A. M., & Lindner, D. L. (2013). Phylogenetic evaluation of *Geomyces* and allies reveals no close relatives of *Pseudogymnoascus destructans*, comb. Nov., in bat hibernacula of eastern North America. *Fungal Biology*, *117*(9), 638–649. https://doi.org/10.1016/j.funbio.2013.07.001

Moore, M. S., Reichard, J. D., Murtha, T. D., Nabhan, M. L., Pian, R. E., Ferreira, J. S., & Kunz, T. H. (2013). Hibernating Little Brown Myotis (*Myotis lucifugus*) Show Variable Immunological Responses to White-Nose Syndrome. *PLOS ONE*, *8*(3), e58976. https://doi.org/10.1371/journal.pone.0058976

Narasimhachari, N., & Vining, L. C. (1963). Studies on the pigments of *Penicillium herquei*. *Canadian Journal of Chemistry*, *41*(3), 641–648. https://doi.org/10.1139/v63-091

Omura, S., Hirano, A., Iwai, Y., & Masuma, R. (1979). Herquline, a new alkaloid produced by *Penicillium herquei* fermentation, isolation and properties. *The Journal of Antibiotics*, *32*(8), 786–790. https://doi.org/10.7164/antibiotics.32.786

Palmer, J. M., Kubatova, A., Novakova, A., Minnis, A. M., Kolarik, M., & Lindner, D. L. (2014). Molecular Characterization of a Heterothallic Mating System in *Pseudogymnoascus*

destructans , the Fungus Causing White-Nose Syndrome of Bats. *G3 Genes|Genomes|Genetics*, *4*(9), 1755–1763. https://doi.org/10.1534/g3.114.012641

Patel, S., & Sharma, S. (2022). Respiratory Acidosis. In *StatPearls*. StatPearls Publishing. http://www.ncbi.nlm.nih.gov/books/NBK482430/

Pirt, S. J. (1967). A Kinetic Study of the Mode of Growth of Surface Colonies of Bacteria and Fungi. *Microbiology*, *47*(2), 181–197. https://doi.org/10.1099/00221287-47-2-181

Porras-Alfaro, A., Liu, K.-L., Kuske, C. R., & Xie, G. (2014). From Genus to Phylum: Large-Subunit and Internal Transcribed Spacer rRNA Operon Regions Show Similar Classification Accuracies Influenced by Database Composition. *Applied and Environmental Microbiology*, *80*(3), 829–840. https://doi.org/10.1128/AEM.02894-13

Puechmaille, S. J., Wibbelt, G., Korn, V., Fuller, H., Forget, F., Mühldorfer, K., Kurth, A., Bogdanowicz, W., Borel, C., Bosch, T., Cherezy, T., Drebet, M., Görföl, T., Haarsma, A.-J., Herhaus, F., Hallart, G., Hammer, M., Jungmann, C., Le Bris, Y., Lutsar, L., Masing, M., Mulkens, B., Passior, K., Starrach, M., Wojtaszewski, A., Zöphel, U., Teeling, E. C., Arlettaz, R. (2011). Pan-European Distribution of White-Nose Syndrome Fungus (Geomyces destructans) Not Associated with Mass Mortality. *PLoS ONE*, *6*(4), e19167. https://doi.org/10.1371/journal.pone.0019167

Rachowicz, L. J., Hero, J.-M., Alford, R. A., Taylor, J. W., Morgan, J. A. T., Vredenburg, V. T., Collins, J. P., & Briggs, C. J. (2005). The Novel and Endemic Pathogen Hypotheses: Competing Explanations for the Origin of Emerging Infectious Diseases of Wildlife. *Conservation Biology*, *19*(5), 1441–1448. https://doi.org/10.1111/j.1523-1739.2005.00255.x

Reeder, D. M., Frank, C. L., Turner, G. G., Meteyer, C. U., Kurta, A., Britzke, E. R., Vodzak, M. E., Darling, S. R., Stihler, C. W., Hicks, A. C., Jacob, R., Grieneisen, L. E., Brownlee, S. A., Muller, L. K., & Blehert, D. S. (2012). Frequent Arousal from Hibernation Linked to Severity of Infection and Mortality in Bats with White-Nose Syndrome. *PLOS ONE*, *7*(6), e38920. https://doi.org/10.1371/journal.pone.0038920

Saint Mary's University. (n.d.). *Work Instructions*. Saint Mary's University. Retrieved January 27, 2023, from https://www.smu.ca/faculty-of-science/science-work-instructions.html

Vanderwolf, K. J., Malloch, D., & McAlpine, D. F. (2016). Detecting Viable *Pseudogymnoascus Destructans* (*ascomycota*: *Pseudeurotiaceae*) from Walls of Bat Hibernacula: Effect of Culture Media. 158–162. https://doi.org/10.4311/2015MB0138

Verant, M. L., Meteyer, C. U., Speakman, J. R., Cryan, P. M., Lorch, J. M., & Blehert, D. S. (2014). White-nose syndrome initiates a cascade of physiologic disturbances in the hibernating bat host. *BMC Physiology*, *14*(1), 10. https://doi.org/10.1186/s12899-014-0010-4

Visagie, C. M., Houbraken, J., Rodriques, C., Pereira, C. S., Dijksterhuis, J., Seifert, K. A., Jacobs, K., & Samson, R. A. (2013). Five new *Penicillium* species in section Sclerotiora: A tribute to the Dutch Royal family. *Persoonia - Molecular Phylogeny and Evolution of Fungi*, *31*(1), 42–62. https://doi.org/10.3767/003158513X667410

Wang, X.-C., Chen, K., Zeng, Z.-Q., & Zhuang, W.-Y. (2017). Phylogeny and morphological analyses of *Penicillium* section Sclerotiora (Fungi) lead to the discovery of five new species. *Scientific Reports*, *7*(1), Article 1. https://doi.org/10.1038/s41598-017-08697-1

Warnecke, L., Turner, J. M., Bollinger, T. K., Lorch, J. M., Misra, V., Cryan, P. M., Wibbelt, G., Blehert, D. S., & Willis, C. K. R. (2012). Inoculation of bats with European *Geomyces destructans* supports the novel pathogen hypothesis for the origin of white-nose syndrome. *Proceedings of the National Academy of Sciences*, *109*(18), 6999–7003. https://doi.org/10.1073/pnas.1200374109

Warnecke, L., Turner, J. M., Bollinger, T. K., Misra, V., Cryan, P. M., Blehert, D. S., Wibbelt, G., & Willis, C. K. R. (2013). Pathophysiology of white-nose syndrome in bats: A mechanistic model linking wing damage to mortality. *Biology Letters*, *9*(4), 20130177. https://doi.org/10.1098/rsbl.2013.0177

West, G., Heard, D., & Caulkett, N. (2014). Zoo Animal and Wildlife Immobilization and Anesthesia. John Wiley & Sons.

Wibbelt, G., Kurth, A., Hellmann, D., Weishaar, M., Barlow, A., Veith, M., Prüger, J., Görföl, T., Grosche, L., Bontadina, F., Zöphel, U., Seidl, H.-P., Cryan, P. M., & Blehert, D. S. (2010). White-Nose Syndrome Fungus (*Geomyces destructans*) in Bats, Europe. *Emerging Infectious Diseases*, *16*(8), 1237–1243. https://doi.org/10.3201/eid1608.100002

Wu, X., Tan, Y., Yi, J., Song, X., Yang, J., Zhou, X., & Chen, G. (2020). Study on Bioactive Secondary Metabolites from *Penicillium herquei* JX4. *Chinese Journal of Organic Chemistry*, *41*(3), 1251. https://doi.org/10.6023/cjoc202009038

Yu, J. S., Jeong, S. Y., Li, C., Oh, T., Kwon, M., Ahn, J. S., Ko, S.-K., Ko, Y.-J., Cao, S., & Kim, K. H. (2022). New phenalenone derivatives from the Hawaiian volcanic soil-associated fungus *Penicillium herquei* FT729 and their inhibitory effects on indoleamine 2,3-

dioxygenase 1 (IDO1). *Archives of Pharmacal Research*, *45*(2), 105–113. https://doi.org/10.1007/s12272-022-01372-8

Zagmajster, M. (2019). Chapter 13—Bats. In W. B. White, D. C. Culver, & T. Pipan (Eds.), *Encyclopedia of Caves (Third Edition)* (pp. 94–101). Academic Press. https://doi.org/10.1016/B978-0-12-814124-3.00013-3

Zhang, T., Chaturvedi, V., & Chaturvedi, S. (2015). Novel Trichoderma polysporum Strain for the Biocontrol of *Pseudogymnoascus destructans*, the Fungal Etiologic Agent of Bat White Nose Syndrome. *PLOS ONE*, *10*(10), e0141316. https://doi.org/10.1371/journal.pone.0141316

Zhou, X.-M., Zheng, C.-J., Song, X.-M., Tang, M.-M., Yang, J.-Y., Yang, X., Peng, S.-J., Cai, J., & Chen, G.-Y. (2019). Bioactive acetaminophen derivatives from *Penicillum herquei* JX4. *Fitoterapia*, *139*, 104400. https://doi.org/10.1016/j.fitote.2019.104400

Zhu, X., McAtee, C. C., & Schindler, C. S. (2019). Total Syntheses of Herqulines B and C. *Journal of the American Chemical Society*, *141*(8), 3409–3413. https://doi.org/10.1021/jacs.8b13849

8. Appendix

8.1 Appendix 1: Quadrupole time-of-flight mass spectrometer analysis report of the acetonitrile extract from S5 plates.

Analysis Report

Agilent | Trusted Answers

Sample Information

Name	ACN frac 1	**Data File Path**	D:\Data\2023\Sit\MM 06-03-2023\ACN frac 1.d
Sample ID		**Acq. Time (Local)**	2023-03-06 9:54:28 PM (UTC-03:00)
Instrument	Instrument 1	**Method Path (Acq)**	D:\Methods\Sit Group\MM 06-03-2023.m
MS Type	QTOF	**Version (Acq SW)**	6200 series TOF/6500 series Q-TOF B.09.00 (B9044.0)
Inj. Vol. (ul)	1.5	**IRM Status**	Success
Position	P1-D10	**Method Path (DA)**	D:\Data\2023\Sit\MM 06-03-2023\ACN frac 1.d\Results\Qual\Version4\SignalToNoiseCheckout.m
Plate Pos.		**Target Source Path**	
Operator		**Result Summary**	

Sample Chromatograms

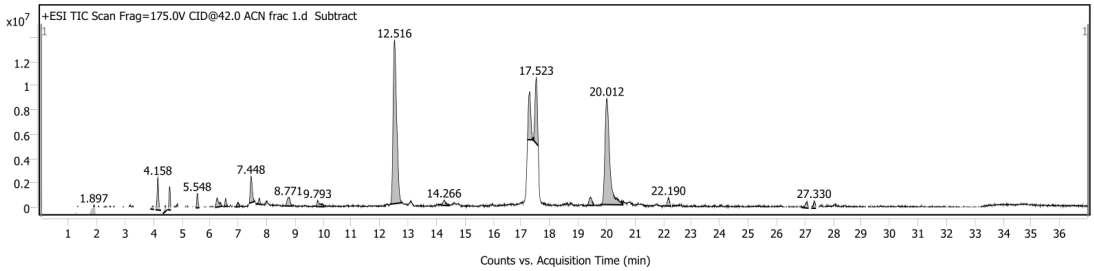

Chromatogram Peaks

Peak	Start	RT	End	Height	Area	Area %	SNR
1	1.109	1.130	1.169	1658265	3708146	3.13	
2	1.180	1.269	1.280	1442355	9323834	7.88	
3	1.719	1.897	1.975	1813167	27435815	23.19	
4	3.908	3.981	4.026	271557	1207026	1.02	
5	4.071	4.158	4.272	2687828	10475120	8.85	
6	4.336	4.431	4.481	461308	2285175	1.93	
7	4.496	4.581	4.622	1934740	6407096	5.41	
8	5.494	5.548	5.623	1189003	4065115	3.44	
9	6.176	6.253	6.415	771395	5248893	4.44	
10	6.496	6.553	6.615	673753	2159058	1.82	
11	6.926	7.004	7.059	344905	1600559	1.35	
12	7.388	7.448	7.563	2166854	10588924	8.95	
13	7.698	7.737	7.803	517418	1775896	1.50	
14	8.665	8.771	8.893	699860	5507859	4.65	
15	9.738	9.793	10.043	501279	4106951	3.47	
16	12.388	12.516	12.766	13486229	118323631	100.00	
17	14.183	14.266	14.455	446133	3278172	2.77	
18	17.209	17.284	17.378	3963879	23546795	19.90	
19	17.428	17.523	17.589	5455466	30025137	25.38	
20	19.329	19.445	19.545	687692	5000496	4.23	
21	19.836	20.012	20.573	8760228	103402450	87.39	
22	22.113	22.190	22.257	706951	3420337	2.89	
23	26.882	27.080	27.136	539908	3346825	2.83	
24	27.227	27.330	27.395	637532	2917838	2.47	

Sample Spectra

+ Scan (rt: 12.427-12.672 min) Sub Peak 16 from + TIC Scan Sub

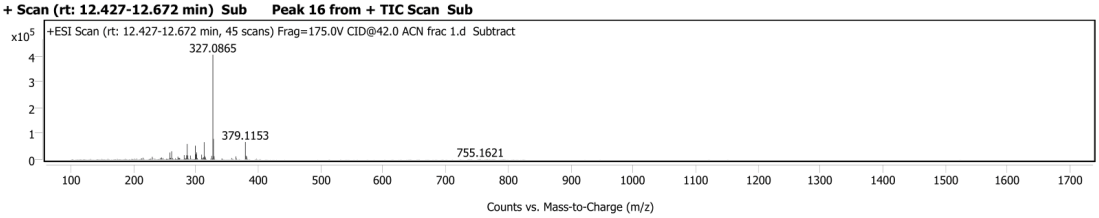

Spectrum Peaks

m/z	z	Abund	Abund %	m/z (Calc)	Diff (ppm)	Ion Species	Formula	Ion Type
131.0544		1273	0.32					
149.0582		1271	0.32					
159.0453		1694	0.42					
174.0666		1500	0.37					
187.0399		1929	0.48					
197.0590		1526	0.38					
199.0406		1080	0.27					
201.0545		1139	0.28					
202.0633		2061	0.51					
205.0500		2758	0.68					
211.0707		878	0.22					
212.0473		2164	0.54					
213.0548		3374	0.84					
215.0350	1	6599	1.64					
216.0407	1	1172	0.29					
217.0498		1190	0.30					
225.0797		1088	0.27					
227.0364		1971	0.49					
227.0642		1679	0.42					
229.0512		1692	0.42					
230.0569	1	9778	2.43					
231.0605	1	1670	0.41					
233.0449		3159	0.78					
235.0742		1509	0.37					
239.0679		890	0.22					
240.0464		902	0.22					
241.0512		1076	0.27					
243.0564		5529	1.37					
245.0452	1	7257	1.80					
246.0503	1	1510	0.37					
247.0598		5072	1.26					
253.0382		990	0.25					
253.0788		2495	0.62					
255.0654		1375	0.34					
256.0712		1186	0.29					
257.0593		2442	0.61					
258.0523	1	26481	6.57					
259.0567	1	5929	1.47					
260.0587	1	1002	0.25					
261.0394	1	31235	7.75					
262.0434	1	4942	1.23					
263.0678		2594	0.64					
267.0654	1	4052	1.01					
268.0653	1	967	0.24					
271.0582		10681	2.65					
272.0654		4448	1.10					
273.0451		3167	0.79					
273.0725		5698	1.41					
274.0498	1	4819	1.20					
275.0537	1	1114	0.28					
281.0800	1	16488	4.09					
282.0834	1	3206	0.80					
283.0616		3190	0.79					
284.0669		4391	1.09					
285.0585		16037	3.98					
286.0476	1	59540	14.78					
287.0522	1	15179	3.77					
288.0554	1	2549	0.63					
289.0427		1139	0.28					
291.0505	1	14806	3.67					
292.0546	1	2427	0.60					
295.0645		1385	0.34					
298.0505		1165	0.29					
298.9812		1198	0.30					
299.0757	1	52717	13.08					
300.0689	1	19661	4.88					
301.0704	1	27093	6.72					
302.0735	1	4892	1.21					
309.0755	1	18524	4.60					
310.0806	1	6317	1.57					
311.0762	1	1109	0.28					
312.0627		7790	1.93					
313.0707	1	66323	16.46					
314.0740	1	12365	3.07					
315.0838	1	7515	1.87					
316.0884	1	1344	0.33					
323.0911		1951	0.48					
324.0980		1127	0.28					
325.1061	1	13494	3.35					
326.1008	1	3451	0.86					
327.0865	1	402906	100.00					
328.0898	1	78958	19.60					
329.0919	1	12241	3.04					
330.0945	1	1433	0.36					
341.1014		1816	0.45					
342.1096		2891	0.72					
357.1317	1	4960	1.23					

Spectrum Peaks

m/z	Z	Abund	Abund %	m/z (Calc)	Diff (ppm)	Ion Species	Formula	Ion Type
358.1366	1	1189	0.30					
359.1140		1409	0.35					
364.0916	1	11504	2.86					
365.0948	1	2393	0.59					
368.9705		950	0.24					
379.1153	1	67086	16.65					
380.1184	1	14405	3.58					
381.0994	1	11001	2.73					
382.1001		2303	0.57					
395.0840		1027	0.25					
397.0589		1988	0.49					
403.0771		994	0.25					
755.1621		1012	0.25					

MassHunter Qual 10.0
(End of Report)

8.2 Appendix 2: Quadrupole time-of-flight mass spectrometer analysis report of the chloroform extract from S5 plates

Analysis Report

Agilent | Trusted Answers

Sample Information

Name	CHCl3 frac 2	**Data File Path**	D:\Data\2023\Sit\MM 06-03-2023\CHCl3 frac 2.d
Sample ID		**Acq. Time (Local)**	2023-03-06 6:03:54 PM (UTC-03:00)
Instrument	Instrument 1	**Method Path (Acq)**	D:\Methods\Sit Group\MM 06-03-2023.m
MS Type	QTOF	**Version (Acq SW)**	6200 series TOF/6500 series Q-TOF B.09.00 (B9044.0)
Inj. Vol. (ul)	1.5	**IRM Status**	Success
Position	P1-D5	**Method Path (DA)**	D:\Data\2023\Sit\MM 06-03-2023\CHCl3 frac 2.d\Results\Qual\Version4\SignalToNoiseCheckout.m
Plate Pos.		**Target Source Path**	
Operator		**Result Summary**	

Sample Chromatograms

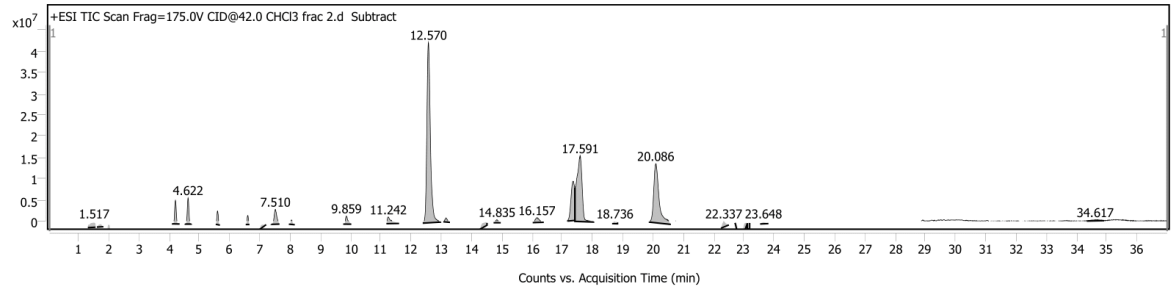

Chromatogram Peaks

Peak	Start	RT	End	Height	Area	Area %	SNR
1	1.308	1.517	1.564	1131972	14030816	4.10	
2	1.608	1.739	1.801	667389	5080607	1.48	
3	1.934	2.001	2.067	3202041	18252581	5.33	
4	4.111	4.205	4.343	5566461	21062591	6.15	
5	4.533	4.622	4.727	6183838	22881082	6.68	
6	5.538	5.599	5.676	3230129	10951192	3.20	
7	6.529	6.599	6.653	2144291	7086118	2.07	
8	6.988	7.188	7.205	153175	5388757	1.57	
9	7.377	7.510	7.645	3511029	22033837	6.43	
10	7.954	8.043	8.151	1072034	4600564	1.34	
11	9.754	9.859	10.020	1918847	11656382	3.40	
12	11.181	11.242	11.600	1566132	14805218	4.32	
13	12.408	12.570	12.969	42468150	342487046	100.00	
14	13.063	13.153	13.282	957462	5266951	1.54	
15	14.271	14.463	14.508	935640	11849098	3.46	
16	14.724	14.835	14.961	742672	4525878	1.32	
17	16.017	16.157	16.384	1142365	10877625	3.18	
18	17.170	17.352	17.413	9248365	75152749	21.94	
19	17.413	17.591	18.030	15470410	190668211	55.67	
20	18.644	18.736	18.825	552964	3855061	1.13	
21	19.880	20.086	20.586	13933915	171319588	50.02	
22	22.241	22.337	22.504	1416475	10839278	3.16	
23	22.709	22.714	22.864	255735	7461989	2.18	
24	22.924	23.076	23.114	935990	12902965	3.77	
25	23.114	23.181	23.192	1405134	6834909	2.00	
26	23.537	23.648	23.813	491191	3656217	1.07	
27	34.339	34.617	34.912	279101	5372455	1.57	

Sample Spectra

+ Scan (rt: 12.479-12.512 ... min) Sub Peak 13 from + TIC Scan Sub

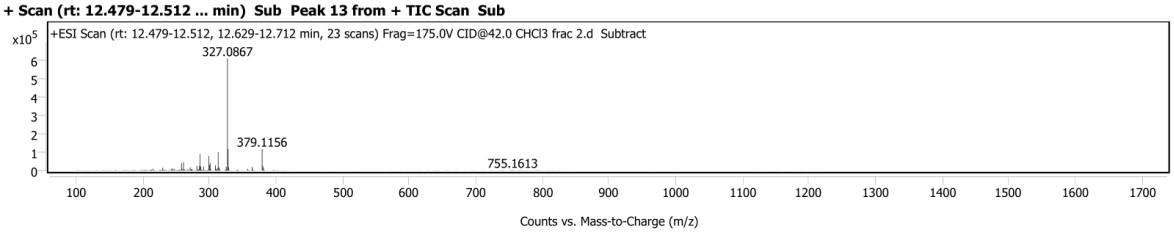

Spectrum Peaks

m/z	z	Abund	Abund %	m/z (Calc)	Diff (ppm)	Ion Species	Formula	Ion Type
131.0534		1736	0.29					
149.0583		1730	0.29					
159.0453		2594	0.43					
174.0640		1509	0.25					
187.0403		2912	0.48					
197.0596		1882	0.31					
199.0401		1753	0.29					
201.0540		1621	0.27					
202.0628		3051	0.50					
205.0501		4134	0.68					
212.0476		3044	0.50					
213.0544		4326	0.72					
215.0343	1	9982	1.65					
216.0395	1	1635	0.27					
217.0490		1670	0.28					
225.0820		1580	0.26					
227.0353		2166	0.36					
227.0668		1556	0.26					
229.0505		2906	0.48					
230.0573	1	14667	2.43					
231.0614	1	2547	0.42					
232.0384		2042	0.34					
233.0451		4651	0.77					
235.0745		2401	0.40					
239.0681		2110	0.35					
241.0518		1368	0.23					
243.0566		8603	1.42					
245.0452	1	10703	1.77					
246.0498	1	2025	0.34					
247.0601		7942	1.31					
253.0416		1870	0.31					
253.0769		4341	0.72					
255.0638		2923	0.48					
256.0710		1621	0.27					
257.0598		3082	0.51					
258.0523	1	39901	6.60					
259.0576	1	8402	1.39					
261.0395	1	45527	7.53					
262.0435	1	7315	1.21					
263.0671		4071	0.67					
267.0662	1	6364	1.05					
268.0652	1	1395	0.23					
271.0585		16552	2.74					
272.0658		6716	1.11					
273.0484		3325	0.55					
273.0697		8312	1.37					
274.0501	1	7419	1.23					
275.0538	1	1995	0.33					
281.0792	1	23627	3.91					
282.0834	1	5146	0.85					
283.0618		4305	0.71					
284.0674		6817	1.13					
285.0590		24274	4.02					
286.0477	1	89342	14.78					
287.0527	1	21962	3.63					
288.0558	1	3668	0.61					
289.0472		1605	0.27					
290.0430		2238	0.37					
291.0508	1	21766	3.60					
292.0551	1	3562	0.59					
295.0649		2296	0.38					
297.0851		1583	0.26					
298.0549		2787	0.46					
298.9825		1674	0.28					
299.0763	1	78704	13.02					
300.0688	1	29010	4.80					
301.0706	1	40294	6.67					
302.0736	1	6935	1.15					
309.0758	1	28061	4.64					
310.0811	1	8894	1.47					
311.0782	1	1549	0.26					
312.0629		11139	1.84					
313.0708	1	99846	16.52					
314.0743	1	18538	3.07					
315.0843	1	11317	1.87					
316.0881	1	2013	0.33					
323.0913		2947	0.49					
324.0971		1657	0.27					
325.1064	1	19751	3.27					
326.0965	1	6314	1.04					
327.0867	1	604534	100.00					
328.0900	1	117228	19.39					
329.0922	1	18402	3.04					
330.0954	1	2057	0.34					
341.1017		2681	0.44					
342.1093		4051	0.67					
357.1315	1	9183	1.52					

Spectrum Peaks

m/z	Z	Abund	Abund %	m/z (Calc)	Diff (ppm)	Ion Species	Formula	Ion Type
358.1357	1	2086	0.35					
359.1157	1	2228	0.37					
364.0919	1	19378	3.21					
365.0950	1	4376	0.72					
379.1156	1	115294	19.07					
380.1187	1	24943	4.13					
381.0997	1	16780	2.78					
382.0996		3254	0.54					
395.0828		1508	0.25					
397.0586		2450	0.41					
403.0765		1817	0.30					
755.1613		1814	0.30					
766.1694		1479	0.24					

+ Scan (rt: 13.084-13.240 min) Sub Peak 14 from + TIC Scan Sub

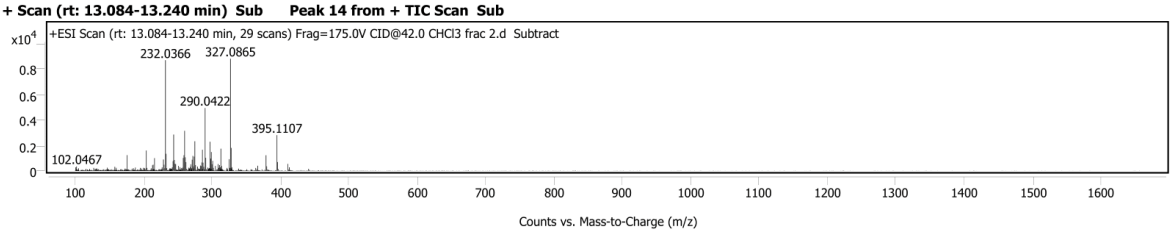

Spectrum Peaks

m/z	Z	Abund	Abund %	m/z (Calc)	Diff (ppm)	Ion Species	Formula	Ion Type
100.9214		270	3.05					
102.0467		334	3.77					
105.0688		193	2.17					
127.0579		222	2.50					
147.0682		244	2.76					
158.0367		311	3.51					
160.0522		232	2.61					
176.0473		1211	13.66					
185.0581		196	2.21					
188.0479		255	2.88					
195.0880		221	2.49					
197.0604		173	1.95					
200.0475		229	2.58					
201.0509		201	2.26					
202.0637		174	1.96					
204.0417	1	1573	17.74					
205.0485	1	225	2.54					
211.0526		197	2.23					
213.0551		433	4.88					
214.0297		471	5.31					
216.0425		981	11.07					
227.0703		265	2.99					
229.0516		827	9.34					
230.0569		478	5.40					
231.0549		192	2.16					
232.0366	1	8730	98.49					
233.0424	1	1340	15.11					
234.0452	1	200	2.26					
238.0985		180	2.03					
239.0345		185	2.09					
242.0568		270	3.04					
243.0648		761	8.58					
244.0382	1	2864	32.32					
245.0453	1	851	9.60					
246.0524		548	6.18					
247.0605		516	5.82					
251.0718		349	3.93					
253.0528		277	3.12					
255.0639		216	2.44					
257.0497		251	2.83					
257.0633		185	2.09					
258.0539		1011	11.41					
259.0599		1228	13.85					
260.0336	1	3089	34.85					
261.0394	1	1025	11.57					
262.0461		681	7.68					
266.0937		239	2.70					
267.0630		194	2.19					
268.0688		304	3.43					
269.0800		493	5.56					
270.0655		204	2.30					
271.0598		872	9.84					
272.0444	1	1171	13.21					
273.0511	1	186	2.10					
273.0687		344	3.88					
274.0470	1	1113	12.55					
275.0546	1	2324	26.22					
276.0612	1	442	4.99					
279.0690		329	3.71					
280.0728		170	1.91					
283.0581		366	4.13					
284.0678		350	3.95					
285.0561		658	7.42					
286.0527		1661	18.74					
287.0555		638	7.20					
288.0578		313	3.53					
290.0422	1	4962	55.98					
291.0473	1	1025	11.56					
294.0871		250	2.82					
295.0829		174	1.96					
296.0679		208	2.35					
297.0060		173	1.95					
297.0771		2146	24.21					
298.0546		954	10.76					
299.0730	1	1385	15.62					
300.0673	1	511	5.77					
301.0710	1	779	8.79					
302.0734	1	226	2.55					
305.0655		378	4.26					
309.0773		527	5.95					
310.0805		228	2.57					
311.0892		447	5.04					
312.0765		270	3.05					
313.0711	1	1749	19.73					
314.0729	1	371	4.19					
322.0809		222	2.51					
325.0678	1	914	10.31					

Spectrum Peaks

m/z	Z	Abund	Abund %	m/z (Calc)	Diff (ppm)	Ion Species	Formula	Ion Type
326.0744	1	225	2.54					
327.0865	1	8864	100.00					
327.9681		194	2.19					
328.0900	1	1805	20.36					
329.0916	1	278	3.13					
364.0912		219	2.47					
367.0460		394	4.44					
379.1149	1	1223	13.80					
380.1176	1	352	3.97					
395.1107	1	2813	31.73					
396.1140	1	685	7.73					
411.0747		541	6.10					
413.2658		271	3.06					

MassHunter Qual 10.0
(End of Report)

8.3 Appendix 3: Quadrupole time-of-flight mass spectrometer analysis report of the *P. destructans* extract

Analysis Report

Agilent | Trusted Answers

Sample Information

Name	Pd 2	**Data File Path**	D:\Data\2022\Sit Group\MM 12.12.20022\Pd s2.d
Sample ID		**Acq. Time (Local)**	2022-12-12 6:14:41 PM (UTC-03:00)
Instrument	Instrument 1	**Method Path (Acq)**	D:\Methods\Sit Group\MM_29_09_22_ver2.m
MS Type	QTOF	**Version (Acq SW)**	6200 series TOF/6500 series Q-TOF B.09.00 (B9044.0)
Inj. Vol. (ul)	1.5	**IRM Status**	Success
Position	P1-B8	**Method Path (DA)**	D:\Data\2022\Sit Group\MM 12.12.20022\Pd s2.d\Results\Qual\Version4\SignalToNoiseCheckout.m
Plate Pos.		**Target Source Path**	
Operator		**Result Summary**	

Sample Chromatograms

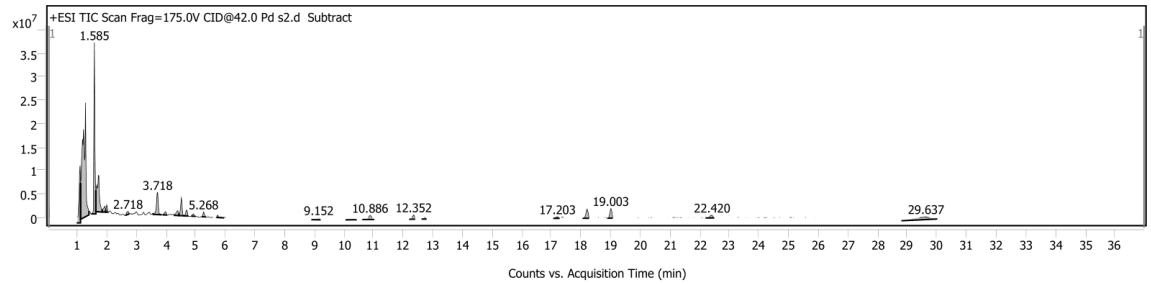

Chromatogram Peaks

Peak	Start	RT	End	Height	Area	Area %	SNR
1	0.987	1.101	1.118	12138612	38182186	21.69	
2	1.118	1.285	1.401	24186699	176026319	100.00	
3	1.501	1.585	1.635	36347083	80686584	45.84	
4	1.635	1.718	1.851	7716649	48734719	27.69	
5	1.851	1.935	1.968	1259148	5888852	3.35	
6	1.968	2.001	2.045	1545050	4012194	2.28	
7	2.635	2.718	2.768	620469	3310234	1.88	
8	3.568	3.718	3.859	4685743	20363332	11.57	
9	3.889	3.985	4.036	680368	3048236	1.73	
10	4.285	4.385	4.435	1036416	5497307	3.12	
11	4.435	4.518	4.618	3773922	13970481	7.94	
12	4.618	4.685	4.754	1260833	4848038	2.75	
13	4.853	4.918	4.999	504613	1976905	1.12	
14	5.204	5.268	5.341	1025887	3451623	1.96	
15	5.699	5.735	5.935	508336	2096991	1.19	
16	8.902	9.152	9.216	427125	3270018	1.86	
17	10.056	10.319	10.419	206625	1872878	1.06	
18	10.636	10.886	11.026	876469	7085550	4.03	
19	12.219	12.352	12.407	915458	4226204	2.40	
20	12.621	12.736	12.792	362929	1797043	1.02	
21	17.062	17.203	17.277	329616	1916329	1.09	
22	18.070	18.203	18.270	1936271	9637765	5.48	
23	18.903	19.003	19.068	2038544	9314399	5.29	
24	22.197	22.420	22.494	598007	4048465	2.30	
25	28.805	29.637	30.016	616332	22425754	12.74	

Sample Spectra

+ Scan (rt: 12.286-12.402 min) Sub Peak 19 from + TIC Scan Sub

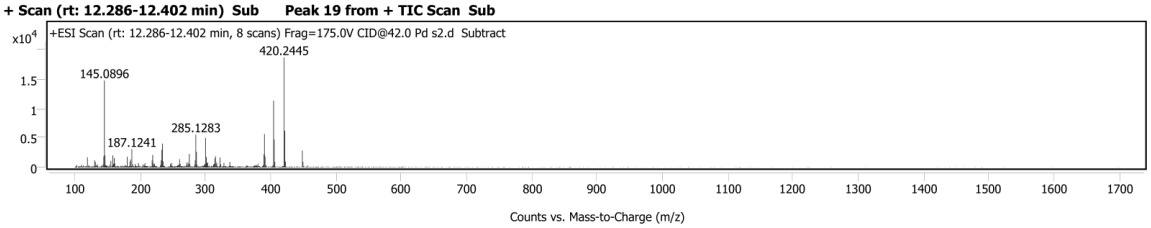

Spectrum Peaks

m/z	Z	Abund	Abund %	m/z (Calc)	Diff (ppm)	Ion Species	Formula	Ion Type
103.0549		379	2.03					
110.0679		404	2.16					
112.9916		267	1.43					
119.0862		1677	8.98					
121.0890		339	1.82					
130.0664		1173	6.28					
131.0801		891	4.78					
132.0834		265	1.42					
133.9815		444	2.38					
134.0988		453	2.43					
143.0800		476	2.55					
144.0817		1834	9.82					
145.0896	1	14747	79.01					
146.0946	1	2022	10.84					
147.1054	1	340	1.82					
148.1133		259	1.39					
152.8916		363	1.95					
155.0619		1084	5.81					
158.0973		2028	10.86					
159.1064		474	2.54					
160.1129		1570	8.41					
160.9910		624	3.34					
176.9311		336	1.80					
180.0580		1757	9.41					
184.1018		967	5.18					
185.1082		1287	6.90					
187.1241	1	3071	16.46					
188.1271	1	506	2.71					
192.0924		560	3.00					
197.1090		690	3.70					
198.1118		285	1.53					
204.0823		484	2.59					
206.1048		348	1.87					
207.1095		595	3.19					
218.0973		1189	6.37					
219.1050		2085	11.17					
220.1118		683	3.66					
221.1190		428	2.29					
222.1285		571	3.06					
231.1014		373	2.00					
232.1123		1179	6.32					
233.1200		2963	15.88					
234.1283	1	3988	21.37					
235.1319	1	976	5.23					
246.1247		603	3.23					
248.1437		704	3.77					
257.1100		300	1.61					
258.1223		314	1.68					
259.1287		484	2.59					
260.1331		1346	7.21					
261.1354		577	3.09					
270.1107		286	1.53					
271.1244	1	765	4.10					
272.1282	1	267	1.43					
273.1401		759	4.07					
274.1462		468	2.51					
275.1548	1	2261	12.12					
276.1595	1	519	2.78					
283.1229		381	2.04					
284.1251		1165	6.24					
285.1283		5529	29.62					
286.1353	1	2620	14.04					
287.1428	1	482	2.58					
295.0962		261	1.40					
298.1423		427	2.29					
299.1402		304	1.63					
300.1508	1	4981	26.68					
301.1599	1	1679	9.00					
302.1726		757	4.05					
303.1862		764	4.09					
312.1611		475	2.55					
313.1669		586	3.14					
314.1668		1503	8.05					
315.1852	1	1855	9.94					
316.1885	1	537	2.88					
317.2021		819	4.39					
322.1601	1	1643	8.80					
323.1628	1	485	2.60					
328.1819		714	3.83					
337.1849		884	4.74					
363.1862		303	1.62					
375.1847		299	1.60					
377.1917		296	1.59					
378.2048		266	1.43					
380.2136		589	3.16					
388.1934		347	1.86					
389.2023		2190	11.73					

Spectrum Peaks

m/z	Z	Abund	Abund %	m/z (Calc)	Diff (ppm)	Ion Species	Formula	Ion Type
390.1983	1	5646	30.25					
391.2034	1	1824	9.77					
392.2103	1	350	1.88					
403.2167		341	1.83					
404.2137	1	11317	60.63					
405.2172	1	4697	25.16					
406.2211	1	899	4.81					
420.2445	1	18665	100.00					
421.2479	1	6191	33.17					
422.2511	1	953	5.10					
448.2510	1	2834	15.19					
449.2552	1	906	4.85					
456.0609		303	1.62					

+ Scan (rt: 12.669-12.786 min) Sub Peak 20 from + TIC Scan Sub

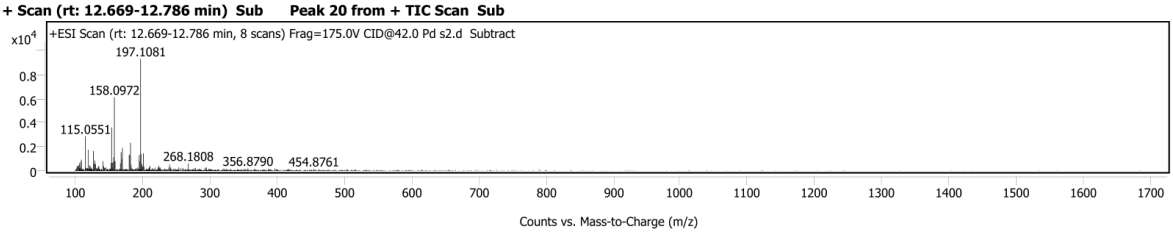

Spectrum Peaks

m/z	Z	Abund	Abund %	m/z (Calc)	Diff (ppm)	Ion Species	Formula	Ion Type
102.0430		236	2.54					
103.0551		391	4.21					
104.0593		363	3.91					
105.0699		450	4.84					
106.0679		633	6.81					
107.0763		174	1.87					
107.9676		733	7.89					
108.0792		320	3.44					
109.0528		920	9.90					
110.1004		181	1.95					
114.9505		159	1.71					
115.0551	1	2860	30.78					
116.0583	1	235	2.53					
117.0698		169	1.82					
117.9298		179	1.93					
118.0698		227	2.44					
119.0621		1746	18.79					
121.0298		176	1.90					
121.0915		441	4.75					
122.0162		399	4.29					
123.0116		192	2.06					
123.0838		304	3.28					
124.9945		202	2.18					
127.0542		1631	17.56					
128.0609		573	6.17					
129.0697		843	9.08					
130.0664		554	5.97					
131.0797		226	2.43					
132.9044		187	2.01					
133.9054		209	2.25					
134.0982		380	4.09					
135.0917		374	4.02					
135.9061		175	1.88					
141.0701		789	8.49					
142.0699		399	4.29					
143.0813		228	2.45					
144.0817		211	2.27					
145.0217		295	3.18					
147.1125		152	1.64					
148.1069		154	1.66					
152.0596		177	1.90					
153.0655		649	6.99					
154.0662	1	3588	38.62					
154.8892		254	2.73					
155.0720	1	616	6.63					
156.0814		707	7.61					
157.0908		1070	11.52					
158.0972	1	6100	65.66					
158.9647		798	8.59					
159.1031	1	711	7.65					
165.0237		178	1.92					
167.0837		616	6.63					
168.0829		1535	16.52					
169.0885		982	10.57					
170.0963		1909	20.55					
174.9115		155	1.67					
180.0808		1335	14.37					
181.0807		1264	13.61					
182.0868	1	2322	25.00					
183.0268		170	1.83					
183.0958	1	504	5.42					
184.1067		202	2.18					
188.9523		162	1.74					
190.8567		188	2.02					
191.0095		174	1.88					
192.8941		268	2.88					
195.0925		1288	13.86					
196.0355		156	1.68					
196.1013		796	8.57					
197.1081	1	9290	100.00					
198.1127	1	1404	15.11					
199.1225		551	5.93					
200.0631		350	3.77					
201.1398	1	1436	15.45					
202.1426	1	344	3.70					
205.9653		180	1.94					
211.1242		354	3.81					
214.9033		203	2.18					
223.1207		277	2.98					
224.1271		422	4.54					
225.1342		251	2.70					
226.1339		269	2.90					
239.1515		231	2.48					
240.1509		519	5.59					
242.1672		283	3.05					
245.9749		170	1.83					
248.8816		163	1.75					

Spectrum Peaks

m/z	Z	Abund	Abund %	m/z (Calc)	Diff (ppm)	Ion Species	Formula	Ion Type
254.1652		280	3.01					
256.8859		184	1.98					
258.8659		187	2.02					
268.1808		612	6.59					
276.8808		201	2.16					
284.9101		165	1.78					
293.0709		233	2.51					
295.1954		276	2.97					
298.8628		168	1.81					
356.8790		203	2.19					
366.8769		160	1.72					
396.8759		190	2.05					
454.8761		153	1.64					

MassHunter Qual 10.0
(End of Report)

8.4 Appendix 4: Quadrupole time-of-flight mass spectrometer analysis report of the S5 and *P. destructans* extract.

Analysis Report

Agilent | Trusted Answers

Sample Information

Name	S5 Pd2	**Data File Path**	D:\Data\2022\Sit Group\MM 12.12.20022\S5 Pd s2.d
Sample ID		**Acq. Time (Local)**	2022-12-12 4:42:34 PM (UTC-03:00)
Instrument	Instrument 1	**Method Path (Acq)**	D:\Methods\Sit Group\MM_29_09_22_ver2.m
MS Type	QTOF	**Version (Acq SW)**	6200 series TOF/6500 series Q-TOF B.09.00 (B9044.0)
Inj. Vol. (ul)	1.5	**IRM Status**	Success
Position	P1-B6	**Method Path (DA)**	D:\Data\2022\Sit Group\MM 12.12.20022\S5 Pd s2.d\Results\Qual\Version4\SignalToNoiseCheckout.m
Plate Pos.		**Target Source Path**	
Operator		**Result Summary**	

Sample Chromatograms

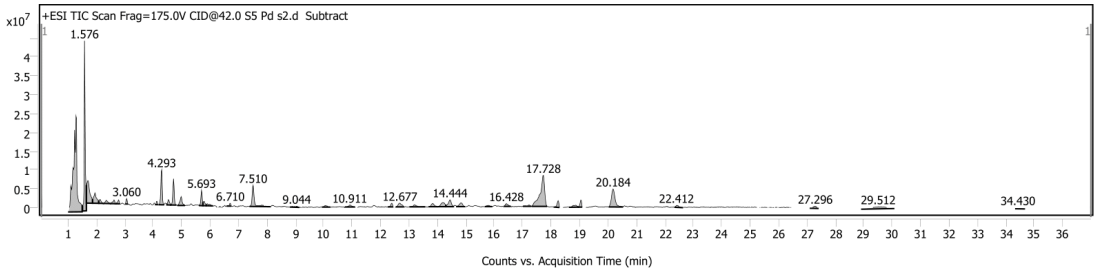

Chromatogram Peaks

Peak	Start	RT	End	Height	Area	Area %	SNR
1	0.998	1.276	1.493	25479109	221091514	100.00	
2	1.510	1.576	1.643	45197992	105272008	47.61	
3	1.643	1.693	1.860	5986372	45854083	20.74	
4	1.860	1.943	2.076	2756906	20317757	9.19	
5	2.076	2.126	2.243	1044106	5464525	2.47	
6	2.243	2.343	2.493	855870	5704429	2.58	
7	2.493	2.610	2.676	996909	4938863	2.23	
8	2.676	2.776	2.826	1036236	3886065	1.76	
9	3.014	3.060	3.104	1441616	3821079	1.73	
10	4.076	4.126	4.161	891654	2492675	1.13	
11	4.186	4.293	4.360	9322285	32085760	14.51	
12	4.477	4.527	4.610	1403224	5904641	2.67	
13	4.610	4.710	4.812	6985737	23128551	10.46	
14	4.844	4.977	5.112	2359091	12759921	5.77	
15	5.627	5.693	5.743	4088264	13179022	5.96	
16	5.743	5.777	5.860	1162800	5658208	2.56	
17	5.860	5.893	6.099	572974	4192978	1.90	
18	6.578	6.710	6.745	742103	2642857	1.20	
19	7.383	7.510	7.727	5621567	27617746	12.49	
20	7.760	7.827	8.110	388860	3261259	1.48	
21	8.803	9.044	9.137	289671	2698589	1.22	
22	9.932	10.060	10.231	412087	2977367	1.35	
23	10.744	10.911	11.094	494819	4066015	1.84	
24	12.250	12.394	12.438	975403	4232277	1.91	
25	12.532	12.677	12.825	982103	8634855	3.91	
26	13.011	13.194	13.573	540800	5069534	2.29	
27	13.685	13.827	14.011	863996	6491732	2.94	
28	14.011	14.211	14.294	1083664	10878110	4.92	
29	14.294	14.444	14.561	1814019	13910249	6.29	
30	14.678	14.828	14.972	971020	8163245	3.69	
31	15.666	15.794	15.911	313426	2595913	1.17	
32	16.336	16.428	16.585	730460	4968901	2.25	
33	17.004	17.228	17.304	370076	2727697	1.23	
34	17.314	17.728	17.859	8244164	90482194	40.93	
35	18.111	18.245	18.292	1790993	7440465	3.37	
36	18.631	18.861	18.961	518303	5479900	2.48	
37	18.961	19.045	19.090	1874856	6856287	3.10	
38	20.029	20.184	20.511	4761988	42061655	19.02	
39	22.341	22.412	22.645	530739	4298390	1.94	
40	27.100	27.296	27.416	571847	4915721	2.22	
41	28.910	29.512	30.082	565717	19499958	8.82	
42	34.330	34.430	34.680	186605	2327092	1.05	

Sample Spectra

+ Scan (rt: 12.311-12.427 min) Sub Peak 24 from + TIC Scan Sub

+ Scan (rt: 12.577-12.811 min) Sub Peak 25 from + TIC Scan Sub

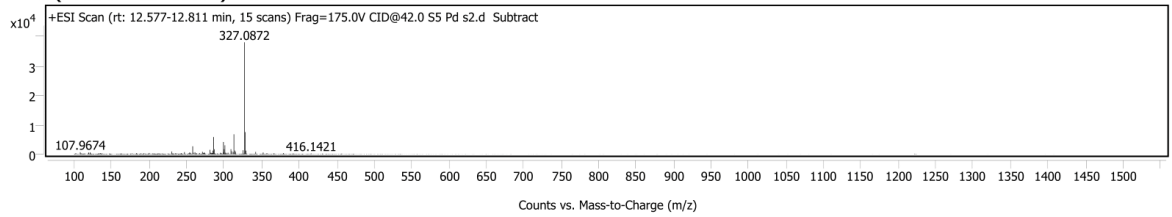

Spectrum Peaks

m/z	Z	Abund	Abund %	m/z (Calc)	Diff (ppm)	Ion Species	Formula	Ion Type
102.0388		357	0.94					
107.9674		693	1.82					
111.0891		205	0.54					
113.9676		248	0.65					
119.0622		532	1.40					
119.0841		527	1.39					
121.0833		611	1.60					
122.0752		212	0.56					
132.9926		270	0.71					
133.9884		222	0.58					
135.1144		415	1.09					
136.9203		336	0.88					
147.1150		223	0.59					
162.9193		251	0.66					
174.8789		201	0.53					
176.9312		305	0.80					
183.0893		384	1.01					
184.1047		195	0.51					
189.0566		313	0.82					
192.8910		223	0.59					
193.0519		320	0.84					
194.8862		193	0.51					
199.0380		212	0.56					
200.0628		434	1.14					
204.9165		286	0.75					
207.0968		215	0.56					
211.1236		227	0.60					
212.0523		240	0.63					
213.0565		225	0.59					
214.0571		224	0.59					
217.0897		247	0.65					
225.0146		243	0.64					
230.0603	1	872	2.29					
231.0641	1	241	0.63					
233.0414		206	0.54					
235.0661		331	0.87					
236.8624		266	0.70					
237.0582		198	0.52					
242.0557		230	0.60					
243.0293		302	0.79					
243.0619		202	0.53					
247.0619		729	1.92					
253.0827		394	1.03					
254.0478		639	1.68					
255.0627		447	1.17					
258.0544	1	2697	7.08					
259.0599	1	546	1.43					
261.0436		635	1.67					
262.8584		240	0.63					
262.9219		191	0.50					
263.0696		311	0.82					
267.0689		421	1.11					
271.0604		829	2.18					
272.0655		411	1.08					
273.0760		623	1.64					
274.0512		441	1.16					
281.0810	1	1505	3.95					
282.0861	1	500	1.31					
283.0664	1	454	1.19					
284.0647		428	1.12					
284.8871		200	0.53					
285.0419		401	1.05					
285.0636		1245	3.27					
286.0497	1	5849	15.37					
287.0549	1	1666	4.38					
287.1327		210	0.55					
288.0548	1	220	0.58					
291.0627		226	0.59					
295.1954		530	1.39					
296.0581		372	0.98					
297.0796		223	0.59					
299.0578		739	1.94					
299.0780		4180	10.98					
300.0711		1697	4.46					
301.0718	1	3000	7.88					
302.0746	1	565	1.48					
303.1860		282	0.74					
305.2020		551	1.45					
309.0777		1718	4.51					
310.0844		1018	2.67					
312.0658		746	1.96					
313.0715	1	6785	17.82					
314.0740	1	1247	3.28					
314.8532		197	0.52					
315.0856		874	2.30					
325.1051		1368	3.59					
327.0872	1	38066	100.00					

Spectrum Peaks

m/z	Z	Abund	Abund %	m/z (Calc)	Diff (ppm)	Ion Species	Formula	Ion Type
328.0911	1	7536	19.80					
329.0922	1	1222	3.21					
330.0969		212	0.56					
342.1339		805	2.12					
352.1194		593	1.56					
357.1231		353	0.93					
366.1320		285	0.75					
379.1193		366	0.96					
392.1165		216	0.57					
392.8797		207	0.54					
416.1421		255	0.67					
431.0996		216	0.57					
457.0642		217	0.57					

MassHunter Qual 10.0
(End of Report)

8.5 Appendix 5: Quadrupole time-of-flight mass spectrometer analysis report of the S5 extract.

Analysis Report

Agilent | Trusted Answers

Sample Information

Name	S5 Control	**Data File Path**	D:\Data\2022\Sit Group\LC\July 28\S5 Control-r001.d
Sample ID		**Acq. Time (Local)**	2022-07-28 6:47:16 PM (UTC-03:00)
Instrument	Instrument 1	**Method Path (Acq)**	D:\Methods\Sit Group\JK_16Mar21.m
MS Type	QTOF	**Version (Acq SW)**	6200 series TOF/6500 series Q-TOF B.09.00 (B9044.0)
Inj. Vol. (ul)	1.5	**IRM Status**	Success
Position	P1-D6	**Method Path (DA)**	D:\Data\2022\Sit Group\LC\July 28\S5 Control-r001.d\Results\Qual\Version4\SignalToNoiseCheckout.m
Plate Pos.		**Target Source Path**	
Operator		**Result Summary**	

Sample Chromatograms

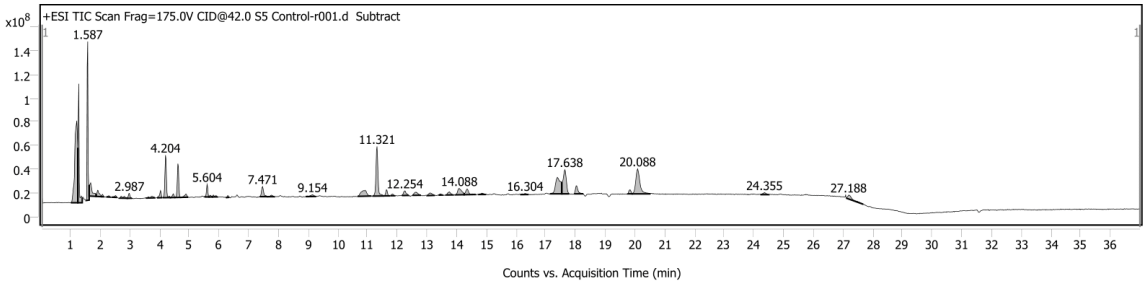

Chromatogram Peaks

Peak	Start	RT	End	Height	Area	Area %	SNR
1	1.021	1.220	1.254	68897545	443045764	100.00	
2	1.254	1.287	1.404	99913729	236983475	53.49	
3	1.537	1.587	1.637	133329644	292202514	65.95	
4	1.637	1.687	1.870	11116735	72784245	16.43	
5	1.870	1.920	2.054	5222917	29188582	6.59	
6	2.054	2.087	2.143	1986316	5680592	1.28	
7	2.216	2.304	2.354	1085393	4506364	1.02	
8	2.393	2.521	2.574	1543563	7726538	1.74	
9	2.654	2.721	2.921	1539409	13874419	3.13	
10	2.921	2.987	3.071	4139478	15897758	3.59	
11	3.539	3.754	3.857	1399826	13470743	3.04	
12	3.921	4.037	4.093	6012987	22448165	5.07	
13	4.111	4.204	4.371	35649087	126563412	28.57	
14	4.371	4.471	4.521	3084413	12661092	2.86	
15	4.521	4.621	4.721	28358499	97270144	21.95	
16	4.721	4.887	4.971	2672731	16381056	3.70	
17	5.537	5.604	5.671	10516141	32696912	7.38	
18	5.671	5.704	5.787	1387819	6103961	1.38	
19	5.787	5.821	5.954	1549480	7749882	1.75	
20	6.237	6.304	6.354	1640556	5474214	1.24	
21	7.372	7.471	7.637	8450639	42669521	9.63	
22	7.637	7.771	7.871	1359059	9320986	2.10	
23	8.920	9.154	9.254	1508946	13733057	3.10	
24	10.666	10.921	11.132	4973978	65918251	14.88	
25	11.188	11.321	11.538	41644940	195041410	44.02	
26	11.571	11.638	11.768	5223312	22065742	4.98	
27	11.773	11.838	11.921	1497367	6795700	1.53	
28	12.156	12.254	12.391	3880563	24944987	5.63	
29	12.511	12.638	12.799	2626262	23511202	5.31	
30	13.004	13.104	13.269	2272138	18700352	4.22	
31	13.388	13.471	13.538	1069061	5093882	1.15	
32	13.638	13.754	13.888	2629591	18227124	4.11	
33	13.954	14.088	14.254	5305908	51185009	11.55	
34	14.254	14.354	14.638	4725005	35371815	7.98	
35	14.738	14.854	14.971	1192430	8721504	1.97	
36	16.138	16.304	16.421	975709	7577676	1.71	
37	17.154	17.388	17.538	13851279	164368890	37.10	
38	17.538	17.638	17.787	20291683	157974779	35.66	
39	17.953	18.021	18.261	6689846	40690735	9.18	
40	19.755	19.838	19.905	3391617	17897192	4.04	
41	19.905	20.088	20.521	21021713	204738531	46.21	
42	24.221	24.355	24.505	1681758	13276042	3.00	
43	27.109	27.188	27.683	3293330	38145734	8.61	

Sample Spectra

+ Scan (rt: 12.171-12.354 min) Sub Peak 28 from + TIC Scan Sub

+ Scan (rt: 12.521-12.754 min) Sub Peak 29 from + TIC Scan Sub

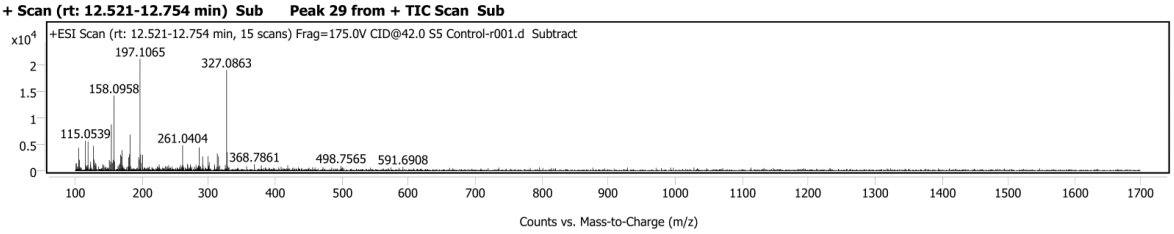

Spectrum Peaks

m/z	Z	Abund	Abund %	m/z (Calc)	Diff (ppm)	Ion Species	Formula	Ion Type
100.9518		1398	6.58					
102.9265		811	3.82					
103.0535		816	3.84					
104.9568		1653	7.77					
105.0335		897	4.22					
105.0667		4381	20.60					
106.0676		2095	9.85					
115.0539		5724	26.92					
116.0608		1043	4.91					
117.0685		765	3.60					
118.0669		975	4.58					
118.9268		1157	5.44					
119.0773		5578	26.23					
122.9485		1131	5.32					
123.0441		1744	8.20					
127.0534		4759	22.38					
128.0607		2146	10.09					
129.0687		1125	5.29					
130.0652		1543	7.26					
130.9022		840	3.95					
131.0771		1303	6.13					
135.0980		833	3.92					
141.0685		1289	6.06					
142.0691		1040	4.89					
143.0780		997	4.69					
146.0937		764	3.59					
151.0547		2046	9.62					
152.0588		1746	8.21					
153.0659		1232	5.79					
154.0650	1	8811	41.44					
155.0714	1	1700	7.99					
156.0798		1454	6.84					
157.0869		2092	9.84					
158.0958	1	14287	67.19					
159.1002	1	1794	8.44					
164.0614		986	4.64					
167.0824		1389	6.53					
168.0807		3069	14.43					
169.0861		2753	12.95					
170.0940		3923	18.45					
171.1000		1048	4.93					
178.9024		745	3.50					
178.9544		836	3.93					
180.0794		2569	12.08					
181.0800		3137	14.76					
182.0854	1	6852	32.22					
183.0951	1	917	4.31					
195.0921		2609	12.27					
196.0991		2132	10.03					
197.1065	1	21264	100.00					
198.1102	1	3102	14.59					
199.1205		1493	7.02					
201.1369		3035	14.27					
223.1211		844	3.97					
225.8535		1205	5.67					
235.1280		884	4.16					
236.9849		846	3.98					
238.8722		841	3.95					
240.1491		1077	5.06					
245.0430		828	3.89					
258.0564		1134	5.33					
259.0585		771	3.63					
260.8510		1015	4.78					
260.8884		741	3.48					
261.0404	1	4857	22.84					
262.0429	1	1034	4.86					
268.1819		1355	6.37					
268.8533		1077	5.07					
272.8238		865	4.07					
272.8831		1236	5.81					
274.8367		752	3.54					
278.8411		747	3.51					
281.0777		1142	5.37					
284.8644		994	4.68					
285.0610		987	4.64					
286.0492	1	4444	20.90					
287.0499	1	876	4.12					
287.8362		819	3.85					
291.0488		2727	12.82					
291.8048		1169	5.50					
298.9853		1004	4.72					
299.0728	1	2817	13.25					
300.0734	1	1002	4.71					
301.0711	1	1638	7.70					
309.0781		1214	5.71					
313.0708	1	3285	15.45					
314.0721	1	838	3.94					

Spectrum Peaks

m/z	Z	Abund	Abund %	m/z (Calc)	Diff (ppm)	Ion Species	Formula	Ion Type
314.8491		2797	13.16					
316.8454		973	4.58					
325.1077		1158	5.44					
327.0863	1	19171	90.16					
328.0913	1	3219	15.14					
329.0889	1	784	3.69					
357.1199		836	3.93					
368.7861		1255	5.90					
379.1134		1026	4.82					
408.8051		794	3.73					
418.7643		1057	4.97					
498.7565		974	4.58					
591.6908		778	3.66					

MassHunter Qual 10.0
(End of Report)